GOAL-ORIENTED ADAPTIVE MESH REFINEMENT FOR NON-SYMMETRIC FUNCTIONAL SETTINGS

BRENDAN KEITH, ALI VAZIRI ASTANEH, AND LESZEK DEMKOWICZ

ABSTRACT. In this article, a Petrov-Galerkin duality theory is developed. This theory is then used to motivate goal-oriented adaptive mesh refinement strategies for use with discontinuous Petrov-Galerkin (DPG) methods. The focus of this article is mainly on broken ultraweak variational formulations of steady boundary value problems, however, many of the ideas presented within are general enough that they be extended to any such well-posed variational formulation. The proposed goal-oriented adaptive mesh refinement procedures require the construction of refinement indicators for both a primal problem and a dual problem. In the DPG context, the primal problem is simply the system of linear equations coming from a standard DPG method and the dual problem is a similar system of equations, coming from a new method which is dual to DPG. This new method has the same coefficient matrix as the associated DPG method but has a different load. We refer to this new finite element method as a DPG* method. A thorough analysis of DPG* methods, as stand-alone finite element methods, is not given here but will be provided in subsequent articles. For DPG methods, the current theory of a posteriori error estimation is reviewed and the reliability estimate in [13, Theorem 2.1] is improved on. For DPG* methods, three different classes of refinement indicators are derived and several contributions are made towards rigorous a posteriori error estimation. At the closure of the article, results of numerical experiments with Poisson's boundary value problem in a three-dimensional domain are provided. These results clearly demonstrate the utility of the goal-oriented adaptive mesh refinement strategies for quantities of interest with either interior or boundary terms.

1. Introduction

With a natural capacity to accommodate problems with non-symmetric functional settings, the discontinuous Petrov–Galerkin (DPG) methodology [24, 27] has proven its merit in many areas of engineering interest [36, 37, 39, 40, 48, 60, 65, 66]. Desirable features of DPG methods include intrinsic numerical stability [17, 25, 30], a positive definite stiffness matrix for all well-posed boundary value problems [49], flexibility of variational formulation for the treatment of said boundary value problems [14, 37, 47], and a "built-in" *a posteriori* error estimator which can be used for adaptive mesh refinement [13,29]. The methodology incorporates a user-defined test norm, which, if chosen well, allows DPG methods to deliver a nearly optimal projection of the solution variable in a desired norm [8,70]. By exploiting properties of the underlying variational formulation, some DPG methods (ultraweak DPG methods) also permit irregular polytopal meshes [68].

For steady boundary value problems, all DPG methods begin with the declaration of a minimum residual principle. It is the first-order optimality condition for this minimum principle which delivers the variational equation determining the ideal DPG solution [49]. One advantage of this process is that it induces a very robust framework for analysis [12–14,42]. From the implementation point of view, this universal methodology also has many significant advantages and so has led to very general and very user-friendly DPG software [62–64].

Adaptive mesh refinement (AMR) and *a posteriori* error estimation [1,5,15,32,34,55] has been fundamental since the inception of DPG methods and so AMR has been incorporated into most applied research involving DPG [8, 18, 29, 33, 47, 62]. In each of these studies, the same "built-in" DPG *a posteriori* error estimator was used to drive AMR. This error estimator solely relies upon an intrinsic so-called "energy norm" estimate of the

Date: November 6, 2017.

²⁰¹⁰ Mathematics Subject Classification. 65N30, 65N12.

Key words and phrases. DPG methods, ultraweak formulations, a posteriori error analysis, duality, adaptivity, goal-oriented adaptivity. Acknowledgments. This work was partially supported with grants by NSF (DMS-1418822), AFOSR (FA9550-12-1-0484), and ONR (N00014-15-1-2496). The authors express their gratitude to Socratis Petrides for his assistance with certain features of the hp3D software during the numerical experiments.

solution error. The energy norm is induced by the chosen underlying minimum residual principle, and cannot be otherwise geared towards any specific extrinsic purpose. In the context of AMR, this is an example of what we will later on refer to as solution-adaptive mesh refinement (SMR).

Although SMR is sufficient in many circumstances, AMR geared towards a specified quantity of interest (QoI)—an output of the simulation which is defined through a function of the solution variables—instead of a global intrinsic energy, can be much more efficient for predictive modeling. In practical circumstances, a simulation is usually invoked to yield an estimate of a particular QoI. As a motivating principle, the effect of solution error on any such estimate will depend upon the QoI under consideration. Therefore, an intelligent AMR strategy should take the influence of the given QoI into account and therein possibly sacrifice a minimal global solution error (energy error) in order to minimize the more important QoI error. In many circumstances, if it is done well, an extrinsically-motivated AMR strategy can significantly reduce the ratio of QoI error to computational cost. In the framework developed in this manuscript, a primal and a dual problem is solved and refinement indicators for both problems are used to mark elements for refinement. We will refer to this form of AMR broadly as goal-oriented adaptive mesh refinement (GMR). In the DPG context, the associated dual problem can be identified with *a new class of methods* which we call DPG* methods [46] (see Section 4).

2. OVERVIEW

Elements of goal-oriented *a posteriori* error estimation and GMR have been the subject of significant practical interest in computational science for a few decades [4,7,41,50,52,58,61] and so a significant amount of its theory has been developed for a large variety of specific applications (see [51] and references therein). The lack of any sophisticated GMR framework for DPG methods was only recently identified as a shortcoming in [48]. Therefore, at the outset, the principal motivation of this article was to address the present DPG shortcoming in GMR. However, along the way, we uncovered a rich Petrov–Galerkin duality theory which has now started to take on a life of its own.

Main contributions and outline. The remainder of this article is organized as follows:

- In Section 3, the general Petrov–Galerkin duality theory is outlined in an idealized minimum residual principle setting. Here, important notions based on optimality are introduced along with a review of relevant material from the literature on test norms, variational formulations, and DPG methods.
- In Section 4, the discrete setting for the primal and dual problems and the main duality theorem (Theorem 4.2) is presented. Here, generality is maintained so that all results hold for the broad category of discrete least-squares (DLS) finite element methods [49], not only DPG methods. It is in this section that DPG* methods (and DLS* methods) are first introduced.
- In Section 5, the error in the discrete primal and dual solutions from Section 4 are identified with norms of specific residuals. As a consequence of Theorem 4.2, the product of these residuals is shown to bound the QoI error.
- In Section 6, standard ideas in goal-oriented adaptive mesh refinement are reviewed and compared to those in standard adaptive mesh refinement.
- In Section 7, conventional energy-based DPG *a posteriori* error estimation is presented. Here, an improved on version of [13, Theorem 2.1] is given (see Theorem 7.4, here).
- In Sections 8–10, three different classes of refinement indicators for DPG* methods are derived.
- In Section 11, the broken ultraweak formulation of Poisson's boundary value problem is presented and three different refinement indicators from Sections 8–10 are given for the corresponding DPG* methods.
- Finally, in Section 12, numerical experiments are presented. Here, a wide variety of possible quantities of interest are considered.

Notation. Throughout this document, $\Omega \subseteq \mathbb{R}^d$ will denote a bounded connected Lipschitz domain and \mathcal{T} , referred to as the mesh, will be a finite open disjoint partition of Ω into Lipschitz subdomains $K \in \mathcal{T}$. Specifically, \mathcal{T} is collection of open subsets $K \subseteq \Omega$, $|\mathcal{T}| < \infty$, $\bigcup_{K \in \mathcal{T}} \overline{K} = \overline{\Omega}$, and $K \cap \widetilde{K} = \emptyset$, for all $K \neq \widetilde{K} \in \mathcal{T}$. Here, each $K \in \mathcal{T}$, referred to as an element, is necessarily Lipschitz.

Occasionally, we will write $A \lesssim B$ or $B \lesssim A$ if there exists a constant C > 0, independent of the maximal mesh size, h, or the individual element size, h_K , such that $A \leq CB$ or $B \leq CA$, respectively. Similarly, $A \approx B$ is understood to mean that $A \lesssim B$ and $B \lesssim A$.

Lastly, we will often deal with bounded linear operators $\mathcal{L} \in B(\mathcal{X}, \mathcal{Y})$ between Banach spaces \mathcal{X} and \mathcal{Y} . From now on, when dealing with quotients, such as in the definition of the norm $\|\mathcal{L}\|_{B(\mathcal{X},\mathcal{Y})} = \sup_{\mathbf{r} \in \mathcal{X} \setminus \{0\}} \frac{\|\mathcal{L}\mathbf{r}\|_{\mathcal{Y}}}{\|\mathbf{r}\|_{\mathcal{X}}}$, we will assume that the infinima and suprema ignore zero, wherein such quotients are not defined. Furthermore, because the meaning can often be understood by context in the case of such linear operators, instead of writing out $\|\mathcal{L}\|_{B(\mathcal{X},\mathcal{Y})}$ in totality, we will usually suppress the subscript above and simply write $\|\mathcal{L}\|$.

3. PRELIMINARY THEORY

3.1. The Riesz operator. Let $\mathcal W$ be a Hilbert space over $\mathbb R$. We will denote the norm on $\mathcal W$ by $\|\cdot\|_{\mathcal W}=(\cdot,\cdot)^{1/2}_{\mathcal W}$, where $(\cdot,\cdot)_{\mathcal W}$ is the associated inner product. In the case $\mathcal W=L^2(K)$ for any subset $K\subseteq\Omega$, we will simply just write $\|\cdot\|_K=(\cdot,\cdot)^{1/2}_K=\left(\int_K\cdot^2\right)^{1/2}$. Denote the duality pairing between $\mathcal W$ and $\mathcal W'$ by $\langle\cdot,\cdot\rangle_{\mathcal W',\mathcal W}$. That is, for all bounded linear functionals

Denote the duality pairing between W and W' by $\langle \cdot, \cdot \rangle_{W',W}$. That is, for all bounded linear functionals $f \in W'$ and all $\mathfrak{w} \in W$, $\langle f, \mathfrak{w} \rangle_{W',W} = f(\mathfrak{w})$. Now, recalling the Riesz representation theorem [20], the topological dual of W, denoted W', is isometrically isomorphic to W. Moreover, this isomorphism $\mathcal{R}_W : W \to W'$ can be defined explicitly:

$$(3.1) \qquad \langle \mathcal{R}_{\mathcal{W}} \, \mathfrak{w}, \widetilde{\mathfrak{w}} \rangle_{\mathcal{W}', \mathcal{W}} = \langle \mathfrak{w}, \mathcal{R}_{\mathcal{W}} \, \widetilde{\mathfrak{w}} \rangle_{\mathcal{W}, \mathcal{W}'} = (\mathfrak{w}, \widetilde{\mathfrak{w}})_{\mathcal{W}} = (\mathcal{R}_{\mathcal{W}} \, \mathfrak{w}, \mathcal{R}_{\mathcal{W}} \, \widetilde{\mathfrak{w}})_{\mathcal{W}'}, \quad \forall \, \mathfrak{w}, \widetilde{\mathfrak{w}} \in \mathcal{W}.$$

We call $\mathcal{R}_{\mathcal{W}}: \mathcal{W} \to \mathcal{W}'$, defined above, the *Riesz operator*. Note that $\|\mathcal{R}_{\mathcal{W}} \mathfrak{w}\|_{\mathcal{W}'} = \|\mathfrak{w}\|_{\mathcal{W}}$, for all $\mathfrak{w} \in \mathcal{W}$, $\|f\|_{\mathcal{W}'} = \|\mathcal{R}_{\mathcal{W}}^{-1} f\|_{\mathcal{W}}$, for all $f \in \mathcal{W}'$, $\mathcal{R}_{\mathcal{W}} = \mathcal{R}'_{\mathcal{W}}$, and $\mathcal{R}_{\mathcal{W}'} = \mathcal{R}^{-1}_{\mathcal{W}}$ (under the identification $\mathcal{W} \sim \mathcal{W}''$). From now on, we will not explicitly declare the spaces in a duality pairing, $\langle \cdot, \cdot \rangle_{\mathcal{W}',\mathcal{W}}$, because they can be deduced from context.

With the Riesz operator now introduced, it is appropriate to immediately present a key lemma which will get significant mileage throughout this article. Our proof will rely upon the key properties established above.

Lemma 3.1. Let $f \in W'$, where W is Hilbert, and let $W_0 \subseteq W$ be a closed subspace. Define $W_1 = W_0^{\perp}$. Then

$$\sup_{\mathbf{w} \in \mathcal{W}} \frac{|f(\mathbf{w})|^2}{\|\mathbf{w}\|_{\mathcal{W}}^2} = \sup_{\mathbf{w}_0 \in \mathcal{W}_0} \frac{|f(\mathbf{w}_0)|^2}{\|\mathbf{w}_0\|_{\mathcal{W}}^2} + \sup_{\mathbf{w}_1 \in \mathcal{W}_1} \frac{|f(\mathbf{w}_1)|^2}{\|\mathbf{w}_1\|_{\mathcal{W}}^2}.$$

Proof. Recall the Riesz operator, $\mathcal{R}_{\mathcal{W}}: \mathcal{W} \to \mathcal{W}'$, from (3.1). Let $\mathfrak{f} = \mathcal{R}_{\mathcal{W}}^{-1} f$ and so $(\mathfrak{f}, \mathfrak{w})_{\mathcal{W}} = f(\mathfrak{w})$, for all $\mathfrak{w} \in \mathcal{W}$. Moreover, $\|\mathfrak{f}\|_{\mathcal{W}} = \|f\|_{\mathcal{W}'}$. If we orthogonally decompose $\mathfrak{f} = \mathfrak{f}_0 + \mathfrak{f}_1$, where $\mathfrak{f}_0 \in \mathcal{W}_0$ and $\mathfrak{f}_1 \in \mathcal{W}_1$, then, by orthogonality,

$$f(\mathfrak{w}_0) + f(\mathfrak{w}_1) = (\mathfrak{f}_0, \mathfrak{w}_0)_{\mathcal{W}} + (\mathfrak{f}_1, \mathfrak{w}_1)_{\mathcal{W}}, \quad \forall \mathfrak{w}_0 \in \mathcal{W}_0, \mathfrak{w}_1 \in \mathcal{W}_1.$$

Therefore, $\mathfrak{f}_0=\mathcal{R}^{-1}_{\mathcal{W}_0}(f|_{\mathcal{W}_0})$ and $\mathfrak{f}_1=\mathcal{R}^{-1}_{\mathcal{W}_1}(f|_{\mathcal{W}_1}).$ Finally,

$$\|f\|_{\mathcal{W}'}^2 = \|\mathfrak{f}\|_{\mathcal{W}}^2 = \|\mathfrak{f}_0\|_{\mathcal{W}_0}^2 + \|\mathfrak{f}_1\|_{\mathcal{W}_1}^2 = \|f|_{\mathcal{W}_0}\|_{\mathcal{W}_0'}^2 + \|f|_{\mathcal{W}_1}\|_{\mathcal{W}_1'}^2.$$

3.2. Variational boundary value problems with a linear quantity of interest. Let \mathcal{U} and \mathcal{V} be Hilbert spaces over \mathbb{R} . In the abstract setting, the variational boundary value problems we consider are posed over such spaces using a continuous bilinear form $b: \mathcal{U} \times \mathcal{V} \to \mathbb{R}$. Here, \mathcal{U} is called the *trial space* and \mathcal{V} is called the *test space*. The members of both spaces \mathcal{U} and \mathcal{V} may have many components but are routinely called *functions*. For instance, *trial functions* $\mathbf{u} \in \mathcal{U}$ and *test functions* $\mathbf{v} \in \mathcal{V}$.

For a given functional $\ell \in \mathcal{V}'$, called the *load*, we define the *(primal) solution* to be the unique function $\mathbf{u}^* \in \mathcal{U}$ satisfying

$$(3.2) b(\mathbf{u}^{\star}, \mathbf{v}) = \ell(\mathbf{v}), \quad \forall \, \mathbf{v} \in \mathcal{V}.$$

Note that the bilinear form b naturally generates a linear, continuous operator $\mathcal{B}:\mathcal{U}\to\mathcal{V}'$ and, taking into account the reflexivity of \mathcal{V} , also generates its dual $\mathcal{B}':\mathcal{V}\to\mathcal{U}'$:

$$\langle \mathfrak{B}\mathfrak{u}, \mathfrak{v} \rangle = \langle \mathfrak{u}, \mathfrak{B}'\mathfrak{v} \rangle = b(\mathfrak{u}, \mathfrak{v}), \quad \forall \mathfrak{u} \in \mathfrak{U}, \mathfrak{v} \in \mathfrak{V}.$$

Often, in practical simulations, we are not altogether interested in the global features of the solution $\mathbf{u}^* = \mathcal{B}^{-1}\ell$ of a given problem of type (3.2). Instead, we are interested in a derived quantity $g(\mathbf{u}^*)$, called the *quantity* of interest (QoI). In this context, we choose to call the corresponding functional $g \in \mathcal{U}'$ the goal. Although we do not require it immediately, note that, for every goal $g \in \mathcal{U}'$, there exists a function $\mathbf{g} \in \mathcal{U}$ such that

$$(3.3) g(\mathbf{u}) = (\mathbf{g}, \mathbf{u})_{\mathcal{U}}, \quad \forall \, \mathbf{u} \in \mathcal{U}.$$

Namely, $\mathfrak{g} = \mathfrak{R}_{\mathfrak{U}}^{-1} g$ is the Riesz representation of the goal functional.

Formally, observe that

(3.4)
$$g(\mathbf{u}^{\star}) = \langle g, \mathcal{B}^{-1} \ell \rangle = \langle \ell, (\mathcal{B}')^{-1} g \rangle = \ell(\mathbf{v}^{\star}),$$

where $\mathbf{v}^* = (\mathcal{B}')^{-1}g$. Here, we call $\mathbf{v}^* \in \mathcal{V}$ the (*test space*) *influence function* and note that it is a test function satisfying

$$(3.5) b(\mathbf{u}, \mathbf{v}^*) = g(\mathbf{u}), \quad \forall \, \mathbf{u} \in \mathcal{U}.$$

From (3.4), observe that the QoI can be calculated from the solution of the primal problem (3.2) or from a solution of the dual problem (3.5).

3.3. Well-posedness. Clearly, in order for solutions to (3.2) and (3.5) to exist, we must assume that $\ell \in \operatorname{Range}(\mathcal{B})$ and $g \in \operatorname{Range}(\mathcal{B}')$. In order to simplify our analysis in this section, we will often choose to assume $\operatorname{Range}(\mathcal{B}') = \mathcal{U}'$ and $\operatorname{Range}(\mathcal{B}) = \mathcal{V}'$. These assumptions will make both \mathfrak{u}^* and \mathfrak{v}^* unique, but only the first assumption will ultimately be necessary for our analysis in later sections. In the general scenario, therefore, $g \in \mathcal{U}'$ can always be completely arbitrary.

In the sequel, we will occasionally embellish our assumptions on structure of the bilinear form b as well as the trial and test spaces \mathcal{U} and \mathcal{V} . Such assumptions will be introduced as and when they become necessary. For now, however, let us pose the following universal assumption, which will ensure that (3.2) is well-posed.

Assumption 1. The bilinear form $b: \mathcal{U} \times \mathcal{V} \to \mathbb{R}$ is bounded with continuity constant $M < +\infty$, where

(3.6)
$$\sup_{\mathbf{u} \in \mathcal{U}} \sup_{\mathbf{v} \in \mathcal{V}} \frac{b(\mathbf{u}, \mathbf{v})}{\|\mathbf{u}\|_{\mathcal{U}} \|\mathbf{v}\|_{\mathcal{V}}} = M,$$

and it satisfies the Banach-Babuška-Nečas inf-sup condition with stability constant $\gamma > 0$, where

(3.7)
$$\inf_{\mathbf{u} \in \mathcal{U}} \sup_{\mathbf{v} \in \mathcal{V}} \frac{b(\mathbf{u}, \mathbf{v})}{\|\mathbf{u}\|_{\mathcal{U}} \|\mathbf{v}\|_{\mathcal{V}}} = \gamma.$$

Throughout this section, we make the following additional assumption to ensure that (3.5) is also well-posed. When this assumption is or is not valid, it will be referred to as the *surjective* or *non-surjective setting*, respectively.

Assumption 2. The null space of \mathcal{B}' is trivial, $\text{Null}(\mathcal{B}') = \{0\}$, and, therefore, the Banach-Babuška-Nečas inf-sup condition is satisfied for the dual problem (3.5) and $\text{Range}(\mathcal{B}) = \mathcal{V}'$. That is,

$$\inf_{\mathfrak{v}\in\mathcal{V}}\sup_{\mathfrak{u}\in\mathcal{U}}\frac{b(\mathfrak{u},\mathfrak{v})}{\|\mathfrak{u}\|_{\mathcal{U}}\|\mathfrak{v}\|_{\mathcal{V}}}=\gamma\,.$$

Assumptions 1 and 2, together, imply that $\|\mathcal{B}\| = \|\mathcal{B}'\| = M$ and $\|\mathcal{B}^{-1}\| = \|(\mathcal{B}')^{-1}\| = \gamma^{-1}$. In this case, \mathcal{B} and \mathcal{B}' are Banach space isomorphisms. Namely,

(3.8)
$$\gamma \|\mathbf{u}\|_{\mathcal{U}} \leq \|\mathcal{B}\mathbf{u}\|_{\mathcal{V}'} \leq M \|\mathbf{u}\|_{\mathcal{U}}, \quad \forall \, \mathbf{u} \in \mathcal{U},$$

and

(3.9)
$$\gamma \|\mathbf{v}\|_{\mathcal{V}} \leq \|\mathcal{B}'\mathbf{v}\|_{\mathcal{U}'} \leq M\|\mathbf{v}\|_{\mathcal{V}}, \quad \forall \mathbf{v} \in \mathcal{V}.$$

When only Assumption 1 holds, then only (3.8) is satisfied.

3.4. **Minimum residual principles.** Let $\mathcal{U}_h \subseteq \mathcal{U}$ be a discrete subspace of the trial space. It desirable for us to seek, in some practical sense, the *optimal* (i.e. minimal error) solution $\mathbf{u}_h^{\text{opt}} \in \mathcal{U}_h$ to the primal problem (3.2). Because the exact solution $\mathbf{u}^* = \mathcal{B}^{-1}\ell$ is inaccessible *a priori*, the optimal solution $\mathbf{u}_h^{\text{opt}}$ cannot be defined by explicitly invoking it. For illustration, the most convenient (but impractical) notion of "optimal solution" is the so-called best approximation error solution: $\mathbf{u}_h^{\text{opt}} = \mathbf{u}_h^*$, where

$$\mathbf{u}_h^{\star} = \operatorname*{arg\,min}_{\mathbf{u}_h \in \mathcal{U}_h} \|\mathbf{u}^{\star} - \mathbf{u}_h\|_{\mathcal{U}}^2.$$

The discrete solution \mathbf{u}_h^{\star} naturally corresponds to the orthogonal projection of the exact solution in the trial space norm $\|\cdot\|_{\mathcal{U}}$. Meanwhile, the minimum value attained, $\|\mathbf{u}^{\star} - \mathbf{u}_h^{\star}\|_{\mathcal{U}}$, is referred to as the *best approximation error*.

Instead of adopting the best approximation error notion (or any similar explicit concept), we will pose optimality implicitly through a minimum residual principle:

(3.10)
$$\mathbf{u}_h^{\text{opt}} = \underset{\mathbf{u}_h \in \mathcal{U}_h}{\arg \min} \|\mathcal{B}\mathbf{u}_h - \ell\|_{\mathcal{V}'}^2.$$

Define the *condition number* of ${\mathfrak B}$ to be

$$\kappa(\mathfrak{B}) = \|\mathfrak{B}\|_{B(\mathfrak{U}, \mathcal{V}')} \|\mathfrak{B}^{-1}\|_{B(\mathcal{V}', \mathfrak{U})} = \frac{M}{\gamma} \ge 1.$$

It can be shown that the accuracy of the optimal solution in (3.10) depends upon the condition number of \mathcal{B} , viz.,

(3.11)
$$\|\mathbf{u} - \mathbf{u}_h^{\star}\|_{\mathcal{U}} \leq \|\mathbf{u} - \mathbf{u}_h^{\text{opt}}\|_{\mathcal{U}} \leq \kappa(\mathcal{B})\|\mathbf{u} - \mathbf{u}_h^{\star}\|_{\mathcal{U}}.$$

One potential issue with using a minimum residual principle like (3.10) is handling the dual norm $\|\cdot\|_{\mathcal{V}'} = \sup_{\mathbf{v} \in \mathcal{V}} \frac{\langle \cdot, \mathbf{v} \rangle}{\|\mathbf{v}\|_{\mathcal{V}}}$. As we will come to see, DPG methods are designed to overcome this impediment.

Observe that $\|\mathfrak{B}\mathbf{u}_h - \ell\|_{\mathcal{V}'}^2 = \langle \mathfrak{B}\mathbf{u}_h - \ell, \mathfrak{R}_{\mathcal{V}}^{-1}(\mathfrak{B}\mathbf{u}_h - \ell) \rangle$, for all $\mathbf{u}_h \in \mathcal{U}_h$. Therefore, the first-order optimality condition associated with (3.10) is equivalent to the variational equation

$$(3.12) \qquad \langle \mathfrak{B}\mathbf{\mathfrak{u}}_{h}^{\text{opt}}, \mathfrak{R}_{\mathcal{V}}^{-1} \, \mathfrak{B}\mathbf{\mathfrak{u}}_{h} \rangle = \langle \ell, \mathfrak{R}_{\mathcal{V}}^{-1} \, \mathfrak{B}\mathbf{\mathfrak{u}}_{h} \rangle, \quad \forall \, \mathbf{\mathfrak{u}}_{h} \in \mathcal{U}_{h} \,.$$

We will now introduce a number of definitions which will be important soon. Define the *trial-to-test* operator $\Theta: \mathcal{U} \to \mathcal{V}$,

$$\Theta = \mathcal{R}_{\mathcal{V}}^{-1} \mathcal{B}$$
,

the *induced (trial space) Riesz operator* $A : \mathcal{U} \to \mathcal{U}'$,

$$\mathcal{A} = \mathcal{B}' \, \mathcal{R}_{\mathcal{V}}^{-1} \, \mathcal{B} = \mathcal{B}' \Theta = \Theta' \mathcal{B} \,,$$

its association energy inner product $a:\mathcal{U}\times\mathcal{U}\to\mathbb{R}$,

$$a(\mathfrak{u}, \widetilde{\mathfrak{u}}) = \langle A\mathfrak{u}, \widetilde{\mathfrak{u}} \rangle = \langle \mathfrak{u}, A\widetilde{\mathfrak{u}} \rangle, \quad \forall \mathfrak{u}, \widetilde{\mathfrak{u}} \in \mathcal{U},$$

and, also, the *induced load* $f \in \mathcal{U}'$,

$$f = \mathcal{B}' \mathcal{R}_{\mathcal{V}}^{-1} \ell = \Theta' \ell$$
.

With these definitions, we can reexpress (3.12) as either

$$(3.13) b(\mathbf{u}_h^{\text{opt}}, \mathbf{v}_h) = \ell(\mathbf{v}_h), \quad \forall \, \mathbf{v}_h \in \Theta(\mathcal{U}_h),$$

which is known as the optimal test function expression [25, 27], or as

(3.14)
$$a(\mathbf{u}_h^{\text{opt}}, \mathbf{u}_h) = f(\mathbf{u}_h), \quad \forall \, \mathbf{u}_h \in \mathcal{U}_h,$$

which we will refer to as the *coercive expression*. Clearly, both expressions (3.13) and (3.14) are equivalent. They can be shown to be well-posed—therefore, having unique solutions—given only Assumption 1 [26, 27]. Both expressions will help give insight into the goal-oriented analysis and duality theory which follows. In (3.13), the subspace $\Theta(\mathcal{U}_h) \subseteq \mathcal{V}$ is referred to as the *optimal test space*, and its members are called *optimal test functions*.

Note that the trial-to-test operator Θ is an isomorphism under Assumptions 1 and 2. Also note that, with only Assumption 1, the energy inner product $a: \mathcal{U} \times \mathcal{U} \to \mathbb{R}$, induces a norm

(3.15)
$$\|\mathbf{u}\|_{\mathcal{U}}^2 = a(\mathbf{u}, \mathbf{u}) = \langle \mathcal{A}\mathbf{u}, \mathbf{u} \rangle = \|\mathcal{B}\mathbf{u}\|_{\mathcal{V}'}^2, \quad \forall \, \mathbf{u} \in \mathcal{U}.$$

We will refer to $\|\cdot\|_{\mathcal{H}}$ as the *energy norm*.

3.5. **Dual minimum residual principles in the surjective setting.** Let us return to (3.2) and (3.5). As we have used when deducing (3.4), these problems can be rewritten $\mathcal{B}\mathbf{u}^* = \ell$ and $\mathcal{B}'\mathbf{v}^* = g$, respectively. Applying the dual of trial-to-test operator, Θ' , to both sides of the former expression delivers $\mathcal{A}\mathbf{u}^* = f$. When $\mathcal{U}_h = \mathcal{U}$, comparison with (3.14) then demonstrates that $\mathbf{u}_h^{\text{opt}} = \mathbf{u}^*$. Meanwhile, if we define $\boldsymbol{\omega}^* = \Theta^{-1}\mathbf{v}^*$ the latter expression gives us the equation $\mathcal{A}\boldsymbol{\omega}^* = g$. With ambiguity, we shall refer to $\boldsymbol{\omega}^* \in \mathcal{U}$ as the (trial space) influence function. Its distinction from the (test space) influence function $\mathbf{v}^* \in \mathcal{V}$ should always be clear from context.

A Bubnov-Galerkin approximation, ω_h , of the influence function ω^* can be readily characterized:

(3.16)
$$a(\boldsymbol{\omega}_h, \boldsymbol{\mathfrak{u}}_h) = g(\boldsymbol{\mathfrak{u}}_h), \quad \forall \, \boldsymbol{\mathfrak{u}}_h \in \mathcal{U}_h.$$

The discrete solution above, $\omega_h = \omega_h^{\rm en}$, can easily be seen to come from the Ritz method following from the quadratic energy principle

$$\boldsymbol{\omega}_h^{\text{en}} = \operatorname*{arg\,min}_{\boldsymbol{\mathfrak{u}}_h \in \mathcal{U}_h} \left(a(\boldsymbol{\mathfrak{u}}_h, \boldsymbol{\mathfrak{u}}_h) - 2g(\boldsymbol{\mathfrak{u}}_h) \right).$$

Similarly, $\omega_h=\omega_h^{\rm opt}$, where $\omega_h^{\rm opt}$ is defined as the minimum residual solution

$$\boldsymbol{\omega}_h^{\text{opt}} = \underset{\boldsymbol{\mathfrak{u}}_h \in \mathcal{U}_h}{\operatorname{arg\,min}} \| \mathcal{A} \boldsymbol{\mathfrak{u}}_h - g \|_{\mathcal{U}'}.$$

For an expanded discussion, see [49, Section 2.3]. As this second perspective will be the most useful to us, from now on we will only denote ω_h in (3.16) as ω_h^{opt} .

Observe that an approximation of the influence function $\mathbf{v}^{\star} \in \mathcal{V}$, denoted $\mathbf{v}_h^{\text{opt}}$, where

$$b(\mathbf{u}_h, \mathbf{v}_h^{\text{opt}}) = g(\mathbf{u}_h), \quad \forall \, \mathbf{u}_h \in \mathcal{U}_h,$$

can be recovered by post-processing the computed ω_h^{opt} : simply apply the trial-to-test operator Θ to the solution ω_h^{opt} . That is, $\mathbf{v}_h^{\text{opt}} = \Theta \omega_h^{\text{opt}}$. Note that this makes the discrete influence function $\mathbf{v}_h^{\text{opt}} \in \Theta(\mathcal{U}_h)$ an optimal test function and

$$\boldsymbol{\mathfrak{v}}_h^{\text{opt}} = \underset{\boldsymbol{\mathfrak{v}}_h \in \Theta(\mathfrak{U}_h)}{\text{arg min}} \| | \mathcal{B}' \boldsymbol{\mathfrak{v}}_h - g \|_{\mathcal{U}'}.$$

3.6. The optimal test norm. With the minimum residual principle (3.10), we have the flexibility of choosing the test space norm $\|\cdot\|_{\mathcal{V}}$. Naturally, the accuracy of the computed solution, measured in the trial norm $\|\cdot\|_{\mathcal{U}}$, will depend upon the chosen test norm $\|\cdot\|_{\mathcal{V}}$. In an ideal scenario, one would probably use a test norm $\|\cdot\|_{\mathcal{V}} = \|\|\cdot\|_{\mathcal{V}}$ where the norm of the residual is equal to best approximation error of the solution.

Suppose that a test norm $\|\cdot\|_{\mathcal{V}}$ is indeed used where

(3.17)
$$\|\mathbf{u}^{\star} - \mathbf{u}\|_{\mathcal{U}} = \|\mathcal{B}\mathbf{u} - \ell\|_{\mathcal{V}}, \quad \forall \mathbf{u} \in \mathcal{U},$$

and therefore $\mathbf{u}_h^{\mathrm{opt}} = \mathbf{u}_h^{\star}$. Note that $\|\|\mathcal{B}\mathbf{u} - \ell\|\|_{\mathcal{V}'} = \|\|\mathcal{B}(\mathbf{u}^{\star} - \mathbf{u})\|\|_{\mathcal{V}'}$, for all $\mathbf{u} \in \mathcal{U}$. Therefore, if (3.17) holds for all $\mathbf{u}^{\star} = \mathcal{B}^{-1}\ell \in \mathcal{U}$, then we may declare $\|\|\mathcal{B} \cdot \|\|_{\mathcal{V}'} = \| \cdot \|_{\mathcal{U}}$. With this norm,

$$\langle \mathcal{R}_{\mathcal{U}} \, \mathfrak{u}, \widetilde{\mathfrak{u}} \rangle \stackrel{\star}{=} (\mathfrak{u}, \widetilde{\mathfrak{u}})_{\mathcal{U}} \stackrel{\star}{=} (\mathcal{B}\mathfrak{u}, \mathcal{B}\widetilde{\mathfrak{u}})_{\mathcal{V}'} \stackrel{\star}{=} \langle \mathcal{B}' \, \mathcal{R}_{\mathcal{V}}^{-1} \, \mathcal{B}\mathfrak{u}, \widetilde{\mathfrak{u}} \rangle, \quad \forall \, \mathfrak{u}, \widetilde{\mathfrak{u}} \in \mathcal{U}.$$

Therefore, $\mathcal{R}_{\mathcal{U}} \stackrel{\star}{=} \mathcal{B}' \mathcal{R}_{\mathcal{V}}^{-1} \mathcal{B} = \mathcal{A}$ and, likewise, the Riesz operator for the optimal test norm is $\mathcal{R}_{\mathcal{V}} \stackrel{\star}{=} \mathcal{B} \mathcal{R}_{\mathcal{U}}^{-1} \mathcal{B}'$. Here, we have written the equalities above with the \star -notation to remind the reader they only hold in this idealized setting. We will continue to use this notation throughout this article.

The definitions of these idealized Riesz operators are easy to remember by observing that they are the unique isometries where the following diagram commutes:

$$\begin{array}{ccc} \mathcal{U}' & \stackrel{\mathcal{B}'}{\longleftarrow} & \mathcal{V} \\ \mathbb{R}_{\mathcal{U}} & & & \downarrow \mathbb{R}_{\mathcal{V}} \\ \mathcal{U} & \stackrel{\mathcal{B}}{\longrightarrow} & \mathcal{V}' \end{array}$$

Notice that the trial space Riesz operator $\mathcal{A}:\mathcal{U}\to\mathcal{U}'$ and the corresponding energy norm $\|\|\cdot\|\|_{\mathcal{U}}$ has been defined previously in (3.15). We will call $\|\|\cdot\|\|_{\mathcal{V}}$ the *optimal test norm*, however, in some articles it is also referred to as the "ideal test norm" [21]. Note that if $\|\cdot\|_{\mathcal{V}} \stackrel{\star}{=} \|\|\cdot\|\|_{\mathcal{V}}$, then $M \stackrel{\star}{=} \gamma \stackrel{\star}{=} 1$ in (3.8) and (3.9), $\kappa(\mathcal{B}) \stackrel{\star}{=} 1$ in (3.11), and $b(\mathbf{u}, \mathbf{v})$ becomes a duality pairing [11].

Note the definition $\|\mathbf{v}\|_{\mathcal{V}} = \|\mathcal{B}'\mathbf{v}\|_{\mathcal{U}'}$ and the identity $\|\mathbf{u}\|_{\mathcal{U}} = \|\mathcal{B}\mathbf{u}\|_{\mathcal{V}'}$. That is,

Observe that

$$(3.19) b(\mathbf{u}, \mathbf{v}) \leq \|\mathbf{u}\|_{\mathcal{U}} \|\mathbf{v}\|_{\mathcal{V}} \text{and} b(\mathbf{u}, \mathbf{v}) \leq \|\mathbf{u}\|_{\mathcal{U}} \|\mathbf{v}\|_{\mathcal{V}},$$

simultaneously, for all $u \in \mathcal{U}$ and $v \in \mathcal{V}$. Moreover, observe that

$$\|\mathbf{u}^{\star} - \mathbf{u}\|_{\mathcal{U}} = \|\mathcal{B}\mathbf{u} - \ell\|_{\mathcal{V}'}$$
 and $\|\mathbf{v}^{\star} - \mathbf{v}\|_{\mathcal{V}} = \|\mathcal{B}'\mathbf{v} - g\|_{\mathcal{U}'}$,

simultaneously, for all $\mathfrak{u} \in \mathcal{U}$ and $\mathfrak{v} \in \mathcal{V}$. Therefore,

$$\|\mathbf{u}^{\star} - \mathbf{u}_h^{\text{opt}}\|_{\mathcal{U}} = \|\mathcal{B}\mathbf{u}_h^{\text{opt}} - \ell\|_{\mathcal{V}'} \quad \text{and} \quad \|\mathbf{v}^{\star} - \mathbf{v}_h^{\text{opt}}\|_{\mathcal{V}} = \|\mathcal{B}'\mathbf{v}_h^{\text{opt}} - g\|_{\mathcal{U}'} = \|\mathcal{A}\boldsymbol{\omega}_h^{\text{opt}} - g\|_{\mathcal{U}'}.$$

As we have just seen, in the hypothetical scenario that $\mathcal{R}_{\mathcal{V}} \stackrel{\star}{=} \mathcal{B} \, \mathcal{R}_{\mathcal{U}}^{-1} \, \mathcal{B}'$, we also have $\mathcal{A} \stackrel{\star}{=} \mathcal{R}_{\mathcal{U}}$ and, accordingly, $\|\cdot\|_{\mathcal{U}} \stackrel{\star}{=} \|\cdot\|_{\mathcal{U}}$. Furthermore, recall from (3.3) that $\mathfrak{g} = \mathcal{R}_{\mathcal{U}}^{-1} \, g$ is the Riesz representation of $g \in \mathcal{U}'$. Therefore, the use of the optimal test norm implies that $\boldsymbol{\omega}^{\star} = \mathfrak{g}$ and

(3.20)
$$\|\mathbf{v}^{\star} - \mathbf{v}_{h}^{\text{opt}}\|_{\mathcal{V}} \stackrel{\star}{=} \|\mathcal{R}_{\mathcal{U}} \boldsymbol{\omega}_{h}^{\text{opt}} - g\|_{\mathcal{U}'} \stackrel{\star}{=} \|\mathbf{g} - \boldsymbol{\omega}_{h}^{\text{opt}}\|_{\mathcal{U}}.$$

We note one final identity. Let $\mathbf{u} \in \mathcal{U}$ be arbitrary and define the error representation function as $\psi = \mathcal{R}_{\mathcal{V}}^{-1}(\mathcal{B}\mathbf{u} - \ell)$. With the optimal test norm, note that

$$g(\mathbf{u}^{\star} - \mathbf{u}) = g(\mathcal{B}^{-1} \mathcal{R}_{\mathcal{V}} \mathcal{R}_{\mathcal{V}}^{-1} \mathcal{B}(\mathbf{u}^{\star} - \mathbf{u})) \stackrel{\star}{=} -g(\mathcal{R}_{\mathcal{U}}^{-1} \mathcal{B}' \psi) \stackrel{\star}{=} -b(\mathbf{g}, \psi).$$

This indicates an explicit relationship, in an ideal scenario, between error in the QoI and the residual.

Unfortunately, actually working directly with the optimal test norm is not computationally feasible. This is, in part, due to presence of the inverse of the trial space Riesz operator in the expression $\mathcal{R}_{\mathcal{V}} \stackrel{\star}{=} \mathcal{B} \, \mathcal{R}_{\mathcal{U}}^{-1} \, \mathcal{B}'$. Nevertheless, for special bilinear forms, we can often still come suitably close as we will motivate in the next subsection.

3.7. Ultraweak variational formulations. Let $\mathcal{L}^*: \mathcal{V} \to L^2(\Omega)$ be a closed linear operator where $\mathcal{V} = \mathrm{Dom}(\mathcal{L}^*) \subseteq L^2(\Omega)$ is dense. An (unbroken) ultraweak variation formulation is a boundary value problem in a special functional setting that is expressed as

(3.21)
$$\begin{cases} \operatorname{Find} \, \boldsymbol{\mathfrak{u}}^{\star} \in L^{2}(\Omega) : \\ (\boldsymbol{\mathfrak{u}}^{\star}, \mathcal{L}^{*}\boldsymbol{\mathfrak{v}})_{\Omega} = \ell(\boldsymbol{\mathfrak{v}}) , \quad \forall \, \boldsymbol{\mathfrak{v}} \in \mathcal{V}. \end{cases}$$

Define

$$(3.22) b(\mathbf{u}, \mathbf{v}) = (\mathbf{u}, \mathcal{L}^* \mathbf{v})_{\Omega}, \quad \forall \, \mathbf{u} \in L^2(\Omega), \, \mathbf{v} \in \mathcal{V}.$$

In this setting, observe that $\mathcal{U} = L^2(\Omega)$ and $\mathcal{B} = \mathcal{R}_{L^2(\Omega)} \mathcal{L}^*$, and so the optimal test norm (3.18) is readily computable for all $\mathbf{v} \in \mathcal{V}$:

$$\|\|\mathbf{v}\|\|_{\mathcal{V}} = \sup_{\mathbf{u} \in L^2(\Omega)} \frac{(\mathbf{u}, \mathcal{L}^*\mathbf{v})_{\Omega}}{\|\mathbf{u}\|_{\Omega}} = \|\mathcal{L}^*\mathbf{v}\|_{\Omega}.$$

The corresponding test space Riesz map is defined

$$(3.23) \qquad \langle \mathcal{R}_{\mathcal{V}} \, \mathbf{v}, \widetilde{\mathbf{v}} \rangle \stackrel{\star}{=} (\mathcal{L}^* \mathbf{v}, \mathcal{L}^* \widetilde{\mathbf{v}}), \quad \forall \, \mathbf{v}, \widetilde{\mathbf{v}} \in \mathcal{V},$$

which is indeed a norm, by (3.7): $\|\mathcal{L}^*\mathbf{v}\|_{\Omega} \ge \gamma \|\mathbf{v}\|_{\Omega}$ for all $\mathbf{v} \in \mathcal{V}$, where $\gamma > 0$.

Note that, in general, when $\mathcal{U} = L^2(\Omega)$, all QoI can be expressed

$$g(\mathfrak{u}) = (\mathfrak{g}, \mathfrak{u})_{\Omega} = \int_{\Omega} \mathfrak{g} \cdot \mathfrak{u}, \quad \forall \, \mathfrak{u} \in L^2(\Omega),$$

for some unique function $\mathfrak{g} \in L^2(\Omega)$. This will become useful when deriving one set of refinement indicators (see Section 10).

3.8. **Broken variational formulations and DPG methods.** With a well-posed ultraweak variational formulation, it is now clear that the optimal test norm is readily computable. Unfortunately, practical computation with the minimum residual principle (3.10) must include an accurate and efficiently computable inverse of the test space Riesz operator, $\Re^{-1}_{\mathcal{V}}$. In the scenarios we are preparing for, \mathcal{L}^* in (3.21) is a globally-defined differential operator. Therefore, any matrix representation, G, of an approximation of the optimal test space Riesz map (3.23) coming from a conforming discrete subspace of \mathcal{V} would have an enormous dense matrix inverse G^{-1} . This would be impractical to compute or even to store in memory. At this juncture, therefore, an ultraweak variational formulation not allow $\mathfrak{u}_h^{\mathrm{opt}}$ to be efficiently estimated. The compromise considered in this work is a hybridization approach to ultraweak variational formulations using the general theory of *broken variational formulations* [14]. This way, the formulations we use still locally satisfy (3.22) but allow $\Re^{-1}_{\mathcal{V}}$ to be discretized through element-wise computations and produce a sparse matrix representation $\mathsf{G}^{-1} = \mathrm{diag}_{K \in \mathcal{T}}(\mathsf{G}_{K}^{-1})$.

Without necessarily having the corresponding product norm, a test space $\mathcal{V} = \prod_{K \in \mathcal{T}} \mathcal{V}_K$ is *broken* if it does not require in its members any form of continuity across element boundaries, ∂K . Meanwhile, a test space norm $\|\cdot\|_{\mathcal{V}}$ is *localizable* if it induces a finite orthogonal direct sum, $\mathcal{V} = \bigoplus_{K \in \mathcal{T}} \mathcal{V}_K$, where $\mathfrak{v}_K|_{\widetilde{K}} = 0$ for all $\mathfrak{v}_K \in \mathcal{V}_K$, $K \neq \widetilde{K}$. Here, it is helpful to envision each \mathcal{V}_K as an element-wise test space. In a DPG method the following assumptions holds:

Assumption 3. The test space \mathcal{V} is broken and the corresponding test space norm $\|\cdot\|_{\mathcal{V}}$ is localizable.

It is the broken test space assumption which permits discontinuous test functions in DPG methods, but it is the localizable norm assumption which make DPG methods practical. These two properties, together, ensure that $\mathcal{R}_{\mathcal{V}} = \bigoplus_{K \in \mathcal{T}} \mathcal{R}_{\mathcal{V}_K}$ and $\mathcal{R}_{\mathcal{V}}^{-1} = \bigoplus_{K \in \mathcal{T}} \mathcal{R}_{\mathcal{V}_K}^{-1}$ and that the Gram matrix $\mathsf{G} = \mathrm{diag}_{K \in \mathcal{T}}(\mathsf{G}_K)$ can be block diagonal [49] (with a block-diagonal inverse).

3.9. Broken ultraweak variational formulations. Consider a broken test space $\mathcal{V} = \prod_{K \in \mathcal{T}} \mathcal{V}_K$ and $\mathcal{L}^* : \mathcal{V} \to L^2(\Omega)$ as in Section 3.7 where $(\mathfrak{u}, \mathcal{L}^* \mathfrak{v})_{\Omega} = \sum_{K \in \mathcal{T}} (\mathfrak{u}, \mathcal{L}^* \mathfrak{v})_K$, for all $\mathfrak{u} \in L^2(\Omega)$ and $\mathfrak{v} \in \mathcal{V}$. A broken ultraweak variation formulation is a boundary value problem in a special functional setting expressed as

$$\begin{cases} \operatorname{Find}\, \boldsymbol{\mathfrak{u}}^{\star} = (\boldsymbol{\mathfrak{u}}^{\star}, \hat{\boldsymbol{\mathfrak{u}}}^{\star}) \in \mathcal{U} = L^{2}(\Omega) \times \hat{\mathcal{U}}: \\ (\boldsymbol{\mathfrak{u}}^{\star}, \mathcal{L}^{*}\boldsymbol{\mathfrak{v}})_{\Omega} + \langle \hat{\boldsymbol{\mathfrak{u}}}^{\star}, \boldsymbol{\mathfrak{v}} \rangle_{\partial \mathcal{T}} = \ell(\boldsymbol{\mathfrak{v}}) \,, \quad \forall \, \boldsymbol{\mathfrak{v}} \in \mathcal{V} \,. \end{cases}$$

Here, $\langle \cdot, \cdot \rangle_{\partial \mathcal{T}}$ denotes the mesh-dependent functional pairing:

$$\langle \hat{\mathfrak{u}}, \boldsymbol{\mathfrak{v}} \rangle_{\partial \mathcal{T}} = \sum_{K \in \mathcal{T}} \langle \hat{\mathfrak{u}}, \operatorname{tr}_{\mathcal{V}}^{\partial K} \boldsymbol{\mathfrak{v}} \rangle \,, \quad \forall \, \hat{\mathfrak{u}} \in \hat{\mathcal{U}}, \boldsymbol{\mathfrak{v}} \in \mathcal{V} \,,$$

where $\operatorname{tr}_{\mathcal{V}}^{\partial K}: \mathcal{V}|_K \to \hat{\mathcal{V}}_{\partial K}$ is a continuous trace operator. Define

$$b(\boldsymbol{\mathfrak u},\boldsymbol{\mathfrak v})=(\boldsymbol{\mathfrak u},\mathcal L^*\boldsymbol{\mathfrak v})_{\scriptscriptstyle\Omega}+\langle\hat{\boldsymbol{\mathfrak u}},\boldsymbol{\mathfrak v}\rangle_{\scriptscriptstyle\partial\mathcal T}\,,\quad\forall\,\boldsymbol{\mathfrak u}\in L^2(\Omega)\times\hat{\mathcal U},\,\boldsymbol{\mathfrak v}\in\prod_{K\in\mathcal T}\mathcal V_K\,.$$

If the interface space $\hat{\mathcal{U}}$ is chosen correctly, Assumption 1 can be shown to hold under very general circumstances [28].

Using Lemma 3.1, the optimal test norm (3.18) for a broken ultraweak variational formulation can be expressed as

$$\left\|\left\|\boldsymbol{v}\right\|\right\|_{\mathcal{V}}^{2} = \left(\sup_{\boldsymbol{\mathfrak{u}}\in\mathcal{U}}\frac{(\boldsymbol{\mathfrak{u}},\mathcal{L}^{*}\boldsymbol{v})_{\Omega}+\langle\hat{\boldsymbol{\mathfrak{u}}},\boldsymbol{v}\rangle_{\partial\mathcal{T}}}{\left(\left\|\boldsymbol{\mathfrak{u}}\right\|_{\Omega}^{2}+\left\|\hat{\boldsymbol{\mathfrak{u}}}\right\|_{\hat{\Omega}}^{2}\right)^{1/2}}\right)^{2} = \left\|\mathcal{L}^{*}\boldsymbol{v}\right\|_{\Omega}^{2} + \sup_{\hat{\boldsymbol{\mathfrak{u}}}\in\hat{\mathcal{U}}}\frac{\langle\hat{\boldsymbol{\mathfrak{u}}},\boldsymbol{v}\rangle_{\partial\mathcal{T}}^{2}}{\left\|\hat{\boldsymbol{\mathfrak{u}}}\right\|_{\Omega}^{2}}.$$

Here, the first term is readily computable but the second term is not. Moreover, due to the second term, the optimal test norm is generally not localizable. To compromise on these issues, a related norm is often used in practice, called the (*adjoint*) *graph norm*:

$$\|\mathbf{v}\|_{\mathcal{L}^*,\alpha}^2 = \|\mathcal{L}^*\mathbf{v}\|_{\Omega}^2 + \alpha^2 \|\mathbf{v}\|_{\Omega}^2.$$

Note that the graph norm easily decomposes into the sum $\|\mathbf{v}\|_{\mathcal{L}^*,\alpha}^2 = \sum_{K\in\mathcal{T}} \left(\|\mathcal{L}^*\mathbf{v}\|_K^2 + \alpha^2\|\mathbf{v}\|_K^2\right)$ and so, with this norm, the test space \mathcal{V} decomposes into the orthogonal direct sum $\mathcal{V} = \bigoplus_{K\in\mathcal{T}} \mathcal{V}_K$, and $\|\mathbf{v}\|_{\mathcal{L}^*,\alpha}$ is localizable.

Computations with the graph norm $\|\cdot\|_{\mathcal{L}^*,\alpha}^2$, for sufficiently small values of the parameter α , give quasi-optimal results for a wide variety of problems. For much deeper examinations of test norm choices as well as improvements over the graph norm for some singular perturbation problems, see [17,44] and references therein.

4. DISCRETIZATION, DUALITY, AND DISCRETE LEAST-SQUARES METHODS

Many of the expressions in the previous section were derived with the assumption that the test space Riesz map $\mathcal{R}_{\mathcal{V}}$ can be inverted over the entire space \mathcal{V} . Although this assumption is a helpful guide for designing DPG methods, it cannot be made during careful numerical analysis. In practice, the inversion of the Riesz map is carried out only approximately, on a subspace $\mathcal{V}_r \subsetneq \mathcal{V}$. To rigorously account for the error inherited from this discretization, it is helpful to first consider (practical) DPG methods—and all similar minimum residual methods—from the saddle-point perspective. That is the subject of this section.

In this section as well as the next two, there are no specifically DPG-related assumptions. All of the analysis here holds for any minimum residual method where the test space has also been discretized. In this context, a discretized minimum residual principle gives rise to a general class of methods called discrete least-squares (DLS) methods [49]. In later sections, when DPG-specific properties are used, we will remark upon it to emphasize that the pertaining results do not hold for all DLS methods.

4.1. **The mixed method interpretation.** Reflect upon (3.14) and (3.16):

$$a(\mathbf{u}_h^{\mathrm{opt}}, \mathbf{u}_h) = f(\mathbf{u}_h)$$
 and $a(\boldsymbol{\omega}_h^{\mathrm{opt}}, \mathbf{u}_h) = g(\mathbf{u}_h), \quad \forall \, \mathbf{u}_h \in \mathcal{U}_h$.

Note that both optimal discrete solutions $\mathbf{u}_h^{\mathrm{opt}}$ and $\boldsymbol{\omega}_h^{\mathrm{opt}}$ are unique, even when Assumption 2 does not hold. Define $\boldsymbol{\psi}_h^{\mathrm{opt}} = \mathcal{R}_{\mathcal{V}}^{-1}(\mathcal{B}\mathbf{u}_h^{\mathrm{opt}} - \ell)$ and recall that $\mathbf{v}_h^{\mathrm{opt}} = \mathcal{R}_{\mathcal{V}}^{-1}\,\mathcal{B}\boldsymbol{\omega}_h^{\mathrm{opt}}$. Note that both $\boldsymbol{\psi}_h^{\mathrm{opt}}$ and $\mathbf{v}_h^{\mathrm{opt}}$ must also be unique. Finally, observe that

$$b(\mathbf{u}_h, \boldsymbol{\psi}_h^{\text{opt}}) = \langle \mathcal{B}' \, \mathcal{R}_{\mathcal{V}}^{-1}(\mathcal{B}\mathbf{u}_h^{\text{opt}} - \ell), \mathbf{u}_h \rangle = a(\mathbf{u}_h^{\text{opt}}, \mathbf{u}_h) - f(\mathbf{u}_h) = 0, \quad \forall \, \mathbf{u}_h \in \mathcal{U}_h,$$

and

$$b(\mathbf{u}_h,\mathbf{v}_h^{\mathrm{opt}}) = \langle \mathcal{B}' \, \mathcal{R}_{\mathcal{V}}^{^{-1}} \, \mathcal{B} \boldsymbol{\omega}_h^{\mathrm{opt}}, \mathbf{u}_h \rangle = a(\boldsymbol{\omega}_h^{\mathrm{opt}}, \mathbf{u}_h) = g(\mathbf{u}_h) \,, \quad \forall \, \mathbf{u}_h \in \mathcal{U}_h \,.$$

Therefore, note the following saddle-point characterizations of the primal and dual problems:

(4.1)
$$\begin{cases} (\boldsymbol{\psi}_{h}^{\text{opt}}, \boldsymbol{\mathfrak{v}})_{\mathcal{V}} - b(\boldsymbol{\mathfrak{u}}_{h}^{\text{opt}}, \boldsymbol{\mathfrak{v}}) = -\ell(\boldsymbol{\mathfrak{v}}), & \forall \, \boldsymbol{\mathfrak{v}} \in \mathcal{V}, \\ b(\boldsymbol{\mathfrak{u}}_{h}, \boldsymbol{\psi}_{h}^{\text{opt}}) & = 0, & \forall \, \boldsymbol{\mathfrak{u}}_{h} \in \mathcal{U}_{h}, \end{cases}$$

and

(4.2)
$$\begin{cases} (\boldsymbol{\mathfrak{v}}_{h}^{\text{opt}}, \boldsymbol{\mathfrak{v}})_{\mathcal{V}} - b(\boldsymbol{\omega}_{h}^{\text{opt}}, \boldsymbol{\mathfrak{v}}) = 0, & \forall \, \boldsymbol{\mathfrak{v}} \in \mathcal{V}, \\ b(\boldsymbol{\mathfrak{u}}_{h}, \boldsymbol{\mathfrak{v}}_{h}^{\text{opt}}) & = g(\boldsymbol{\mathfrak{u}}_{h}), & \forall \, \boldsymbol{\mathfrak{u}}_{h} \in \mathcal{U}_{h}, \end{cases}$$

respectively. We will refer to these as the idealized mixed methods.

Similarly, by introducing the functions $\psi^* = \mathcal{R}^{-1}_{\mathcal{V}}(\mathcal{B}\mathfrak{u}^* - \ell)$ and $\mathfrak{v}^* = \mathcal{R}^{-1}_{\mathcal{V}}\mathcal{B}\omega^*$, note that

(4.3)
$$\begin{cases} (\boldsymbol{\psi}^{\star}, \boldsymbol{\mathfrak{v}})_{\mathcal{V}} - b(\boldsymbol{\mathfrak{u}}^{\star}, \boldsymbol{\mathfrak{v}}) = -\ell(\boldsymbol{\mathfrak{v}}), & \forall \, \boldsymbol{\mathfrak{v}} \in \mathcal{V}, \\ b(\boldsymbol{\mathfrak{u}}, \boldsymbol{\psi}^{\star}) & = 0, & \forall \, \boldsymbol{\mathfrak{u}} \in \mathcal{U}, \end{cases}$$

and

(4.4)
$$\begin{cases} (\mathbf{v}^{\star}, \mathbf{v})_{\mathcal{V}} - b(\boldsymbol{\omega}^{\star}, \mathbf{v}) = 0, & \forall \mathbf{v} \in \mathcal{V}, \\ b(\mathbf{u}, \mathbf{v}^{\star}) & = g(\mathbf{u}), & \forall \mathbf{u} \in \mathcal{U}. \end{cases}$$

Because the null space of \mathcal{B}' may be non-trivial, an important distinction between (3.5) and (4.4) is that (4.4) always has a unique solution. Indeed, for arbitrary $\ell \in \mathcal{V}'$ and $g \in \mathcal{U}'$, existence and uniqueness can be proven for each saddle point problem (4.1)–(4.4) by simply checking Brezzi's conditions [10], which are readily satisfied. In fact, for arbitrary $\ell \in \operatorname{Range}(\mathcal{B}')$ and $g \in \mathcal{U}'$, $\psi^* = 0$ and $\mathfrak{v}^* \in \operatorname{Null}(\mathcal{B}')^{\perp}$ is a unique test space influence function satisfying (3.5), as the following theorem demonstrates.

Theorem 4.1. Let Assumption 1 hold. Let $\ell \in \text{Range}(\mathcal{B})$ and $g \in \mathcal{U}'$. Let $(\mathbf{u}^*, \boldsymbol{\psi}^*) \in \mathcal{U} \times \mathcal{V}$ be a solution of (4.3) and $(\boldsymbol{\omega}^*, \mathbf{v}^*) \in \mathcal{U} \times \mathcal{V}$ be a solution of (4.4). Then, $(\mathbf{u}^*, \boldsymbol{\psi}^*)$ and $(\boldsymbol{\omega}^*, \mathbf{v}^*)$ exist and are unique. Furthermore, $\boldsymbol{\psi}^* = 0$ and $\mathbf{v}^* \in \text{Null}(\mathcal{B}')^{\perp}$, where $b(\mathbf{u}, \mathbf{v}^*) = g(\mathbf{u})$, for all $\mathbf{u} \in \mathcal{U}$.

Proof. As stated above, Brezzi's conditions can be used to prove existence and uniqueness of solutions. In this case, however, we prefer a more constructive approach.

The operator form of (4.3) is

$$\begin{cases} \mathcal{R}_{\mathcal{V}} \boldsymbol{\psi}^{\star} - \mathcal{B} \boldsymbol{\mathfrak{u}}^{\star} = -\ell, \\ \mathcal{B}' \boldsymbol{\psi}^{\star} = 0. \end{cases}$$

Applying $\Theta'=\mathcal{B}'\mathcal{R}_{\mathcal{V}}^{-1}$ to the first equation and substituting the second gives $\mathcal{B}'\mathcal{R}_{\mathcal{V}}^{-1}\mathcal{B}\mathbf{u}^\star=\mathcal{B}'\mathcal{R}_{\mathcal{V}}^{-1}\ell$ or, equivalently, $\mathcal{A}\mathbf{u}^\star=f$. Since this equation has a unique solution, under Assumption 1, as discussed in Section 3, \mathbf{u}^\star exists and is unique. Note that $\ell\in\mathrm{Range}(\mathcal{B})=\mathrm{Null}(\mathcal{B}')^\perp$ and $\mathcal{B}\mathbf{u}^\star=\ell$. Therefore, $\mathbf{u}^\star=\mathcal{B}^{-1}\ell$ and $\psi_1^\star=\mathcal{R}_{\mathcal{V}}^{-1}(\mathcal{B}\mathbf{u}^\star-\ell)\in\mathrm{Null}(\mathcal{B}')^\perp$ is at least one candidate for the second solution component, ψ^\star . Let $\psi^\star=\psi_0^\star+\psi_1^\star$, where $\psi_0^\star\in\mathrm{Null}(\mathcal{B}')$ and $\psi_1^\star\in\mathrm{Null}(\mathcal{B}')^\perp$. Testing the first equation of (4.3) with ψ_0^\star , we find $\|\psi_0^\star\|_{\mathcal{V}}^2=0$. Therefore $\psi^\star=\psi_1^\star=\mathcal{R}_{\mathcal{V}}^{-1}(\mathcal{B}\mathbf{u}^\star-\ell)=\mathcal{R}_{\mathcal{V}}^{-1}(\mathcal{B}\mathcal{B}^{-1}\ell-\ell)=0$. Observe that $\mathrm{Null}((\mathcal{B}')')^\perp=\mathrm{Null}(\mathcal{B})^\perp=\mathcal{U}'$, by Assumption 1. Therefore, as for \mathbf{u}^\star above, $\boldsymbol{\omega}^\star$ can be

Observe that $\text{Null}((\mathcal{B}')')^{\perp} = \text{Null}(\mathcal{B})^{\perp} = \mathcal{U}'$, by Assumption 1. Therefore, as for \mathfrak{u}^* above, ω^* can be shown to be the unique solution to $\mathcal{A}\omega^* = g$. Clearly, $b(\mathfrak{u}, \mathfrak{v}^*) = g(\mathfrak{u})$, for all $\mathfrak{u} \in \mathcal{U}$, by the second equation in (4.4). As argued above for $\psi^* = \psi_0^* + \psi_1^*$, it also follows that $\mathfrak{v}^* \in \text{Null}(\mathcal{B}')^{\perp}$.

Remark 4.1. A similarity between (4.3) and least squares finite element methods is well known [49]. Likewise, a similarly between (4.4) and \mathcal{LL}^* methods can be shown. This latter relationship as well as *a priori* convergence estimates will be explored in future studies.

4.2. **Discretization.** In computation, the infinite dimensional test space \mathcal{V} in (4.1) and (4.2) often must be replaced by a discrete subspace $\mathcal{V}_r \subseteq \mathcal{V}$. In the case of (4.1), this leads to the special class of mixed methods called DLS methods [49]. In the case of (4.2), this leads to a separate special class of mixed methods, which we here refer to as DLS* methods.

In the DPG setting, the discrete test space $\mathcal{V}_r \subseteq \mathcal{V}$ should also satisfy Assumption 3. That is, \mathcal{V}_r should be broken, just like \mathcal{V} : $\mathcal{V} = \prod_{K \in \mathcal{T}} \mathcal{V}_K$, and $\mathcal{V}_r = \prod_{K \in \mathcal{T}} \mathcal{V}_{K,r}$, where $\mathcal{V}_{K,r} \subseteq \mathcal{V}_K$, for all $K \in \mathcal{T}$. When this is the case, the special corresponding DLS* will be referred to as a DPG* method, instead.

DLS methods correspond to the saddle-point problem

$$\begin{cases}
(\boldsymbol{\psi}_{h,r}^{\text{opt}}, \boldsymbol{\mathfrak{v}}_r)_{\mathcal{V}} - b(\boldsymbol{\mathfrak{u}}_{h,r}^{\text{opt}}, \boldsymbol{\mathfrak{v}}_r) = -\ell(\boldsymbol{\mathfrak{v}}_r) & \forall \, \boldsymbol{\mathfrak{v}}_r \in \mathcal{V}_r \,, \\
b(\boldsymbol{\mathfrak{u}}_h, \boldsymbol{\psi}_{h,r}^{\text{opt}}) & = 0 \,, & \forall \, \boldsymbol{\mathfrak{u}}_h \in \mathcal{U}_h \,.
\end{cases}$$

Conversely, DLS* methods correspond to the saddle-point problem

$$\begin{cases}
(\mathbf{v}_{h,r}^{\text{opt}}, \mathbf{v}_r)_{\mathcal{V}} - b(\boldsymbol{\omega}_{h,r}^{\text{opt}}, \mathbf{v}_r) = 0, & \forall \mathbf{v}_r \in \mathcal{V}_r, \\
b(\mathbf{u}_h, \mathbf{v}_{h,r}^{\text{opt}}) & = g(\mathbf{u}_h), & \forall \mathbf{u}_h \in \mathcal{U}_h.
\end{cases}$$

Notice that the solutions of the above problems, $\mathbf{u}_{h,r}^{\mathrm{opt}}, \boldsymbol{\omega}_{h,r}^{\mathrm{opt}} \in \mathcal{U}_h$ and $\boldsymbol{\psi}_{h,r}^{\mathrm{opt}}, \mathbf{v}_{h,r}^{\mathrm{opt}} \in \mathcal{V}_r$, are not necessarily equal to their ideal counterparts in (4.1) and (4.2). That is, $\mathbf{u}_{h,r}^{\mathrm{opt}} \neq \mathbf{u}_h^{\mathrm{opt}}, \mathbf{v}_{h,r}^{\mathrm{opt}} \neq \mathbf{v}_h^{\mathrm{opt}}$, etc.

Since the bilinear form is identical for both DLS and DLS* methods, much of the existing theory for DLS and DPG methods can be used to prove well-posedness and convergence rates for DLS* and DPG* methods. For instance, from [42, Theorem 2.1], well-posedness of both (4.5) and (4.6) is equivalent to the existence of a so-called Fortin operator. Construction of such operators has been considered in several DPG scenarios [13, 16, 42, 54]—including for our example problem (see Section 11)—and so we will not be concerned with proving its existence. However, existence of this operator constitutes our two final assumptions.

Assumption 4. For the closed subspaces $\mathcal{U}_h \subseteq \mathcal{U}$ and $\mathcal{V}_r \subseteq \mathcal{V}$, there exists a bounded linear operator $\Pi_r : \mathcal{V} \to \mathcal{V}_r$ such that

$$(4.7) b(\mathbf{u}_h, \mathbf{v} - \Pi_r \mathbf{v}) = 0, \quad \forall \, \mathbf{u}_h \in \mathcal{U}_h, \, \mathbf{v} \in \mathcal{V}.$$

Although only Assumption 4 is actually required for well-posedness of (4.5) and (4.6), when Π_r is constructed for DPG methods, it is often additionally designed to be a projection. This additional structure can be exploited, so we also include the following stronger assumption.

Assumption 5. In addition to Assumption 4, Π_r is projection, $\Pi_r \circ \Pi_r = \Pi_r$.

4.3. **Error in the quantity of interest.** We close this section with the following crucial theorem which relates the error in the QoI to the errors in the discrete solutions of the primal and dual problems.

Theorem 4.2. Let Assumptions 1 and 4 hold. Let $\ell \in \text{Range}(\mathcal{B})$ and $g \in \mathcal{U}'$. Let $(\mathbf{u}^*, \boldsymbol{\psi}^*) \in \mathcal{U} \times \mathcal{V}$ be the solution of (4.3), $(\boldsymbol{\omega}^*, \mathbf{v}^*) \in \mathcal{U} \times \mathcal{V}$ be the solution of (4.4), $(\boldsymbol{\psi}_h^{\text{opt}}, \mathbf{u}_h^{\text{opt}}) \in \mathcal{V} \times \mathcal{U}_h$ be the solution of (4.1), $(\mathbf{v}_h^{\text{opt}}, \boldsymbol{\omega}_h^{\text{opt}}) \in \mathcal{V} \times \mathcal{U}_h$ be the solution of (4.2), $(\mathbf{u}_{h,r}^{\text{opt}}, \boldsymbol{\psi}_{h,r}^{\text{opt}}) \in \mathcal{U}_h \times \mathcal{V}_r$ be the solution of (4.5), and $(\boldsymbol{\omega}_{h,r}^{\text{opt}}, \mathbf{v}_{h,r}^{\text{opt}}) \in \mathcal{U}_h \times \mathcal{V}_r$ be the solution of (4.6). Then, the following equalities hold:

$$(4.8) g(\mathbf{u}^{\star} - \mathbf{u}_h^{\text{opt}}) = a(\mathbf{u}^{\star} - \mathbf{u}_h^{\text{opt}}, \boldsymbol{\omega}^{\star} - \boldsymbol{\omega}_h^{\text{opt}}) = f(\boldsymbol{\omega}^{\star} - \boldsymbol{\omega}_h^{\text{opt}})$$

and

$$(4.9) g(\mathbf{u}^{\star} - \mathbf{u}_{h,r}^{\text{opt}}) = b(\mathbf{u}^{\star} - \mathbf{u}_{h,r}^{\text{opt}}, \mathbf{v}^{\star} - \mathbf{v}_{h,r}^{\text{opt}}) = \ell(\mathbf{v}^{\star} - \mathbf{v}_{h,r}^{\text{opt}}).$$

Remark 4.2. Note that (4.8) does not imply (4.9). Indeed, for every $\mathfrak{u} \in \mathcal{U}$,

$$a(\mathfrak{u},\boldsymbol{\omega}^{\star}-\boldsymbol{\omega}_h^{\mathrm{opt}})=b(\mathfrak{u},\Theta(\boldsymbol{\omega}^{\star}-\boldsymbol{\omega}_h^{\mathrm{opt}}))=b(\mathfrak{u},\mathfrak{v}^{\star}-\mathfrak{v}_h^{\mathrm{opt}})$$

which is not equal to $b(\mathbf{u}, \mathbf{v}^* - \mathbf{v}_{h,r}^{\text{opt}})$, in general. If $\mathcal{V}_r = \mathcal{V}$, however, then clearly $\mathbf{u}_{h,r}^{\text{opt}} = \mathbf{u}_h^{\text{opt}}$ and $\mathbf{v}_{h,r}^{\text{opt}} = \mathbf{v}_h^{\text{opt}}$ and (4.8) and (4.9) become equivalent. In the next section, we will come to see that identity (4.9) will be far more useful than (4.8) in our analysis.

Proof of Theorem 4.2. Assumption 1 guarantees existence of the solutions to (4.1)–(4.4). Assumptions 1 and 4 guarantee existence and uniqueness of solutions to (4.5) and (4.6). Therefore, both expressions (4.8) and (4.9) are well-defined.

To prove (4.8), observe that $g(\mathbf{u}) = a(\mathbf{u}^\star, \mathbf{u}) = a(\mathbf{u}, \boldsymbol{\omega}^\star)$ for all $\mathbf{u} \in \mathcal{U}$. Meanwhile, as a consequence of Galerkin orthogonality in (3.14) —namely, $a(\mathbf{u}^\star - \mathbf{u}_h^{\mathrm{opt}}, \mathbf{u}_h) = 0$, for all $\mathbf{u}_h \in \mathcal{U}_h$ —it holds that

$$g(\mathbf{u}^{\star} - \mathbf{u}_h^{\mathrm{opt}}) = a(\mathbf{u}^{\star} - \mathbf{u}_h^{\mathrm{opt}}, \boldsymbol{\omega}^{\star}) = a(\mathbf{u}^{\star} - \mathbf{u}_h^{\mathrm{opt}}, \boldsymbol{\omega}^{\star} - \mathbf{u}_h), \quad \forall \, \mathbf{u}_h \in \mathcal{U}_h.$$

Setting $\mathfrak{u}_h = \omega_h^{\mathrm{opt}}$ delivers the leftmost equality in (4.8). Likewise, note that

$$f(\boldsymbol{\omega}^{\star} - \boldsymbol{\omega}_h^{\mathrm{opt}}) = a(\boldsymbol{\mathfrak{u}}^{\star}, \boldsymbol{\omega}^{\star} - \boldsymbol{\omega}_h^{\mathrm{opt}}) = a(\boldsymbol{\mathfrak{u}}^{\star} - \boldsymbol{\mathfrak{u}}_h, \boldsymbol{\omega}^{\star} - \boldsymbol{\omega}_h^{\mathrm{opt}}) \,, \quad \forall \, \boldsymbol{\mathfrak{u}}_h \in \mathcal{U}_h \,.$$

Setting $u_h = u_h^{\text{opt}}$ completes (4.8).

The proof we present of (4.9) is slightly more subtle and relies upon the fact that $\psi^* = 0$ (see Theorem 4.1). We proceed by defining the bilinear form from the mixed problems above:

$$a((\mathfrak{u}, \psi), (\omega, \mathfrak{v})) = (\psi, \mathfrak{v})_{\mathcal{V}} - b(\omega, \psi) + b(\mathfrak{u}, \mathfrak{v}), \quad \forall (\mathfrak{u}, \psi), (\omega, \mathfrak{v}) \in \mathcal{U} \times \mathcal{V}.$$

Now, by Galerkin orthogonality,

$$\begin{split} g(\boldsymbol{\mathfrak{u}}^{\star} - \boldsymbol{\mathfrak{u}}_{h,r}^{\mathrm{opt}}) &= \boldsymbol{a} \big((\boldsymbol{\mathfrak{u}}^{\star} - \boldsymbol{\mathfrak{u}}_{h,r}^{\mathrm{opt}}, \boldsymbol{\psi}^{\star} - \boldsymbol{\psi}_{h,r}^{\mathrm{opt}}), (\boldsymbol{\omega}^{\star}, \boldsymbol{\mathfrak{v}}^{\star}) \big) \\ &= \boldsymbol{a} \big((\boldsymbol{\mathfrak{u}}^{\star} - \boldsymbol{\mathfrak{u}}_{h,r}^{\mathrm{opt}}, \boldsymbol{\psi}^{\star} - \boldsymbol{\psi}_{h,r}^{\mathrm{opt}}), (\boldsymbol{\omega}^{\star} - \boldsymbol{\omega}_{h,r}^{\mathrm{opt}}, \boldsymbol{\mathfrak{v}}^{\star} - \boldsymbol{\mathfrak{v}}_{h,r}^{\mathrm{opt}}) \big) \\ &= \boldsymbol{a} \big((\boldsymbol{\mathfrak{u}}^{\star} - \boldsymbol{\mathfrak{u}}_{h,r}^{\mathrm{opt}}, \boldsymbol{\psi}^{\star}), (\boldsymbol{\omega}^{\star} - \boldsymbol{\omega}_{h,r}^{\mathrm{opt}}, \boldsymbol{\mathfrak{v}}^{\star} - \boldsymbol{\mathfrak{v}}_{h,r}^{\mathrm{opt}}) \big) \\ &= \boldsymbol{b} \big(\boldsymbol{\mathfrak{u}}^{\star} - \boldsymbol{\mathfrak{u}}_{h,r}^{\mathrm{opt}}, \boldsymbol{\mathfrak{v}}^{\star} - \boldsymbol{\mathfrak{v}}_{h,r}^{\mathrm{opt}} \big) \\ &= b \big(\boldsymbol{\mathfrak{u}}^{\star} - \boldsymbol{\mathfrak{u}}_{h,r}^{\mathrm{opt}}, \boldsymbol{\mathfrak{v}}^{\star} - \boldsymbol{\mathfrak{v}}_{h,r}^{\mathrm{opt}} \big) \\ &= b \big(\boldsymbol{\mathfrak{u}}^{\star} - \boldsymbol{\mathfrak{u}}_{h,r}^{\mathrm{opt}}, \boldsymbol{\mathfrak{v}}^{\star} - \boldsymbol{\mathfrak{v}}_{h,r}^{\mathrm{opt}} \big) \\ &= b \big(\boldsymbol{\mathfrak{u}}^{\star} - \boldsymbol{\mathfrak{u}}_{h,r}^{\mathrm{opt}}, \boldsymbol{\mathfrak{v}}^{\star} - \boldsymbol{\mathfrak{v}}_{h,r}^{\mathrm{opt}} \big) \\ &= b \big(\boldsymbol{\mathfrak{u}}^{\star} - \boldsymbol{\mathfrak{u}}_{h,r}^{\mathrm{opt}}, \boldsymbol{\mathfrak{v}}^{\star} - \boldsymbol{\mathfrak{v}}_{h,r}^{\mathrm{opt}} \big) \\ &= b \big(\boldsymbol{\mathfrak{u}}^{\star} - \boldsymbol{\mathfrak{u}}_{h,r}^{\mathrm{opt}}, \boldsymbol{\mathfrak{v}}^{\star} - \boldsymbol{\mathfrak{v}}_{h,r}^{\mathrm{opt}} \big) \\ &= b \big(\boldsymbol{\mathfrak{u}}^{\star} - \boldsymbol{\mathfrak{u}}_{h,r}^{\mathrm{opt}}, \boldsymbol{\mathfrak{v}}^{\star} - \boldsymbol{\mathfrak{v}}_{h,r}^{\mathrm{opt}} \big) \\ &= b \big(\boldsymbol{\mathfrak{u}}^{\star} - \boldsymbol{\mathfrak{u}}_{h,r}^{\mathrm{opt}}, \boldsymbol{\mathfrak{v}}^{\star} - \boldsymbol{\mathfrak{v}}_{h,r}^{\mathrm{opt}} \big) \\ &= b \big(\boldsymbol{\mathfrak{u}}^{\star} - \boldsymbol{\mathfrak{u}}_{h,r}^{\mathrm{opt}}, \boldsymbol{\mathfrak{v}}^{\star} - \boldsymbol{\mathfrak{v}}_{h,r}^{\mathrm{opt}} \big) \\ &= b \big(\boldsymbol{\mathfrak{u}}^{\star} - \boldsymbol{\mathfrak{u}}_{h,r}^{\mathrm{opt}}, \boldsymbol{\mathfrak{v}}^{\star} - \boldsymbol{\mathfrak{v}}_{h,r}^{\mathrm{opt}} \big) \\ &= b \big(\boldsymbol{\mathfrak{u}}^{\star} - \boldsymbol{\mathfrak{u}}_{h,r}^{\mathrm{opt}}, \boldsymbol{\mathfrak{v}}^{\star} - \boldsymbol{\mathfrak{v}}_{h,r}^{\mathrm{opt}} \big) \\ &= b \big(\boldsymbol{\mathfrak{u}}^{\star} - \boldsymbol{\mathfrak{u}}_{h,r}^{\mathrm{opt}}, \boldsymbol{\mathfrak{v}}^{\star} - \boldsymbol{\mathfrak{v}}_{h,r}^{\mathrm{opt}} \big) \\ &= b \big(\boldsymbol{\mathfrak{u}}^{\star} - \boldsymbol{\mathfrak{u}}_{h,r}^{\mathrm{opt}}, \boldsymbol{\mathfrak{u}}^{\star} - \boldsymbol{\mathfrak{u}}_{h,r}^{\mathrm{opt}} \big) \\ &= b \big(\boldsymbol{\mathfrak{u}}^{\star} - \boldsymbol{\mathfrak{u}}_{h,r}^{\mathrm{opt}}, \boldsymbol{\mathfrak{u}}^{\star} - \boldsymbol{\mathfrak{u}}_{h,r}^{\mathrm{opt}} \big) \\ &= b \big(\boldsymbol{\mathfrak{u}}^{\star} - \boldsymbol{\mathfrak{u}}_{h,r}^{\mathrm{opt}}, \boldsymbol{\mathfrak{u}}^{\star} - \boldsymbol{\mathfrak{u}}_{h,r}^{\mathrm{opt}} \big) \\ &= b \big(\boldsymbol{\mathfrak{u}}^{\star} -$$

Here, we have used Galerkin orthogonality in the primal problem and then Galerkin orthogonality in the dual problem. Similarly,

$$\begin{split} \ell(\boldsymbol{\mathfrak{v}}^{\star} - \boldsymbol{\mathfrak{v}}_{h,r}^{\mathrm{opt}}) &= \boldsymbol{a} \big((\boldsymbol{\mathfrak{u}}^{\star}, \boldsymbol{\psi}^{\star}), (\boldsymbol{\omega}^{\star} - \boldsymbol{\omega}_{h,r}^{\mathrm{opt}}, \boldsymbol{\mathfrak{v}}^{\star} - \boldsymbol{\mathfrak{v}}_{h,r}^{\mathrm{opt}}) \big) \\ &= \boldsymbol{a} \big((\boldsymbol{\mathfrak{u}}^{\star} - \boldsymbol{\mathfrak{u}}_{h,r}^{\mathrm{opt}}, \boldsymbol{\psi}^{\star}), (\boldsymbol{\omega}^{\star} - \boldsymbol{\omega}_{h,r}^{\mathrm{opt}}, \boldsymbol{\mathfrak{v}}^{\star} - \boldsymbol{\mathfrak{v}}_{h,r}^{\mathrm{opt}}) \big) \\ &= b(\boldsymbol{\mathfrak{u}}^{\star} - \boldsymbol{\mathfrak{u}}_{h,r}^{\mathrm{opt}}, \boldsymbol{\mathfrak{v}}^{\star} - \boldsymbol{\mathfrak{v}}_{h,r}^{\mathrm{opt}}) \\ &= b(\boldsymbol{\mathfrak{u}}^{\star} - \boldsymbol{\mathfrak{u}}_{h,r}^{\mathrm{opt}}, \boldsymbol{\mathfrak{v}}^{\star} - \boldsymbol{\mathfrak{v}}_{h,r}^{\mathrm{opt}}) \end{split} \qquad \text{(Galerkin orthogonality)}$$

5. Crude upper bounds on the QoI error

5.1. A comparison of crude upper bounds. Reflect upon Theorem 4.2. For the *idealized* problems (3.2) and (3.5) (equivalently, (4.1) and (4.2)), one may simply use (4.8) to bound the error in the QoI by the product of two errors in the energy norm:

$$(5.1) |g(\mathbf{u}^{\star}) - g(\mathbf{u}_h^{\text{opt}})| = |a(\mathbf{u}^{\star} - \mathbf{u}_h^{\text{opt}}, \boldsymbol{\omega}^{\star} - \boldsymbol{\omega}_h^{\text{opt}})| \le ||\mathbf{u}^{\star} - \mathbf{u}_h^{\text{opt}}||_{\mathcal{H}} ||\boldsymbol{\omega}^{\star} - \boldsymbol{\omega}_h^{\text{opt}}||_{\mathcal{H}}.$$

Alternatively, with *practical* DLS methods (4.1) and (4.2), the QoI error can be bounded with the energy norm and the corresponding test norm:

$$(5.2) |g(\mathbf{u}^{\star}) - g(\mathbf{u}_{h,r}^{\text{opt}})| = |b(\mathbf{u}^{\star} - \mathbf{u}_{h,r}^{\text{opt}}, \mathbf{v}^{\star} - \mathbf{v}_{h,r}^{\text{opt}})| \le ||\mathbf{u}^{\star} - \mathbf{u}_{h,r}^{\text{opt}}||_{\mathcal{U}} ||\mathbf{v}^{\star} - \mathbf{v}_{h,r}^{\text{opt}}||_{\mathcal{V}}.$$

Recalling (3.19) and (3.8), similar bounds can also be made with the trial norm and the corresponding optimal test norm:

$$(5.3) |g(\mathbf{u}^{\star}) - g(\mathbf{u}_{h,r}^{\text{opt}})| \leq \|\mathbf{u}^{\star} - \mathbf{u}_{h,r}^{\text{opt}}\|_{\mathcal{U}} \|\mathbf{v}^{\star} - \mathbf{v}_{h,r}^{\text{opt}}\|_{\mathcal{V}} \leq \gamma^{-1} \|\mathbf{u}^{\star} - \mathbf{u}_{h,r}^{\text{opt}}\|_{\mathcal{U}} \|\mathbf{v}^{\star} - \mathbf{v}_{h,r}^{\text{opt}}\|_{\mathcal{V}}.$$

The simplicity of (5.2) and (5.3) is actually surprising when compared with analogous upper bounds for other mixed methods [56]. Notably, these bounds do not involve the auxiliary functions $\psi_{h,r}^{\text{opt}}$ and $\omega_{h,r}^{\text{opt}}$. The algorithms in the next section will be motivated by some form of these inequalities. Nevertheless, we note that for some idealized minimum residual methods, like first-order system least squares (FOSLS) methods [19], inequality (5.1) is more natural and useful.

5.2. **Bounding the QoI error by residuals.** In Section 3.6, it was demonstrated that the energy error in the primal problem is precisely the norm of the primal problem residual. Indeed, $\|\mathbf{u}^* - \mathbf{u}_h\|_{\mathcal{U}} = \|\mathcal{B}\mathbf{u}_h - \ell\|_{\mathcal{V}}$, for all $\mathbf{u}_h \in \mathcal{U}_h$. The main purpose of this section is to likewise relate the error in a DLS* problem to the norm of the dual residual in the general setting where $\mathcal{B}: \mathcal{U} \to \mathcal{V}'$ is not surjective. Now, if Assumption 2 holds along with continuity of \mathcal{B} (3.6), then $\|\|\mathbf{v}^* - \mathbf{v}_r\|\|_{\mathcal{V}} = \|\mathcal{B}'\mathbf{v}_r - g\|_{\mathcal{U}'}$, for all $\mathbf{v}_r \in \mathcal{V}_r$. This was demonstrated in Section 3.6. It remains to derive the corresponding relationship when Assumption 2 does not hold.

Once this is done, the upper bounds given above can be used to formulate a new bound on the QoI error using only residuals of the two solutions. Residuals of the solutions will be frequently used later on, especially in Sections 7–10, in order to motivate and construct a posteriori error estimators and refinement indicators.

The main theorem of this section is the following.

Theorem 5.1 (General upper bound on the QoI error). *In the setting of Theorem 4.2*,

$$(5.4) |g(\mathbf{u}^{\star}) - g(\mathbf{u}_{h,r}^{\text{opt}})| \leq \|\mathcal{B}\mathbf{u}_{h,r}^{\text{opt}} - \ell\|_{\mathcal{V}'} \|\mathcal{B}'\mathbf{v}_{h,r}^{\text{opt}} - g\|_{\mathcal{U}'} \leq \gamma^{-1} \|\mathcal{B}\mathbf{u}_{h,r}^{\text{opt}} - \ell\|_{\mathcal{V}'} \|\mathcal{B}'\mathbf{v}_{h,r}^{\text{opt}} - g\|_{\mathcal{U}'}.$$

The proof of Theorem 5.1 is nearly immediate, once following lemma is established.

Lemma 5.2. Let Assumption 1 hold. Let $g \in \mathcal{U}'$ and let $(\boldsymbol{\omega}^{\star}, \boldsymbol{v}^{\star}) \in \mathcal{U} \times \mathcal{V}$ be the unique solution of (4.4). Define $\mathcal{V}_0 = \operatorname{Null}(\mathcal{B}')$. Then

$$\|\mathbf{v}^{\star} - \mathbf{v}\|_{\mathcal{V}}^{2} = \|\mathcal{P}_{\mathcal{V}_{0}}\mathbf{v}\|_{\mathcal{V}}^{2} + \|\mathcal{B}'\mathbf{v} - g\|_{\mathcal{U}'}^{2}, \quad \forall \, \mathbf{v} \in \mathcal{V}.$$

Proof. Define $V_1 = V_0^{\perp}$. By the Closed Range Theorem, observe that $V_1' = \text{Range}(\mathcal{B})$ and both V_0 and V_1 are closed. Therefore,

$$\sup_{\widetilde{\mathbf{v}}_1 \in \mathcal{V}_1} \frac{(\mathbf{v}^* - \mathbf{v}, \widetilde{\mathbf{v}}_1)_{\mathcal{V}}}{\|\widetilde{\mathbf{v}}_1\|_{\mathcal{V}}} = \sup_{\mathbf{u} \in \mathcal{U}} \frac{(\mathbf{v}^* - \mathbf{v}, \mathcal{R}_{\mathcal{V}}^{-1} \mathcal{B} \mathbf{u})_{\mathcal{V}}}{\|\mathcal{R}_{\mathcal{V}}^{-1} \mathcal{B} \mathbf{u}\|_{\mathcal{V}}} = \sup_{\mathbf{u} \in \mathcal{U}} \frac{\langle \mathbf{v}^* - \mathbf{v}, \mathcal{B} \mathbf{u} \rangle}{\|\mathcal{B} \mathbf{u}\|_{\mathcal{V}'}} = \|\mathcal{B}' \mathbf{v} - g\|_{\mathcal{U}'}.$$

Now, if $\mathcal{V}_0 = \{0\}$, then $\mathcal{V}_1 = \mathcal{V}$ and we are done.

Assume that $V_0 \neq \{0\}$ is non-trivial and recall Lemma 3.1. Observe that

$$\|\boldsymbol{\mathfrak{v}}^{\star}-\boldsymbol{\mathfrak{v}}\|_{\mathcal{V}}^{2}=\left(\sup_{\widetilde{\boldsymbol{\mathfrak{v}}}\in\mathcal{V}}\frac{(\boldsymbol{\mathfrak{v}}^{\star}-\boldsymbol{\mathfrak{v}},\widetilde{\boldsymbol{\mathfrak{v}}})_{\mathcal{V}}}{\|\widetilde{\boldsymbol{\mathfrak{v}}}\|_{\mathcal{V}}}\right)^{2}=\left(\sup_{\widetilde{\boldsymbol{\mathfrak{v}}}_{0}\in\mathcal{V}_{0}}\frac{(\boldsymbol{\mathfrak{v}}^{\star}-\boldsymbol{\mathfrak{v}},\widetilde{\boldsymbol{\mathfrak{v}}}_{0})_{\mathcal{V}}}{\|\widetilde{\boldsymbol{\mathfrak{v}}}_{0}\|_{\mathcal{V}}}\right)^{2}+\left(\sup_{\widetilde{\boldsymbol{\mathfrak{v}}}_{1}\in\mathcal{V}_{1}}\frac{(\boldsymbol{\mathfrak{v}}^{\star}-\boldsymbol{\mathfrak{v}},\widetilde{\boldsymbol{\mathfrak{v}}}_{1})_{\mathcal{V}}}{\|\widetilde{\boldsymbol{\mathfrak{v}}}_{1}\|_{\mathcal{V}}}\right)^{2}.$$

By Theorem 4.1, $\mathbf{v}^* \in \mathcal{V}_1$. Therefore, the first term on the right-hand side is just equal to $\|\mathcal{P}_{\mathcal{V}_0}\mathbf{v}\|_{\mathcal{V}}^2$.

Proof of Theorem 5.1. Observe that $b(\mathbf{u}^* - \mathbf{u}_{h,r}^{\text{opt}}, \mathbf{v}_0) = 0$, for all $\mathbf{v}_0 \in \mathcal{V}_0 = \text{Null}(\mathcal{B}')$. Therefore, by Theorem 4.2.

$$|g(\mathfrak{u}^{\star}) - g(\mathfrak{u}_{h,r}^{\text{opt}})| = |b(\mathfrak{u}^{\star} - \mathfrak{u}_{h,r}^{\text{opt}}, \mathfrak{v}^{\star} - (\mathfrak{v}_{h,r}^{\text{opt}} - \mathfrak{v}_{0}))| \leq \|\mathfrak{u}^{\star} - \mathfrak{u}_{h,r}^{\text{opt}}\|_{\mathcal{U}} \|\mathfrak{v}^{\star} - (\mathfrak{v}_{h,r}^{\text{opt}} - \mathfrak{v}_{0})\|_{\mathcal{V}},$$

for all $\mathbf{v}_0 \in \mathcal{V}_0$. Invoking (5.5), observe that

$$|g(\mathbf{u}^{\star}) - g(\mathbf{u}_{h,r}^{\text{opt}})| \leq \|\mathcal{B}\mathbf{u}_{h,r}^{\text{opt}} - \ell\|_{\mathcal{V}'} (\|\mathcal{P}_{\mathcal{V}_0}\mathbf{v}_{h,r}^{\text{opt}} - \mathbf{v}_0\|_{\mathcal{V}}^2 + \|\mathcal{B}'\mathbf{v}_{h,r}^{\text{opt}} - g\|_{\mathcal{U}'}^2)^{1/2}, \quad \forall \, \mathbf{v}_0 \in \mathcal{V}_0.$$

Here, setting $\mathbf{v}_0 = \mathcal{P}_{\mathcal{V}_0} \mathbf{v}_{h,r}^{\text{opt}}$ delivers the required result.

6. GOAL-ORIENTED ADAPTIVE MESH REFINEMENT ALGORITHMS

In the literature, there are goal-oriented adaptive mesh refinement (GMR) strategies for elliptic PDEs that can be proven to be optimally convergent [35, 45, 52]. At each refinement step, such GMR strategies are designed to minimize an upper bound on the error in the QoI similar to (5.4). Likewise, it is this upper bound which is proven to decrease at an optimal rate with each mesh refinement, at least asymptotically. Notably, in many circumstances, the upper bound can actually be a very crude approximation of the true error.

The authors of the present manuscript are not aware of similar proofs of optimal convergence for non-coercive problems. Consequently, because we are dealing with mixed methods—albeit, very special mixed methods—we cannot simply rely on existing GMR literature to conclude optimal convergence rates with our adaptive algorithms. Our intentions are not to develop such a theory here so, therefore, a careful treatment of this issue awaits a follow-up study.

It is remarkable to note that, without a rigorous mathematical explanation, exceptional convergence rates in QoI error are routinely demonstrated with algorithms falling far outside the context of [35,52]. Notable examples include [2, 19, 43, 57]. For this reason, without the ability to rely upon a rigorous mathematical justification, we chose our GMR algorithms in analogy to one of the most simple—yet, also usually very successful—strategies in the literature [1,61].

In order to properly introduce our specific approach, it is necessary to feature it in the context of other established adaptive mesh refinement (AMR) algorithms for finite element analysis. A brief summary of this is given, presently.

6.1. **Refinement indicators and adaptive mesh refinement algorithms.** In the context of finite element analysis, the most pervasive strategy for AMR can be described by the following loop [32, 34]:

```
... solve; estimate; mark; refine; ...
```

Normally, at the first stage of the "estimate" step, a special dedicated estimate of the global error is computed. If this estimate is below a specific tolerance, the loop is broken. Otherwise, it continues until ample time or computational resources have been consumed. Usually, this global *a posteriori* error estimate, η_{QoI} , comes in the form of dedicated upper and, sometimes, lower bounds [51, 59]. We will forgo the global error estimate feature of a complete AMR strategy and leave the analysis of this ingredient for a future study.

Recall Theorem 5.1:

$$|g(\mathbf{u}^{\star}) - g(\mathbf{u}_{h,r}^{\text{opt}})| \leq \|\mathcal{B}\mathbf{u}_{h,r}^{\text{opt}} - \ell\|_{\mathcal{V}'} \|\mathcal{B}'\mathbf{v}_{h,r}^{\text{opt}} - g\|_{\mathcal{U}'}.$$

In this manuscript, GMR will involve the following repeated sequence of actions common to AMR: (1) compute the approximate solutions $\mathbf{u}_{h,r}^{\text{opt}}$ and $\mathbf{v}_{h,r}^{\text{opt}}$; (2) construct computable and reliable a posteriori error estimators

$$(6.1) \qquad \qquad \|\mathcal{B}\mathbf{u}_{h,r}^{\mathrm{opt}} - \ell\|_{\mathcal{V}'} \approx \eta(\mathbf{u}_{h,r}^{\mathrm{opt}}) \qquad \text{and} \qquad \|\mathcal{B}'\mathbf{v}_{h,r}^{\mathrm{opt}} - g\|_{\mathcal{U}'} \approx \eta^*(\mathbf{v}_{h,r}^{\mathrm{opt}});$$

(3) decompose the error estimators $\eta(\mathbf{u}_{h,r}^{\text{opt}})$ and $\eta^*(\mathbf{v}_{h,r}^{\text{opt}})$ into element-wise components, called *refinement indicators*,

$$\eta(\mathbf{u}_{h,r}^{\mathrm{opt}})^2 = \sum_{K \in \mathcal{T}} (\eta_{\scriptscriptstyle{K}})^2 \qquad \text{and} \qquad \eta^*\!(\mathbf{v}_{h,r}^{\mathrm{opt}}) = \sum_{K \in \mathcal{T}} (\eta_{\scriptscriptstyle{K}}^*)^2\,;$$

(4) mark suitable elements for refinement using a marking convention influenced by contributions of both sets of refinement indicators $\{\eta_{\kappa}\}_{K\in\mathcal{T}}$ and $\{\eta_{\kappa}^*\}_{K\in\mathcal{T}}$; (5) refine all marked elements with the intention of driving the upper bound (5.4) to zero with an exceptional rate.

The general AMR strategy above is summarized in Algorithm 1. In this manuscript, the only difference between GMR and solution-adaptive mesh refinement (SMR), which has usually driven DPG AMR in the past, will be in the marking strategy (step (4)).

Note that the product $\eta(\mathbf{u}_{h,r}^{\text{opt}}) \cdot \eta^*(\mathbf{v}_{h,r}^{\text{opt}})$ could be used for the global error estimate η_{QoI} . However, in many scenarios, this can be such an unpredictably poor overestimate of the true global error, it would be inefficient to formulate a stopping criterion based on it alone.

Algorithm 1 Adaptive mesh refinement

Input: initial mesh \mathcal{T} , marking strategy, tolerance $\eta_{\text{tol.}}$.

loop

- (1) Solve for $\mathfrak{u}_{h,r}^{\mathrm{opt}}$ and $\mathfrak{v}_{h,r}^{\mathrm{opt}}$ on \mathcal{T} .
- (2) Compute global error estimate η_{QoI} .

if $\eta_{\mathrm{QoI}} < \eta_{\mathrm{tol.}}$ then

break

- (3) Compute the two sets of refinement indicators $\{\eta_{\kappa}\}_{\kappa\in\mathcal{T}}$ and $\{\eta_{\kappa}^*\}_{\kappa\in\mathcal{T}}$.
- (4) Mark elements for refinement $\mathcal{M} \subseteq \mathcal{T}$, as dictated by *the marking strategy*.
- (5) Refine all marked elements $K \in \mathcal{M}$ and construct new mesh \mathcal{T} .

return acceptably accurate solution $\mathfrak{u}_{h,r}^{\text{opt}}$ and QoI $g(\mathfrak{u}_{h,r}^{\text{opt}})$.

At step (5) of Algorithm 1, we assume that a minimal set of additional elements are also refined, beyond the set of marked elements $\mathcal{M} \subseteq \mathcal{T}$, to ensure that the new mesh has only one level of hanging nodes. Under this assumption, the freedom to construct refinement indicators $\{\eta_K\}_{K\in\mathcal{T}}$ and $\{\eta_K^*\}_{K\in\mathcal{T}}$ as well as the choice of marking strategy are the largest sources of flexibility in GMR.

We will consider only one class of refinement indicators for the DPG problem $\{\eta_K\}_{K\in\mathcal{T}}$, presented in Section 7. This class coincides with the same well-established, standard energy norm refinement indicators that have been used for SMR in many previous DPG studies [13,17,29,36,48,62,68]. Alternatively, we will consider

three different classes of refinement indicators $\{\eta_K^*\}_{K\in\mathcal{T}}$ for the DPG* problem. These are each presented, in sequence, in Sections 8–10. The specific AMR marking strategies are discussed in the next subsection.

Remark 6.1. Note that Algorithm 1 permits the computation of the primal and dual solutions, $\mathbf{u}_{h,r}^{\mathrm{opt}}$ and $\mathbf{v}_{h,r}^{\mathrm{opt}}$, on the same mesh, with the same polynomial order. This is contrary to other established techniques which require the solution of the dual problem on a finer trial space [19, 43]. Often, this space $\mathcal{U}_H \supseteq \mathcal{U}_h$ is obtained by a global enrichment or refinement of the given trial space \mathcal{U}_h . For the category of GMR algorithms which we have considered, it is easy to demonstrate—at least in the coercive setting—that no additional accuracy bounding the QoI error is achieved by using different nested spaces, as opposed to just simply using the finer space \mathcal{U}_H for both problems [52, Remark 5.1].

6.2. **Marking strategies.** Marking strategies are the primary distinguishing factor in many AMR algorithms [6, 32, 35, 52]. In our experience, the so-called "greedy" strategy is usually very competitive with—and sometimes even outperforms—more complicated Dörfler-influenced marking strategies. Since we have forgone mathematical proof of the optimality of our GMR algorithms, we present only two naive greedy marking strategies, featured below. We have performed experiments with more elaborate SMR and GMR marking strategies, but witnessed only marginal difference in the results.

SMR marking strategy Naive (greedy) energy-based marking strategy

Input: Refinement parameter $0 < \theta < 1$, set of refinement indicators $\{\eta_K\}_{K \in \mathcal{T}}$. Calculate

$$\eta_{\max} = \max_{K \in \mathcal{T}} \, \eta_K \,.$$

Mark all elements $K \in \mathcal{T}$ such that

$$\theta \, \eta_{\max} \leq \eta_K$$
.

GMR marking strategy Naive (greedy) goal-oriented marking strategy

Input: Refinement parameter $0 < \theta < 1$, sets of refinement indicators $\{\eta_K\}_{K \in \mathcal{T}}$ and $\{\eta_K^*\}_{K \in \mathcal{T}}$. Calculate

$$\eta_{\max} = \max_{K \in \mathcal{T}} \eta_K \eta_K^*.$$

Mark all elements $K \in \mathcal{T}$ such that

$$\theta \, \eta_{\max} \leq \eta_K \eta_K^*$$
.

The SMR strategy above is presently the predominant marking strategy for SMR in DPG studies so it is an appropriate reference strategy for comparison. Note that this solution error oriented marking strategy does not require any DPG* refinement indicators and so the DPG* problem need not be solved at all when using it.

For GMR, we will keep the marking strategy described above, fixed. Here, Algorithm 1, paired with the GMR marking strategy above, will be distinguished by the particular DPG* refinement indicator used. Specifically, we consider the following GMR algorithms: the *explicit* GMR algorithm, using $\{\eta_K^{*,\text{expl}}\}_{K\in\mathcal{T}}$ presented in Section 8; the *implicit* GMR algorithm, using $\{\eta_K^{*,\text{impl}}\}_{K\in\mathcal{T}}$ presented in Section 9; and the *ad-hoc* GMR algorithm, using $\{\eta_K^{*,\text{a.h.}}\}_{K\in\mathcal{T}}$ presented in Section 10.

7. A POSTERIORI ERROR ESTIMATION FOR DPG METHODS

Recall (6.1). In this section, we consider a specific well-studied implicit error estimator for the term

$$\|\|\boldsymbol{\mathfrak{u}}^{\star}-\boldsymbol{\mathfrak{u}}_{h,r}^{\mathrm{opt}}\|_{\mathcal{U}}=\|\boldsymbol{\mathfrak{B}}\boldsymbol{\mathfrak{u}}_{h,r}^{\mathrm{opt}}-\ell\|_{\boldsymbol{\mathcal{V}}'}$$

in (5.4). Namely, we consider $\eta(\mathfrak{u}_{h,r}^{\mathrm{opt}})=\eta_r(\mathfrak{u}_{h,r}^{\mathrm{opt}}),$ where

$$\eta_r(\mathfrak{u}) = \sup_{\mathfrak{v}_r \in \mathcal{V}_r} \frac{b(\mathfrak{u},\mathfrak{v}_r) - \ell(\mathfrak{v}_r)}{\|\mathfrak{v}_r\|_{\mathcal{V}}} \,, \quad \forall \, \mathfrak{u} \in \mathcal{U} \,.$$

From now on, we will also denote this error estimator simply as $\eta_r(\mathfrak{u}) = \|\mathfrak{B}\mathfrak{u} - \ell\|_{\mathcal{V}_x^{\prime}}$.

7.1. **Implicit error estimation with DPG.** Let Assumption 3 hold for \mathcal{V} and the subspace $\mathcal{V}_r \subseteq \mathcal{V}$. Specifically, recall that in a DPG method $\mathcal{V} = \bigoplus_{K \in \mathcal{T}} \mathcal{V}_K$ and $\mathcal{V}_r = \bigoplus_{K \in \mathcal{T}} \mathcal{V}_{K,r}$, where $\mathcal{V}_{K,r} \subseteq \mathcal{V}_K$, for all $K \in \mathcal{T}$. Then, as a consequence of Lemma 3.1,

$$\eta_r(\mathbf{u})^2 = \sum_{K \in \mathcal{T}} \| \mathcal{B} \mathbf{u} - \ell \|_{\mathcal{V}'_{K,r}}^2.$$

Define $\eta_K = \|\mathfrak{B}\mathfrak{u}_{h,r}^{\mathrm{opt}} - \ell\|_{\mathcal{V}_{K,r}'}$, for each $K \in \mathcal{T}$, and construct $\{\eta_K\}_{K \in \mathcal{T}}$. If \mathcal{V} is localizable, then each η_K can be computed locally [63]. This is the most frequently used set of refinement indicators in AMR with DPG methods. As mentioned previously, in many DPG studies, SMR was driven solely by use of this refinement indicator and the SMR marking strategy in Section 6.2.

Recall (3.8) and note the following equivalence between the energy norm error and the trial norm error:

$$\gamma \| \mathbf{u}^{\star} - \mathbf{u}_{h,r}^{\text{opt}} \|_{\mathcal{U}} \leq \| \mathbf{u}^{\star} - \mathbf{u}_{h,r}^{\text{opt}} \|_{\mathcal{U}} \leq M \| \mathbf{u}^{\star} - \mathbf{u}_{h,r}^{\text{opt}} \|_{\mathcal{U}}$$

Since $\|\mathbf{u}^{\star} - \mathbf{u}_{h,r}^{\text{opt}}\|_{\mathcal{U}} \approx \|\mathcal{B}\mathbf{u}_{h,r}^{\text{opt}} - \ell\|_{\mathcal{V}'}$, if $\eta_r(\mathbf{u}_{h,r}^{\text{opt}}) \approx \|\mathcal{B}\mathbf{u}_{h,r}^{\text{opt}} - \ell\|_{\mathcal{V}'}$, then $\|\mathbf{u}^{\star} - \mathbf{u}_{h,r}^{\text{opt}}\|_{\mathcal{U}}$ scales with the solution error.

Indeed, in Theorem 7.4, this is demonstrated, up to an unavoidable truncation error in the the load ℓ . Therefore, solely relying upon $\{\eta_K\}_{K\in\mathcal{T}}$ during marking is natural if the purpose is to minimize the solution error $\|\mathbf{u}^* - \mathbf{u}_{h,r}^{\text{opt}}\|_{\mathcal{U}}$ at each refinement step. In this case, it is desirable to choose a test norm $\|\cdot\|_{\mathcal{V}}$ such that the corresponding constants γ and M are as close as possible to unity. Simply using the graph norm (3.24) is sufficient in many circumstances.

7.2. **Discrete subspaces.** Recall Theorem 4.1. Specifically, $\psi^* = 0$. Therefore,

$$\|\mathbf{u}^{\star} - \mathbf{u}_h^{\text{opt}}\|_{\mathcal{H}} = \|\mathcal{B}(\mathbf{u}^{\star} - \mathbf{u}_h^{\text{opt}})\|_{\mathcal{V}'} = \|\boldsymbol{\psi}_h^{\text{opt}}\|_{\mathcal{V}}.$$

When $\mathfrak{u}_h^{\mathrm{opt}}$ is replaced by $\mathfrak{u}_{h,r}^{\mathrm{opt}}$ and ψ_h^{opt} is replaced by $\psi_{h,r}^{\mathrm{opt}}$, there is an additional term:

$$\|\|\boldsymbol{\mathfrak{u}}^{\star} - \boldsymbol{\mathfrak{u}}_{h,r}^{\mathrm{opt}}\|_{\mathcal{U}}^{2} = \|\mathcal{R}_{\mathcal{V}} \boldsymbol{\psi}_{h,r}^{\mathrm{opt}} - \mathcal{B}\boldsymbol{\mathfrak{u}}_{h} + \ell\|_{\mathcal{V}'}^{2} + \|\boldsymbol{\psi}_{h,r}^{\mathrm{opt}}\|_{\mathcal{V}}^{2}.$$

This is an immediate consequence of the following lemma.

Lemma 7.1. Let V_r be any closed subspace of V. Let Assumptions 1 and 4 hold. Let $\ell \in \text{Range}(\mathcal{B})$, $\mathbf{u}^* = \mathcal{B}^{-1}\ell$, and $\mathbf{u}_h \in \mathcal{U}_h$ be arbitrary. Define $\psi_{h,r} \in V_r$ to be the unique solution of $\langle \mathcal{R}_V \psi_{h,r}, \mathbf{v}_r \rangle = \langle \mathcal{B}\mathbf{u}_h - \ell, \mathbf{v}_r \rangle$, for all $\mathbf{v}_r \in V_r$. Then

$$\|\mathcal{B}(\mathbf{u}^{\star} - \mathbf{u}_h)\|_{\mathcal{V}'}^2 = \|\mathcal{R}_{\mathcal{V}} \boldsymbol{\psi}_{h,r} - \mathcal{B}\mathbf{u}_h + \ell\|_{\mathcal{V}'}^2 + \|\boldsymbol{\psi}_{h,r}\|_{\mathcal{V}}^2.$$

Proof. Observe that

$$\begin{split} \|\mathcal{B}(\mathbf{u}^{\star} - \mathbf{u}_{h})\|_{\mathcal{V}'}^{2} &= \|(\mathcal{R}_{\mathcal{V}} \boldsymbol{\psi}_{h,r} - \mathcal{R}_{\mathcal{V}} \boldsymbol{\psi}_{h,r}) - \mathcal{B}\mathbf{u}_{h} + \ell\|_{\mathcal{V}'}^{2} \\ &= \|\mathcal{R}_{\mathcal{V}} \boldsymbol{\psi}_{h,r} - \mathcal{B}\mathbf{u}_{h} + \ell\|_{\mathcal{V}'}^{2} - 2\langle \mathcal{R}_{\mathcal{V}} \boldsymbol{\psi}_{h,r} - \mathcal{B}\mathbf{u}_{h} + \ell, \boldsymbol{\psi}_{h,r} \rangle + \|\mathcal{R}_{\mathcal{V}} \boldsymbol{\psi}_{h,r}\|_{\mathcal{V}'}^{2} \\ &= \|\mathcal{R}_{\mathcal{V}} \boldsymbol{\psi}_{h,r} - \mathcal{B}\mathbf{u}_{h} + \ell\|_{\mathcal{V}'}^{2} + \|\boldsymbol{\psi}_{h,r}\|_{\mathcal{V}}^{2}. \end{split}$$

7.3. **Reliability and efficiency.** In this subsection, we improve on a result from [13] demonstrating reliability and efficiency of the practical *a posteriori* error estimator $\eta_r(\mathbf{u}) = \|\ell - \mathcal{B}\mathbf{u}\|_{\mathcal{V}_r'}$ when the Fortin operator Π_r is a bounded projection (see Assumption 5). In our proof, we require Theorem 7.2 and Theorem 7.3. The first of these has become reasonably well-known in the literature [67] and many different proofs can be found in [67]. The second theorem is perhaps much less well known, so we provide a proof of it in Appendix A.

Theorem 7.2 (Complementary projections). *Let* Π *be any bounded projection on a Hilbert space* W, $\Pi \circ \Pi = \Pi$. *Then*

$$\|\Pi\| = \|1 - \Pi\|$$
.

Theorem 7.3 (Pythagoras). Let W be a Hilbert space and $W_0 \subseteq W$ be a nontrivial closed subspace. Let $\mathcal{P}: \mathcal{W} \to \mathcal{W}_0$ be the orthogonal projection onto W_0 and let $\Pi: \mathcal{W} \to \mathcal{W}_0$ be any other bounded projection onto $W_0 = \Pi(\mathcal{W})$. Then

$$\|\Pi - \mathcal{P}\|^2 + 1 = \|\Pi\|^2$$
.

Theorem 7.4 (Practical a posteriori error estimates, in the trial norm, for DPG). Let Assumptions 1 and 5 hold. Let $\ell \in \text{Range}(\mathfrak{B})$, $\mathfrak{u}^* = \mathfrak{B}^{-1}\ell$, and $\mathfrak{u}_h \in \mathfrak{U}_h$ be arbitrary. Denote the best approximation of \mathfrak{u}^* in \mathfrak{U}_h as

$$\mathbf{u}_h^{\star} = \operatorname*{arg\,min}_{\mathbf{u}_h \in \mathcal{U}_h} \|\mathbf{u}^{\star} - \mathbf{u}_h\|_{\mathcal{U}}.$$

Then the computable residual $\eta_r(\mathbf{u}) = \|\ell - \mathcal{B}\mathbf{u}\|_{\mathcal{V}_r}$ and the data approximation error $\operatorname{osc}(\ell) = \|\ell \circ (1 - \Pi_r)\|_{\mathcal{V}_r}$ satisfy

(7.1)
$$\gamma^2 \|\mathbf{u}^* - \mathbf{u}_h\|_{\mathcal{U}}^2 \le \eta_r(\mathbf{u}_h)^2 + \left(\eta_r(\mathbf{u}_h)\sqrt{\|\Pi_r\|^2 - 1} + \operatorname{osc}(\ell)\right)^2.$$

(7.2)
$$\eta_r(\mathbf{u}_h) \le M \|\mathbf{u}^* - \mathbf{u}_h\|_{\mathcal{U}},$$

(7.3) and
$$\operatorname{osc}(\ell) \leq M \|\Pi_r\| \|\mathbf{u}^* - \mathbf{u}_h^*\|_{\mathcal{U}}$$
.

Replacing the trial norm $\|\cdot\|_{\mathcal{U}}$ with the energy norm $\|\cdot\|_{\mathcal{U}}$, we have the following complementary theorem. The proof of Theorem 7.5 is similar to the proof of Theorem 7.4, so it is left for the reader.

Theorem 7.5 (Practical a posteriori error estimates, in the energy norm, for DPG). Let Assumptions 1 and 5 hold. Let $\ell \in \text{Range}(\mathcal{B})$, $\mathbf{u}^* = \mathcal{B}^{-1}\ell$, and $\mathbf{u}_h \in \mathcal{U}_h$ be arbitrary. Then the computable residual $\eta_r(\mathbf{u}) = \|\ell - \mathcal{B}\mathbf{u}\|_{\mathcal{V}'_r}$ and the data approximation error $\operatorname{osc}(\ell) = \|\ell \circ (1 - \Pi_r)\|_{\mathcal{V}'}$ satisfy

$$\begin{aligned} \|\mathbf{u}^{\star} - \mathbf{u}_h\|_{\mathcal{U}}^2 &\leq \eta_r(\mathbf{u}_h)^2 + \left(\eta_r(\mathbf{u}_h)\sqrt{\|\Pi_r\|^2 - 1} + \operatorname{osc}(\ell)\right)^2. \\ \eta_r(\mathbf{u}_h) &\leq \|\mathbf{u}^{\star} - \mathbf{u}_h\|_{\mathcal{U}}^2, \\ and & \operatorname{osc}(\ell) &\leq \|\Pi_r\| \|\|\mathbf{u}^{\star} - \mathbf{u}_h^{\operatorname{opt}}\|_{\mathcal{U}}^2. \end{aligned}$$

Remark 7.1. The reliability bound in (7.1) is a new version of that found in [13], with the additional assumption that $\Pi_r \circ \Pi_r = \Pi_r$. Note that if $\operatorname{osc}(\ell) = 0$ then

$$\gamma \| \mathbf{u}^* - \mathbf{u}_h \|_{\mathcal{U}} \leq \| \mathbf{u}^* - \mathbf{u}_h \|_{\mathcal{U}} \leq \| \Pi_r \| \eta_r(\mathbf{u}_h) .$$

Moreover, if $\|\Pi_r\|=1$ —that is, if Π_r is an orthogonal projection—then

$$\gamma^2 \|\mathbf{u}^{\star} - \mathbf{u}_h\|_{\mathcal{U}}^2 \leq \|\mathbf{u}^{\star} - \mathbf{u}_h\|_{\mathcal{U}}^2 \leq \eta_r(\mathbf{u}_h)^2 + \operatorname{osc}(\ell)^2.$$

Remark 7.2. Similar to [13, Theorem 2.1], each of the bounds above are sharp.

Proof of Theorem 7.4. To arrive at (7.2), simply observe that

$$\eta_r(\mathbf{u}_h) = \|\mathcal{B}(\mathbf{u}^* - \mathbf{u}_h)\|_{\mathcal{V}'} \le \|\mathcal{B}(\mathbf{u}^* - \mathbf{u}_h)\|_{\mathcal{V}'} \le \|\mathcal{B}\|\|\mathbf{u}^* - \mathbf{u}_h\|_{\mathcal{U}}.$$

To arrive at (7.3), first let $\mathbf{v} \in \mathcal{V}$ where $\|\mathbf{v}\| = 1$ be arbitrary. Then, by (4.7) and Galerkin orthogonality,

$$\ell(\mathbf{v} - \Pi_r \mathbf{v}) = b(\mathbf{u}^*, \mathbf{v} - \Pi_r \mathbf{v}) = b(\mathbf{u}^* - \mathbf{u}_h, \mathbf{v} - \Pi_r \mathbf{v}) \le \|\mathbf{B}\| \|\mathbf{1} - \Pi_r\| \|\mathbf{u}^* - \mathbf{u}_h\|_{\mathbf{U}},$$

for every $u_h \in \mathcal{U}_h$. The result then follows from Assumption 5 and Theorem 7.2: $||1 - \Pi_r|| = ||\Pi_r||$.

The reliability inequality is much more subtle. Begin by defining $\widetilde{\mathcal{V}}_r = \operatorname{Range}(\Pi_r) \subseteq \mathcal{V}_r$. Now, define $\widetilde{\boldsymbol{\psi}}_{h,r} \in \widetilde{\mathcal{V}}_r$ to be the unique solution of $\langle \mathcal{R}_{\mathcal{V}} \, \widetilde{\boldsymbol{\psi}}_{h,r}, \, \widetilde{\boldsymbol{v}}_r \rangle = \langle \ell - \mathcal{B} \boldsymbol{\mathfrak{u}}_h, \, \widetilde{\boldsymbol{v}}_r \rangle$, for all $\widetilde{\boldsymbol{v}}_r \in \widetilde{\mathcal{V}}_r$. Recall that $\gamma \| \boldsymbol{\mathfrak{u}} \|_{\mathcal{U}} \leq \|\mathcal{B} \boldsymbol{\mathfrak{u}}\|_{\mathcal{V}}$, for all $\boldsymbol{\mathfrak{u}} \in \mathcal{U}$, by (3.7). Then, since $\widetilde{\mathcal{V}}_r$ is a closed subspace of \mathcal{V} , note that

(7.4)
$$\gamma^{2} \|\mathbf{u}^{\star} - \mathbf{u}_{h}\|_{\mathcal{U}}^{2} \leq \|\mathcal{B}(\mathbf{u}^{\star} - \mathbf{u}_{h})\|_{\mathcal{V}'}^{2} = \|\mathcal{R}_{\mathcal{V}} \widetilde{\psi}_{h,r} + \mathcal{B}\mathbf{u}_{h} - \ell\|_{\mathcal{V}'}^{2} + \|\widetilde{\psi}_{h,r}\|_{\mathcal{V}}^{2},$$

by Lemma 7.1.

Define $\mathcal{P}_r: \mathcal{V} \to \widetilde{\mathcal{V}}_r$ to be the orthogonal projection onto the range of Π_r . Because $\widetilde{\psi}_{h,r} \in \widetilde{\mathcal{V}}_r$, note that

$$(7.5) \qquad (\widetilde{\boldsymbol{\psi}}_{h,r}, \boldsymbol{\mathfrak{v}} - \Pi_r \boldsymbol{\mathfrak{v}})_{\mathcal{V}} = (\widetilde{\boldsymbol{\psi}}_{h,r}, \mathcal{P}_r (\boldsymbol{\mathfrak{v}} - \Pi_r \boldsymbol{\mathfrak{v}}))_{\mathcal{V}} = (\widetilde{\boldsymbol{\psi}}_{h,r}, \mathcal{P}_r \boldsymbol{\mathfrak{v}} - \Pi_r \boldsymbol{\mathfrak{v}})_{\mathcal{V}}, \quad \forall \, \boldsymbol{\mathfrak{v}} \in \mathcal{V}.$$

Now, employing (4.7)—namely, $b(\mathbf{u}_h, \mathbf{v} - \Pi_r \mathbf{v}) = 0$, for all $\mathbf{v} \in \mathcal{V}$ and $\mathbf{u}_h \in \mathcal{U}_h$ —we find that

$$\|\mathcal{R}_{\mathcal{V}}\widetilde{\psi}_{h,r} + \mathcal{B}\mathbf{u}_{h} - \ell\|_{\mathcal{V}'} = \sup_{\mathbf{v}\in\mathcal{V}} \frac{(\widetilde{\psi}_{h,r}, \mathbf{v})_{\mathcal{V}} + b(\mathbf{u}_{h}, \mathbf{v}) - \ell(\mathbf{v})}{\|\mathbf{v}\|_{\mathcal{V}}}$$

$$= \sup_{\mathbf{v}\in\mathcal{V}} \frac{(\widetilde{\psi}_{h,r}, \mathbf{v} - \Pi_{r}\mathbf{v})_{\mathcal{V}} + b(\mathbf{u}_{h}, \mathbf{v} - \Pi_{r}\mathbf{v}) - \ell(\mathbf{v} - \Pi_{r}\mathbf{v})}{\|\mathbf{v}\|_{\mathcal{V}}}$$

$$= \sup_{\mathbf{v}\in\mathcal{V}} \frac{(\widetilde{\psi}_{h,r}, \mathcal{P}_{r}\mathbf{v} - \Pi_{r}\mathbf{v})_{\mathcal{V}} - \ell(\mathbf{v} - \Pi_{r}\mathbf{v})}{\|\mathbf{v}\|_{\mathcal{V}}}$$

$$\leq \|\widetilde{\psi}_{h,r}\|_{\mathcal{V}} \|\mathcal{P}_{r} - \Pi_{r}\| + \|\ell \circ (1 - \Pi_{r})\|_{\mathcal{V}'}$$

$$= \|\widetilde{\psi}_{h,r}\|_{\mathcal{V}} \sqrt{\|\Pi_{r}\|^{2} - 1} + \operatorname{osc}(\ell).$$

$$(7.6)$$

In the third line, we have used (7.5) and, in the final line, we have used Theorem 7.3. Finally, observe that

$$\|\widetilde{\boldsymbol{\psi}}_{h,r}\|_{\mathcal{V}} = \sup_{\widetilde{\boldsymbol{\mathfrak{v}}}_r \in \widetilde{\mathcal{V}}_r} \frac{b(\boldsymbol{\mathfrak{u}}, \widetilde{\boldsymbol{\mathfrak{v}}}_r) - \ell(\widetilde{\boldsymbol{\mathfrak{v}}}_r)}{\|\widetilde{\boldsymbol{\mathfrak{v}}}_r\|_{\mathcal{V}}} \leq \sup_{\boldsymbol{\mathfrak{v}}_r \in \mathcal{V}_r} \frac{b(\boldsymbol{\mathfrak{u}}, \boldsymbol{\mathfrak{v}}_r) - \ell(\boldsymbol{\mathfrak{v}}_r)}{\|\boldsymbol{\mathfrak{v}}_r\|_{\mathcal{V}}} = \eta_r(\boldsymbol{\mathfrak{u}}_h).$$

With this observation in hand, (7.4) and (7.6) deliver (7.1), as necessary.

8. Explicit error estimators for DPG* methods

This is the first of three sections (Sections 8–10) covering the construction of refinement indicators for DPG* methods. In this section, we define an explicit error estimator $\eta^{*,\text{expl}}(\boldsymbol{\mathfrak{v}}_{h,r}^{\text{opt}})$ for the term $\|\mathcal{B}'\boldsymbol{\mathfrak{v}}_{h,r}^{\text{opt}}-g\|_{\mathcal{U}'}$ present in (5.4). If Assumption 2 holds, then

$$\|\|\mathbf{v}^{\star} - \mathbf{v}_{h,r}^{\text{opt}}\|\|_{\mathcal{V}} = \|\mathcal{B}'\mathbf{v}_{h,r}^{\text{opt}} - g\|_{\mathcal{U}'}$$

and $\eta^{*,\text{expl}}(\mathfrak{v}_{h,r}^{\text{opt}})$ can be also considered an *a posteriori* error estimator for the dual problem.

8.1. **Outline of the general derivation.** This subsection is mostly motivational. A more thorough derivation requires a case-by-case analysis of the interface term appearing on the right-hand side of (8.1). In the setting of Poisson's boundary value problem, a careful analysis is performed in Section 11.5.

Let Assumption 3 hold and consider the broken ultraweak setting (see Section 3.9). Namely, $b(\mathbf{u}, \mathbf{v}) = (\mathbf{u}, \mathcal{L}^*\mathbf{v})_{\Omega} + \langle \hat{\mathbf{u}}, \mathbf{v} \rangle_{\partial \mathcal{T}}$ and $g(\mathbf{u}) = (\mathbf{g}, \mathbf{u})_{\Omega} + \langle \hat{g}, \hat{\mathbf{u}} \rangle_{\partial \mathcal{T}}$, for all $\mathbf{u} = (\mathbf{u}, \hat{\mathbf{u}}) \in \mathcal{U}$ and $\mathbf{v} \in \mathcal{V}$. Then observe that

$$(8.1) \qquad \|\mathcal{B}'\mathbf{v} - g\|_{\mathcal{U}'}^2 = \left(\sup_{\mathbf{u} \in \mathcal{U}} \frac{(\mathbf{u}, \mathcal{L}^*\mathbf{v} - \mathbf{g})_{\Omega} + \langle \hat{\mathbf{u}}, \mathbf{v} - \hat{g} \rangle_{\partial \mathcal{T}}}{\left(\|\mathbf{u}\|_{\Omega}^2 + \|\hat{\mathbf{u}}\|_{\hat{\mathcal{U}}}^2\right)^{1/2}}\right)^2 = \|\mathcal{L}^*\mathbf{v} - \mathbf{g}\|_{\Omega}^2 + \sup_{\hat{\mathbf{u}} \in \hat{\mathcal{U}}} \frac{\langle \hat{\mathbf{u}}, \mathbf{v} - \hat{g} \rangle_{\partial \mathcal{T}}^2}{\|\hat{\mathbf{u}}\|_{\Omega}^2},$$

where the second equality follows from Lemma 3.1. The first term on the right-hand side corresponds to the L^2 -residual, while the second measures the jumps of \mathbf{v} across the element interfaces.

Assume that $\langle \hat{g}, \hat{\mathfrak{u}} \rangle_{\partial \mathcal{T}} = \int_{\partial \Omega} \hat{\mathfrak{g}}_0 \cdot \hat{\mathfrak{u}}$, for all $\hat{\mathfrak{u}} \in \hat{\mathcal{U}}$ and some prescribed function $\hat{\mathfrak{g}}_0$. Next, for the discrete influence function $\mathbf{v}_{h,r}^{\mathrm{opt}} \in \mathcal{V}_r$ and a sufficiently regular $\hat{\mathfrak{g}}_0$, take for granted that the element contributions of the second term can be bounded by a weighted norm of the interface jumps, $[\![\mathbf{v}_{h,r}^{\mathrm{opt}} - \hat{\mathfrak{g}}_0]\!]$:

(8.2)
$$\sup_{\hat{\mathbf{u}} \in \hat{\mathbf{U}}} \frac{\langle \hat{\mathbf{u}}, \mathbf{v}_{h,r}^{\text{opt}} - \hat{g} \rangle_{\partial \mathcal{T}}^2}{\|\hat{\mathbf{u}}\|_{\hat{\mathcal{U}}}^2} \lesssim \sum_{K \in \mathcal{T}} \| [\![\mathbf{v}_{h,r}^{\text{opt}} - \hat{\mathbf{g}}_0]\!] \|_{\partial K, w}^2.$$

Here, the $\|\cdot\|_{\partial K,w}$ -norm is defined $\|\hat{\mathfrak{p}}\|_{\partial K,w}^2 = \int_{\partial K} |\hat{\mathfrak{p}}|^2 w$ (possibly plus face-wise derivative terms) with the weight $w = w(h_K) \in L^\infty(\partial K)$ depending on the element size h_K .

Then, together, (8.1) and imply that (8.2)

(8.3)
$$\|\mathcal{B}'\mathbf{v} - g\|_{\mathcal{U}'}^2 \lesssim \|\mathcal{L}^*\mathbf{v} - \mathfrak{g}\|_{\Omega}^2 + \sum_{K \in \mathcal{T}} \|[\mathbf{v}_{h,r}^{\text{opt}} - \hat{\mathfrak{g}}_0]\|_{\partial K,w}^2 .$$

8.2. Construction of refinement indicators. Naturally, (8.3) motivates the definition

$$\eta^{*,\text{expl}}(\boldsymbol{\mathfrak{v}}_{h,r}^{\text{opt}})^2 = \sum_{K \in \mathcal{T}} \left(\|\mathcal{L}^* \boldsymbol{\mathfrak{v}}_{h,r}^{\text{opt}} - \boldsymbol{\mathfrak{g}}\|_K^2 + \|[\![\boldsymbol{\mathfrak{v}}_{h,r}^{\text{opt}} - \hat{\boldsymbol{\mathfrak{g}}}_{\scriptscriptstyle{0}}]\!]\|_{\partial K,w}^2 \right).$$

Likewise, the corresponding refinement indicators would be

(8.4)
$$(\eta_K^{*,\text{expl}})^2 = \|\mathcal{L}^* \mathbf{v}_{h,r}^{\text{opt}} - \mathfrak{g}\|_K^2 + \|[\mathbf{v}_{h,r}^{\text{opt}} - \hat{\mathfrak{g}}_0]\|_{\partial K,w}^2, \quad \forall K \in \mathcal{T}.$$

Note that $\eta^{*,\text{expl}}(\mathfrak{v}_{h,r}^{\text{opt}})$ defines a viable efficient *and reliable* error estimator for the corresponding DPG* method if a similar lower bound, complementing the upper bound in (8.2), can also be proven (see Remark 11.2). Often, this is also the case.

9. IMPLICIT ERROR ESTIMATORS FOR DPG* METHODS

This is the second of three sections (Sections 8-10) covering the construction of refinement indicators for DPG* methods. In this section, we define an implicit error estimator $\eta^{*,\text{impl}}(\boldsymbol{v}_{h\,r}^{\text{opt}})$ for the term $\|\mathcal{B}'\boldsymbol{v}_{h\,r}^{\text{opt}}-g\|_{\mathcal{U}'}$ present in (5.4). If Assumption 2 holds, then

$$\|\mathbf{v}^{\star} - \mathbf{v}_{h,r}^{\text{opt}}\|_{\mathcal{V}} = \|\mathcal{B}'\mathbf{v}_{h,r}^{\text{opt}} - g\|_{\mathcal{U}'}$$

and $\eta^{*,\mathrm{impl}}(\mathbf{v}_{h.r}^{\mathrm{opt}})$ can be also considered an *a posteriori* error estimator for the dual problem.

9.1. **Derivation.** Recall (4.2). Namely,

$$\begin{cases} (\boldsymbol{\mathfrak{v}}_h^{\mathrm{opt}}, \boldsymbol{\mathfrak{v}})_{\mathcal{V}} - b(\boldsymbol{\omega}_h^{\mathrm{opt}}, \boldsymbol{\mathfrak{v}}) = 0, & \forall \, \boldsymbol{\mathfrak{v}} \in \mathcal{V}, \\ b(\boldsymbol{\mathfrak{u}}_h, \boldsymbol{\mathfrak{v}}_h^{\mathrm{opt}}) & = g(\boldsymbol{\mathfrak{u}}_h), & \forall \, \boldsymbol{\mathfrak{u}}_h \in \mathcal{U}_h. \end{cases}$$

Also, recall that $a(\boldsymbol{\omega}_h^{\mathrm{opt}}, \boldsymbol{\mathfrak{u}}) = b(\boldsymbol{\mathfrak{u}}, \boldsymbol{\mathfrak{v}}_h^{\mathrm{opt}})$, and

(9.1)
$$0 = g(\mathbf{u}_h) - a(\boldsymbol{\omega}_h^{\text{opt}}, \mathbf{u}_h), \quad \forall \, \mathbf{u}_h \in \mathcal{U}_h.$$

Define a representation of the residual in the DPG* solution, $\varepsilon_h^{\text{opt}} \in \mathcal{U}$, to be the unique solution of

$$a(\boldsymbol{\varepsilon}_h^{\mathrm{opt}},\boldsymbol{\mathfrak{u}}) = g(\boldsymbol{\mathfrak{u}}) - a(\boldsymbol{\omega}_h^{\mathrm{opt}},\boldsymbol{\mathfrak{u}}) = g(\boldsymbol{\mathfrak{u}}) - b(\boldsymbol{\mathfrak{u}},\boldsymbol{\mathfrak{v}}_h^{\mathrm{opt}})\,, \quad \forall\, \boldsymbol{\mathfrak{u}} \in \mathcal{U}\,.$$

Clearly, by (9.1), $a(\varepsilon_h^{\text{opt}}, \mathbf{u}_h) = 0$, for all $\mathbf{u}_h \in \mathcal{U}_h$. Observe that $(\varepsilon_h^{\text{opt}}, \mathbf{v}_h^{\text{opt}}) \in \mathcal{U} \times \Theta(\mathcal{U}_h)$ is the unique solution of

$$\begin{cases} a(\boldsymbol{\varepsilon}_h^{\mathrm{opt}}, \boldsymbol{\mathfrak{u}}) + b(\boldsymbol{\mathfrak{u}}, \boldsymbol{\mathfrak{v}}_h^{\mathrm{opt}}) = g(\boldsymbol{\mathfrak{u}}) \,, & \forall \, \boldsymbol{\mathfrak{u}} \in \mathcal{U} \,, \\ b(\boldsymbol{\varepsilon}_h^{\mathrm{opt}}, \boldsymbol{\mathfrak{v}}_h) & = 0 \,, & \forall \, \boldsymbol{\mathfrak{v}}_h \in \Theta(\mathcal{U}_h) \,, \end{cases}$$
 and $\||\boldsymbol{\varepsilon}_h^{\mathrm{opt}}||_{\mathcal{U}} = \||\mathcal{A}^{-1}(\mathcal{B}'\boldsymbol{\mathfrak{v}}_h^{\mathrm{opt}} - g)||_{\mathcal{U}} = \||\mathcal{B}'\boldsymbol{\mathfrak{v}}_h^{\mathrm{opt}} - g||_{\mathcal{U}'}.$ Likewise, we may define $\boldsymbol{\varepsilon}_{h,r}^{\mathrm{opt}}$ as the unique

solution of

(9.2)
$$a(\boldsymbol{\varepsilon}_{h,r}^{\text{opt}}, \boldsymbol{\mathfrak{u}}) = g(\boldsymbol{\mathfrak{u}}) - b(\boldsymbol{\mathfrak{u}}, \boldsymbol{\mathfrak{v}}_{h,r}^{\text{opt}}), \quad \forall \, \boldsymbol{\mathfrak{u}} \in \mathcal{U},$$

and conclude that $\||\boldsymbol{\varepsilon}_{h,r}^{\mathrm{opt}}|\|_{\mathcal{U}} = \||\mathcal{B}'\boldsymbol{v}_{h,r}^{\mathrm{opt}} - g\|_{\mathcal{U}'}$. Notice that not even $\boldsymbol{\varepsilon}_{h,r}^{\mathrm{opt}}$ cannot be computed exactly. Indeed, just as with ψ_h^{opt} , the true residual representation $\boldsymbol{\varepsilon}_{h,r}^{\mathrm{opt}}$ and, therefore, $\||\boldsymbol{\varepsilon}_{h,r}^{\mathrm{opt}}|\|_{\mathcal{U}}$ can only be estimated.

In order to estimate $\varepsilon_{h,r}^{\text{opt}}$, we pose (9.2) on a truncated trail space $\mathcal{U}_H \subseteq \mathcal{U}$ containing the original trial space $\mathcal{U}_h \subsetneq \mathcal{U}_H$. Furthermore, because the inner product $a: \mathcal{U} \times \mathcal{U} \to \mathbb{R}$ has to be approximated on this enriched space, we use a further enriched test space $\mathcal{V}_R \subseteq \mathcal{V}$ to generate its associated approximation $a_R : \mathcal{U}_H \times \mathcal{U}_H \to \mathbb{R}$.

In other words, in order to compute a practical estimate the solution $\varepsilon_{h,r}^{\text{opt}}$ to (9.2), we propose solving a discrete variational problem

$$(9.3) a_R(\boldsymbol{\varepsilon}, \boldsymbol{\mathfrak{u}}_H) = g(\boldsymbol{\mathfrak{u}}_H) - b(\boldsymbol{\mathfrak{u}}_H, \boldsymbol{\mathfrak{v}}_{h,r}^{\text{opt}}), \quad \forall \, \boldsymbol{\mathfrak{u}}_H \in \mathcal{U}_H.$$

Here, $\varepsilon=arepsilon_{H,R}^{
m opt}({f v}_{h,r}^{
m opt})$ is the computable estimate of the representation of the residual in the practical DPG*

(9.4)
$$\eta^{*,\mathrm{impl}}(\boldsymbol{\mathfrak{v}}_{h,r}^{\mathrm{opt}}) = a_R(\boldsymbol{\varepsilon}, \boldsymbol{\varepsilon})^{1/2}.$$

is the associated implicit error estimator. Notice that (9.3) is generally a global problem. Methods for its localization and the corresponding estimation of (9.4) are the topics of the next subsection.

9.2. Construction of refinement indicators. In general, the energy norm $\| \cdot \|_{\mathcal{U}}$ is not localizable and the enriched trial space is not broken $\mathcal{U}_H \neq \prod_{K \in \mathcal{T}} \mathcal{U}_{H,K}$. Therefore, the inverse associated Riesz map cannot be decomposed at the element level, $\mathcal{A}^{-1} \neq \bigoplus_{K \in \mathcal{T}} \mathcal{A}_K^{-1}$. For this reason, a decomposition of $\eta^{*,\mathrm{impl}}(\boldsymbol{v}_{h,r}^{\mathrm{opt}})$ into local element contributions is a slightly more delicate procedure here than with the similar estimator $\eta_r(\boldsymbol{u}_{h,r}^{\mathrm{opt}})$ in Section 7.

Of course, requiring a global inversion over the entire trial space \mathcal{U}_H in the computation of ε in (9.3) is impractical. The refinement indicators must be computable through the solution of independent element-local problems. We have experimented with a small number of different approaches to decompose $a_R(\varepsilon,\varepsilon)$ into a sum of element-wise terms. What is crucial in each of these approaches is that we relax the assumption $\mathcal{U}_H \subseteq \mathcal{U}$, and consider a non-conforming enriched trial space $\mathcal{U}_H = \prod_{K \in \mathcal{T}} \mathcal{U}_{H,K}$. The approaches fall into three categories: (1) null space characterization approaches; (2) Tikhonov regularization approaches; and (3) artificial boundary condition approaches. In all but the first scenario, the element-wise contributions can only be expected to approximately sum to the error estimator:

(9.5)
$$\eta^{*,\mathrm{impl}}(\mathbf{v}_{h,r}^{\mathrm{opt}})^2 \approx \sum_{K \in \mathcal{T}} \left(\eta_K^{*,\mathrm{impl}}\right)^2.$$

Our experiments in Section 12 indicate that such an approximation may be sufficient for GMR. There, results are presented from only the third category of implicit error estimator.

9.2.1. The general approach and null space characterization. From the theory of broken variational formulations [14], if $\mathcal V$ is not a product space already $b:\mathcal U\times\mathcal V\to\mathbb R$ can be extended to a well-posed variational formulation on the non-conforming space $\prod_{K\in\mathcal T}\mathcal V|_K$ by introducing interface terms which act as Lagrange multipliers. Without the interface terms, uniqueness of solutions is lost. Similarly, $\mathcal U$ can be broken into $\prod_{K\in\mathcal T}\mathcal U|_K$ and, without the associated Lagrange multipliers, uniqueness of solutions is also lost.

Consider $\mathcal{U}_h \subsetneq \mathcal{U}_H = \prod_{K \in \mathcal{T}} \mathcal{U}_{H,K} \not\subseteq \mathcal{U}$ where each $\mathcal{U}_{H,K} \subseteq \mathcal{U}|_K$, for all $K \in \mathcal{T}$. Assume that $\mathcal{V}_R = \prod_{K \in \mathcal{T}} \mathcal{V}_{R,K} \supseteq \mathcal{V}_r$ is large enough so that Assumption 4 holds for the new space \mathcal{U}_H . Specifically, assume that there exists a bounded linear operator $\Pi_R : \mathcal{V} \to \mathcal{V}_R$ such that

$$b(\mathbf{u}_H, \mathbf{v} - \Pi_R \mathbf{v}) = 0, \quad \forall \mathbf{u}_H \in \mathcal{U}_H, \mathbf{v} \in \mathcal{V}.$$

Here, we understand $b: \prod_{K \in \mathcal{T}} \mathcal{U}|_K \times \mathcal{V} \to \mathbb{R}$ as this non-conforming analogue of the bilinear form considered elsewhere throughout this manuscript.

In this and the following approaches, the local problem we wish to solve will have a structure similar to (9.3). Specifically, consider $\mathcal{V}_R = \prod_{K \in \mathcal{T}} \mathcal{V}_{R,K}$ and note that

$$a_R(\mathfrak{u}_H,\widetilde{\mathfrak{u}}_H) = \left\langle \mathfrak{B}\mathfrak{u}_H, \mathfrak{R}_{\mathfrak{V}_R}^{^{-1}} \, \mathfrak{B}\widetilde{\mathfrak{u}}_H \right\rangle = \sum_{K \in \mathcal{T}} \left\langle \mathfrak{B}\mathfrak{u}_H, \mathfrak{R}_{\mathfrak{V}_{R,K}}^{^{-1}} \, \mathfrak{B}\widetilde{\mathfrak{u}}_H \right\rangle, \quad \forall \, \mathfrak{u}_H, \widetilde{\mathfrak{u}}_H \in \mathfrak{U}_H \, .$$

Here, each term $a_{R,\kappa}(\mathfrak{u}_H,\widetilde{\mathfrak{u}}_H)=\langle \mathfrak{B}\mathfrak{u}_H,\mathfrak{R}_{\mathcal{V}_{R,\kappa}}^{-1}\,\mathfrak{B}\widetilde{\mathfrak{u}}_H\rangle$ has the symmetric structure of an inner product but is not necessary definite.

Therefore, if we decompose a_R into element-wise contributions $a_{R,\kappa}:\mathcal{U}_{H,\kappa}\times\mathcal{U}_{H,\kappa}\to\mathbb{R}$, then the associated local problem for $\boldsymbol{\varepsilon}_{\kappa}\in\mathcal{U}_{H,\kappa}$,

$$(9.6) a_{R,K}(\boldsymbol{\varepsilon}_K, \boldsymbol{\mathfrak{u}}_H) = g(\boldsymbol{\mathfrak{u}}_H) - b(\boldsymbol{\mathfrak{u}}_H, \boldsymbol{\mathfrak{v}}_{h,r}^{\text{opt}}), \quad \forall \, \boldsymbol{\mathfrak{u}}_H \in \mathcal{U}_{H,K},$$

does not necessarily have a unique solution. Removing the null space of this equation at each element will allow for the construction of the necessary refinement indicators. The precise way that the null space is removed differentiates each category of implicit error estimator. In any case, in (9.5), we may define

(9.7)
$$\eta_K^{*,\mathrm{impl}} = a_{R,K}(\boldsymbol{\varepsilon}_K, \boldsymbol{\varepsilon}_K)^{1/2}, \quad \forall K \in \mathcal{T}.$$

Uniqueness of (9.6) can be built-in by explicitly identifying the null space of the linear operator $A_{R,K}$ associated to the symmetric bilinear form $a_{R,K}$. However, only in limited examples can this space can be easily done

analytically. Generally speaking, the null space of the associated local stiffness matrix can always be characterized through an eigenvalue decomposition after the local Gram matrix for $a_{R,K}$, $A_{R,K}$, is constructed. After the zero eigenvalues have been identified, $A_{R,K}$ can easily be inverted on its range. Eigenvalue decomposition is slow and generally makes null space characterization less practical so the following two other less precise approaches can also be considered.

9.2.2. Tikhonov regularization. In this approach, the decomposition property of the residual in Section 7, $\|\mathfrak{B}\mathfrak{u}-\ell\|_{\mathcal{V}'_r}^2=\sum_{K\in\mathcal{T}}\|\mathfrak{B}\mathfrak{u}-\ell\|_{\mathcal{V}'_{K,r}}^2$, is built into each local problem (9.6) by regularizing the symmetric bilinear form $a_{R,K}$. Abstractly, this approach is equivalent to simply just replacing a_R with the regularized symmetric bilinear form

$$a_{R,w}(\mathfrak{u}_H,\widetilde{\mathfrak{u}}_H) = a_R(\mathfrak{u}_H,\widetilde{\mathfrak{u}}_H) + (\mathfrak{u}_H,\widetilde{\mathfrak{u}}_H)_{L^2_m}, \quad \forall \, \mathfrak{u}_H,\widetilde{\mathfrak{u}}_H \in \mathfrak{U}_H,$$

where $(\cdot,\cdot)_{L^2_w}$ is some weighted L^2 inner product. In this case, because of the L^2_w -term, the local problem

(9.8)
$$a_{R,w}(\boldsymbol{\varepsilon}_{K,w}, \boldsymbol{\mathfrak{u}}_H) = g(\boldsymbol{\mathfrak{u}}_H) - b(\boldsymbol{\mathfrak{u}}_H, \boldsymbol{\mathfrak{v}}_{h,r}^{\text{opt}}), \quad \forall \, \boldsymbol{\mathfrak{u}}_H \in \mathcal{U}_{H,K},$$

is guaranteed to have a unique solution $\varepsilon_{K,w} \in \mathcal{U}_{H,K}$. Hopefully, if the weight is sufficiently small,

$$a_R(\boldsymbol{arepsilon}, \boldsymbol{arepsilon}) pprox \sum_{K \in \mathcal{T}} a_R(\boldsymbol{arepsilon}_{{\scriptscriptstyle{K}},w}, \boldsymbol{arepsilon}_{{\scriptscriptstyle{K}},w}).$$

In practice, when solving for $\varepsilon_{K,w}$ in (9.8), after the local Gram matrix for $a_{R,K}$, $A_{R,K}$, is constructed, a small multiple of the identity can be added. That is, $A_{R,K} \mapsto A_{R,K} + \lambda I$, where $\lambda \ll 1$. This is the procedure is preferred over actually characterizing the inner product $(\cdot,\cdot)_{L^2_w}$ when constructing $A_{R,K}$. Finally, after the regularized solution $\varepsilon_{K,w}$ is computed, the original unweighted inner product $a_R(\cdot,\cdot)$ can easily be used to calculate the refinement indicators, $\eta_{K}^{*,\mathrm{impl}} = a_{R,K}(\varepsilon_{K,w},\varepsilon_{K,w})^{1/2}$.

9.2.3. Artificial boundary conditions. As with the previous approach, the intention here is to introduce uniqueness of solutions to the element-wise problems (9.6) by modifying them in some almost negligible way. With the previous approach, the inner product $a_R(\cdot,\cdot)$ itself was modified to induce uniqueness. With this approach, the trial space \mathcal{U}_H will be modified instead.

The main idea is to formulate a set of well-posed local problems

$$(9.9) a_{R,K}(\boldsymbol{\varepsilon}_K, \boldsymbol{\mathfrak{u}}_H) = g(\boldsymbol{\mathfrak{u}}_H) - b(\boldsymbol{\mathfrak{u}}_H, \boldsymbol{\mathfrak{v}}_{h,r}^{\text{opt}}), \quad \forall \, \boldsymbol{\mathfrak{u}}_H \in \mathcal{U}_{H,K},$$

with uniqueness delivered by placing artificial boundary conditions on ∂K on the variable $\varepsilon_K \in \mathcal{U}_{H,K}$.

Observe that, if $\mathbf{v}_{h.r}^{\text{opt}}$ in (9.2) is replaced with the exact test space influence function \mathbf{v}^* , then

(9.10)
$$a(\boldsymbol{\varepsilon}^{\star}, \boldsymbol{\mathfrak{u}}) = g(\boldsymbol{\mathfrak{u}}) - b(\boldsymbol{\mathfrak{u}}, \boldsymbol{\mathfrak{v}}^{\star}) = 0, \quad \forall \, \boldsymbol{\mathfrak{u}} \in \mathcal{U},$$

and $\varepsilon^{\star}=0$. Due to continuous dependence of the solution ε upon the load above, when a computed test space influence function $\mathfrak{v}_{h,r}^{\mathrm{opt}}\approx\mathfrak{v}^{\star}$ is reinstated, the solution will remain close to zero, $\varepsilon\approx0$.

This suggests a convenient choice for artificial boundary conditions on the localized solution ε_K that may only negligibly affect the discrete solution ε_K . Thus, consider enforcing homogeneous boundary conditions on ∂K on the variable ε_K in (9.9). Obviously, the proper choice of boundary conditions will depend on the problem being solved. Note that, with homogeneous boundary conditions enforced, the modified local problems (9.9) are all consistent with (9.10). That is, if $\mathbf{v}_{h,r}^{\text{opt}} = \mathbf{v}^*$, then the solution ε_K of the modified problem is unique and $\varepsilon_K = \varepsilon^*|_K = 0$, for all $K \in \mathcal{T}$.

10. A SIMPLE CLASS OF AD HOC REFINEMENT INDICATORS FOR DPG* METHODS

This is the last of three sections (Sections 8–10) on the construction of refinement indicators for DPG* methods. In this section, we propose an ad hoc error estimator for the term $\|\mathbf{v}^* - \mathbf{v}_{h,r}^{\text{opt}}\|_{\mathcal{V}}$ present in (5.3) and ignore its relationship to the dual residual. As a bona fide *a posteriori* error estimator for DPG* methods, this ad hoc error estimator has very poor properties and so we do not recommend it for actually estimating error in DPG* problems. Nevertheless, its associated refinement indicators, when combined with the energy

norm refinement indicators $\eta_r(\mathbf{u}_{h,r}^{\mathrm{opt}})$ of Section 7, can still give favorable pre-asymptotic results with our GMR Algorithms. Although we present no theory to justify it, the results of the numerical experiments presented in Section 12 support this conclusion.

In Section 6, 8, and 9, the error estimators for the DPG* problem $\eta^*(\mathbf{v}_{h,r}^{\text{opt}})$ are solely functions of the discrete test space influence function $\mathbf{v}_{h,r}^{\text{opt}}$. Here, we permit error estimators $\eta^*(\boldsymbol{\omega}_{h,r}^{\text{opt}}, \mathbf{v}_{h,r}^{\text{opt}})$ which depend upon both components of the solution to (4.6) and, in particular, depend only upon $\boldsymbol{\omega}_{h,r}^{\text{opt}}$.

10.1. **Derivation.** Recall Section 3.6 and, in particular, (3.20). Namely,

$$\|\mathbf{v}^{\star} - \mathbf{v}_h^{\text{opt}}\|_{\mathcal{V}} \stackrel{\star}{=} \|\boldsymbol{\omega}^{\star} - \boldsymbol{\omega}_h^{\text{opt}}\|_{\mathcal{U}} \stackrel{\star}{=} \|\mathbf{g} - \boldsymbol{\omega}_h^{\text{opt}}\|_{\mathcal{U}},$$

where $\mathbf{g} = \mathcal{R}_{\mathcal{U}}^{-1} g \stackrel{\star}{=} \omega^{\star}$ is the Riesz representation of g, defined in (3.3). Here, recall that the \star -notation exists to remind the reader that the equality only holds in the idealized setting, $\|\cdot\|_{\mathcal{V}} = \|\cdot\|_{\mathcal{V}}$. Also, recall (5.1):

$$|g(\mathfrak{u}^{\star}) - g(\mathfrak{u}_{h,r}^{\text{opt}})| \leq ||\mathfrak{u}^{\star} - \mathfrak{u}_{h,r}^{\text{opt}}||_{\mathcal{U}} ||\mathfrak{v}^{\star} - \mathfrak{v}_{h,r}^{\text{opt}}||_{\mathcal{V}} \stackrel{\star}{=} ||\mathfrak{u}^{\star} - \mathfrak{u}_{h,r}^{\text{opt}}||_{\mathcal{U}} ||\mathfrak{g} - \omega_{h}^{\text{opt}}||_{\mathcal{U}},$$

where the *-equality follows from (3.20). Inspired by this idealized bound, consider the candidate error estimator

$$\eta^{*,\mathrm{proj}}(\boldsymbol{\omega}_{h.r}^{\mathrm{opt}}) = \|\mathbf{\mathfrak{g}} - \boldsymbol{\omega}_{h.r}^{\mathrm{opt}}\|_{\mathcal{U}}$$

for the DPG* problem. This is a surrogate for the ad hoc error estimator that we will eventually derive. Note that only in the idealized setting does $\mathfrak{g} \stackrel{\star}{=} \omega^{\star}$. Therefore, this error estimator is only expected to perform well if $\|\cdot\|_{\mathcal{V}} \approx \|\cdot\|_{\mathcal{V}}$. Similarly, only in the ideal setting will $\eta^{*,\mathrm{proj}}(\omega_{h,r}^{\mathrm{opt}}) \to 0$ as the mesh is refined (see Section 10.3).

In general, the Riesz representation $\mathfrak g$ is not available *a priori*. Consequently, $\eta^{*,\operatorname{proj}}(\omega_{h,r}^{\operatorname{opt}})$ is useless in a general circumstance because it requires the solution of an infinite dimensional problem determining $\mathfrak g$. Nevertheless, as is noted in Section 3.7, $\mathfrak g \in L^2(\Omega)$ is always known from the outset analytically when using an ultraweak variational formulation. Because, at best, we may consider broken ultraweak formulations, the variety of goal functionals have to be restricted with this error estimator.

Specifically, consider the broken ultraweak setting: $\mathbf{u} = (\mathbf{u}, \hat{\mathbf{u}}) \in \mathcal{U} = L^2(\Omega) \times \hat{\mathcal{U}}$. In this case,

$$\|\mathfrak{g} - \boldsymbol{\omega}_{h,r}^{\text{opt}}\|_{\mathcal{U}}^2 = \|(\mathfrak{g}, \hat{\mathfrak{g}}) - (\boldsymbol{\omega}_{h,r}^{\text{opt}}, \hat{\boldsymbol{\omega}}_{h,r}^{\text{opt}})\|_{\mathcal{U}}^2 = \|\mathfrak{g} - \boldsymbol{\omega}_{h,r}^{\text{opt}}\|_{\boldsymbol{\Omega}}^2 + \|\hat{\mathfrak{g}} - \hat{\boldsymbol{\omega}}_{h,r}^{\text{opt}}\|_{\hat{\mathcal{U}}}^2,$$

where $\mathfrak{g}=(\mathfrak{g},\hat{\mathfrak{g}})$ and $\omega_{h,r}^{\mathrm{opt}}=(\omega_{h,r}^{\mathrm{opt}},\hat{\omega}_{h,r}^{\mathrm{opt}})$. Note that, generally, the interface function $\hat{\mathfrak{g}}=\mathcal{R}_{\hat{\mathcal{U}}}^{-1}\hat{g}$ is not available a priori and $\hat{\mathfrak{g}}\neq\hat{\mathfrak{g}}_0=\mathcal{R}_{L^2(\partial\Omega)}^{-1}\hat{g}$ from Section 8.2, which is available a priori. Therefore, for the present ad hoc error estimator, we will only allow goal functionals of the form

$$g(\mathfrak{u}) = \int_{\Omega} \mathfrak{g} \cdot \mathfrak{u} \,, \quad \forall \, \mathfrak{u} \in L^2(\Omega) \,.$$

Here,

$$\|\mathbf{g} - \boldsymbol{\omega}_{h,r}^{\text{opt}}\|_{\mathcal{U}}^2 = \|(\mathbf{g}, 0) - \boldsymbol{\omega}_{h,r}^{\text{opt}}\|_{\mathcal{U}}^2 = \|\mathbf{g} - \boldsymbol{\omega}_{h,r}^{\text{opt}}\|_{\Omega}^2 + \|\hat{\boldsymbol{\omega}}_{h,r}^{\text{opt}}\|_{\hat{\mathcal{U}}}^2$$

Although the second term above can be estimated at the element level, we choose to ignore it. Isolating only the first term, define the ad hoc DPG* error estimator:

$$\eta^{*,\mathrm{a.h.}}(\boldsymbol{\omega}_{h,r}^{\mathrm{opt}}) = \|\mathfrak{g} - \boldsymbol{\omega}_{h,r}^{\mathrm{opt}}\|_{\Omega}.$$

10.2. **Construction of refinement indicators.** In this setting, the construction of refinement indicators is immediate:

(10.1)
$$\eta_K^{*,\text{a.h.}} = \|\mathfrak{g} - \omega_{h,r}^{\text{opt}}\|_K, \quad \forall K \in \mathcal{T}.$$

Clearly,
$$\eta^{*,\mathrm{a.h.}}(\omega_{h,r}^{\mathrm{opt}})^2 = \sum_{K \in \mathcal{T}} (\eta_{\kappa}^{*,\mathrm{a.h.}})^2$$
.

10.3. **Accuracy.** In the ultraweak setting, the test norm of choice is often the adjoint graph norm (3.24). When used on the discrete space \mathcal{V}_r , this norm is often expected to deliver a good approximation of the true optimal test norm, but notable exceptions do exist [17, 30, 44]. Our impression is that good behavior with this error estimator will only be found when the influence function coming from the solution of the dual problem (3.5) is approximately equal to the solution of the dual problem in the idealized setting $\|\cdot\|_{\mathcal{V}} = \|\cdot\|_{\mathcal{V}}$. That is, $\boldsymbol{\omega}_h^{\text{opt}} \approx \mathfrak{g}$. Additionally, it is important to note that

$$\left| \| \mathfrak{g} - \omega^{\star} \|_{\Omega} - \| \omega^{\star} - \omega_{h,r}^{\text{opt}} \|_{\Omega} \right| \leq \| \mathfrak{g} - \omega_{h,r}^{\text{opt}} \|_{\Omega}.$$

Therefore, even with $\|\omega^\star - \omega_{h,r}^{\mathrm{opt}}\|_{\Omega} \to 0$ as the mesh is refined, still $\eta^{*,\mathrm{a.h.}}(\omega_{h,r}^{\mathrm{opt}})^2 \not\to 0$, unless $\omega^\star = \mathfrak{g}$, exactly.

11. A PROTOTYPICAL EXAMPLE PROBLEM

11.1. **Poisson's problem.** In the next section, we will present the results of our DPG experiments with GMR with Poisson's boundary value problem on a convex domain $\Omega \subseteq \mathbb{R}^3$. Specifically, we solved the stationary heat conduction equation

(11.1)
$$\Delta u = f_0, \qquad \iff \qquad \begin{cases} \operatorname{grad} u = \boldsymbol{\sigma}, \\ -\operatorname{div} \boldsymbol{\sigma} = f_0, \end{cases}$$

in Ω ,with boundary conditions $u|_{\Gamma_{\mathrm{D}}} = \hat{\underline{u}}_{0}$ and $\operatorname{grad} u|_{\Gamma_{\mathrm{N}}} \cdot \hat{\boldsymbol{n}} = \hat{\sigma}_{0}$, where Γ_{D} and Γ_{N} are relatively open and form a disjoint partition of $\partial\Omega$. That is, $\overline{\Gamma_{\mathrm{D}} \cup \Gamma_{\mathrm{N}}} = \partial\Omega$ and $\Gamma_{\mathrm{D}} \cap \Gamma_{\mathrm{N}} = \varnothing$.

In (11.1), we have introduced the mathematician's flux variable $\sigma = -q$, where $q = -k \operatorname{grad} u$ is the physical heat flux from Fourier's law with thermal conductivity k = 1. At times, we will refer to the variable u by its physical interpretation (i.e. as temperature).

11.2. A broken ultraweak variational formulation. For all Lipschitz $K \subseteq \Omega$, define the continuous trace operators $\operatorname{tr}_{\operatorname{grad}}^{\partial K}: H^1(K) \to H^{1/2}(\partial K)$ and $\operatorname{tr}_{\operatorname{div}}^{\partial K}: H(\operatorname{div},K) \to H^{-1/2}(\partial K)$, where $(\operatorname{tr}_{\operatorname{grad}}^{\partial K}u)|_{\partial K} = u|_{\partial K}$ and $(\operatorname{tr}_{\operatorname{div}}^{\partial K}\boldsymbol{\sigma})|_{\partial K} = (\boldsymbol{\sigma}\cdot\hat{\boldsymbol{n}}_K)|_{\partial K}$ almost everywhere. Here, by $\hat{\boldsymbol{n}}_K$, we mean the outer unit normal vector on ∂K to the subset $K \subseteq \Omega$. Now, using the trace operators given above, define the Hilbert spaces

$$\begin{split} H^1_{\mathrm{D}}(\Omega) &= \left\{ u \in H^1(\Omega) : (\operatorname{tr}_{\mathrm{grad}}^{\partial\Omega} u)|_{\Gamma_{\mathrm{D}}} = 0 \right\}, \\ \boldsymbol{H}_{\mathrm{N}}(\mathrm{div},\Omega) &= \left\{ \boldsymbol{\sigma} \in \boldsymbol{H}(\mathrm{div},\Omega) : (\operatorname{tr}_{\mathrm{div}}^{\partial\Omega} \boldsymbol{\sigma})|_{\Gamma_{\mathrm{N}}} = 0 \right\}, \end{split} \quad \text{and} \quad \begin{split} H^{1/2}_{\mathrm{D}}(\partial\Omega) &= \operatorname{tr}_{\mathrm{grad}}^{\partial\Omega} H^1_{\mathrm{D}}(\Omega)\,, \\ H^{-1/2}_{\mathrm{N}}(\partial\Omega) &= \operatorname{tr}_{\mathrm{div}}^{\partial\Omega} \boldsymbol{H}_{\mathrm{N}}(\mathrm{div},\Omega)\,, \end{split}$$

and the mesh-dependent trace operators $\operatorname{tr}_{\operatorname{grad}}^{\partial \mathcal{T}} = \prod_{K \in \mathcal{T}} \operatorname{tr}_{\operatorname{div}}^{\partial K}$ and $\operatorname{tr}_{\operatorname{div}}^{\partial \mathcal{T}} = \prod_{K \in \mathcal{T}} \operatorname{tr}_{\operatorname{div}}^{\partial K}$.

Let $L^2(\Omega) = L^2(\Omega)^3$ and assume that the relatively open set $\Gamma_D \subseteq \partial \Omega$ is nonempty, $\Gamma_D \neq \emptyset$. We define the trial and test spaces to be

$$\mathcal{U} = L^2(\Omega) \times \boldsymbol{L}^2(\Omega) \times H_D^{1/2}(\mathcal{S}) \times H_N^{-1/2}(\mathcal{S})$$
 and $\mathcal{V} = H^1(\mathcal{T}) \times \boldsymbol{H}(\mathrm{div}, \mathcal{T})$,

respectively, where

$$\begin{split} H_{\mathrm{D}}^{1/\!_2}(\mathcal{S}) &= \left\{ \hat{u} \in \prod_{K \in \mathcal{T}} H^{1/\!_2}(\partial K) : \exists \, u \in H_{\mathrm{D}}^1(\Omega), \text{ where } \hat{u} = \operatorname{tr}_{\mathrm{grad}}^{\partial K} u, \, \forall K \in \mathcal{T} \right\}, \\ H_{\mathrm{N}}^{-1/\!_2}(\mathcal{S}) &= \left\{ \hat{\sigma} \in \prod_{K \in \mathcal{T}} H^{-1/\!_2}(\partial K) : \exists \, \pmb{\sigma} \in \pmb{H}_{\mathrm{N}}(\mathrm{div}, \Omega), \text{ where } \hat{\sigma} = \mathrm{tr}_{\mathrm{div}}^{\partial K} \, \pmb{\sigma}, \, \forall K \in \mathcal{T} \right\}, \\ H^1(\mathcal{T}) &= \left\{ v \in L^2(\Omega) : v|_K \in H^1(K), \, \forall K \in \mathcal{T} \right\}, \\ \pmb{H}(\mathrm{div}, \mathcal{T}) &= \left\{ \pmb{\tau} \in \pmb{L}^2(\Omega) : \pmb{\tau}|_K \in \pmb{H}(\mathrm{div}, K), \, \forall K \in \mathcal{T} \right\}. \end{split}$$

Multiplication of the first order system in (11.1) by test functions $v \in H^1(\mathcal{T})$ and $\tau \in H(\text{div}, \mathcal{T})$, followed by element-wise integration by parts, yields the broken ultraweak formulation of Poisson's problem. Namely, this defines $b : \mathcal{U} \times \mathcal{V} \to \mathbb{R}$, where

$$(11.2) b(\mathfrak{u},\mathfrak{v}) = (u,\operatorname{div}_{\tau}\tau)_{\mathcal{O}} + (\boldsymbol{\sigma},\boldsymbol{\tau} + \operatorname{grad}_{\tau}v)_{\mathcal{O}} - \langle \hat{\boldsymbol{u}},\boldsymbol{\tau} \cdot \hat{\boldsymbol{n}} \rangle_{\partial \tau} - \langle \hat{\boldsymbol{\sigma}}, v \rangle_{\partial \tau},$$

for all $\mathfrak{u} = (u, \boldsymbol{\sigma}, \hat{u}, \hat{\sigma}) \in \mathcal{U}$ and $\mathfrak{v} = (v, \boldsymbol{\tau}) \in \mathcal{V}$. Here, $\operatorname{grad}_{\tau}$ and $\operatorname{div}_{\tau}$ denote element-wise gradient and divergence, respectively. Meanwhile,

$$\langle \hat{u}, \boldsymbol{\tau} \cdot \hat{\boldsymbol{n}} \rangle_{\partial \mathcal{T}} = \sum_{K \in \mathcal{T}} \langle \hat{u}|_{\partial K}, \boldsymbol{\tau}|_{\partial K} \cdot \hat{\boldsymbol{n}}_{K} \rangle_{\partial K} \qquad \text{and} \qquad \langle \hat{\sigma}, v \rangle_{\partial \mathcal{T}} = \sum_{K \in \mathcal{T}} \langle \hat{\sigma}|_{\partial K}, v|_{\partial K} \rangle_{\partial K} \,.$$

We will consider the trial space \mathcal{U} to be equipped with the norm

$$\|\mathfrak{u}\|_{\mathfrak{U}}^2=\|u\|_{\scriptscriptstyle \Omega}^2+\|\boldsymbol{\sigma}\|_{\scriptscriptstyle \Omega}^2+\|\hat{u}\|_{H^{1/2}(\partial\mathcal{T})}^2+\|\hat{\sigma}\|_{H^{-1/2}(\partial\mathcal{T})}^2,\quad\forall\,\mathfrak{u}=(u,\boldsymbol{\sigma},\hat{u},\hat{\sigma})\in\mathfrak{U}\,.$$

Here, $\|\cdot\|_{H^{1/2}(\partial T)}$ and $\|\cdot\|_{H^{-1/2}(\partial T)}$ denote specific minimum energy extension norms:

$$\begin{split} \|\hat{u}\|_{H^{1/2}(\partial\mathcal{T})}^2 &= \inf_{u \in H^1(\Omega) \cap \left(\operatorname{tr}_{\operatorname{grad}}^{\partial\mathcal{T}}\right)^{-1} \{\hat{u}\}} \left(\|\operatorname{grad}_{\mathcal{T}} u\|_{\Omega}^2 + \|u\|_{\Omega}^2\right) \\ \text{and} & \|\hat{\sigma}\|_{H^{-1/2}(\partial\mathcal{T})}^2 &= \inf_{\boldsymbol{\sigma} \in \boldsymbol{H}(\operatorname{div},\Omega) \cap \left(\operatorname{tr}_{\operatorname{div}}^{\partial\mathcal{T}}\right)^{-1} \{\hat{\sigma}\}} \left(\|\operatorname{div}_{\mathcal{T}} \boldsymbol{\sigma}\|_{\Omega}^2 + \|\boldsymbol{\sigma}\|_{\Omega}^2\right). \end{split}$$

Meanwhile, in the (broken) test space \mathcal{V} , we will consider the adjoint graph norm

(11.3)
$$\|\mathbf{v}\|_{\mathcal{L}^* \alpha}^2 = \|\mathbf{\tau} + \operatorname{grad}_{\tau} v\|_{\Omega}^2 + \|\operatorname{div}_{\tau} \mathbf{\tau}\|_{\Omega}^2 + \alpha^2 (\|v\|_{\Omega}^2 + \|\mathbf{\tau}\|_{\Omega}^2), \quad \forall \mathbf{v} = (v, \mathbf{\tau}) \in \mathcal{V}.$$

This norm is easily derived using the methods of Section 3.9 for the broken ultraweak bilinear form in (11.2). With this bilinear form b, the primal problem is to find the unique solution $\mathfrak{u}^* = (u^*, \sigma^*, \hat{u}^*, \hat{\sigma}^*) \in \mathcal{U}$ satisfying

(11.4)
$$b(\mathfrak{u}^{\star},\mathfrak{v}) = \ell(\mathfrak{v}), \quad \forall \, \mathfrak{v} = (v, \tau) \in \mathcal{V},$$

where $\ell(\mathfrak{v}) = (f_0, v)$. Both Assumptions 1 and 2 can be proven to hold for (11.4) with the choice of norms taken above [14].

11.3. **Quantities of interest.** We will only consider quantities of interest which can be derived from linear functionals acting on the underlying *unbroken* trial space. That is, we will only consider goal functionals $g \in \mathcal{U}'$ where

(11.5)
$$g(\mathfrak{u}) = (g_1, u)_{\Omega} + (\mathbf{g}_2, \boldsymbol{\sigma})_{\Omega} + \langle \hat{g}_3, \hat{u}|_{\partial\Omega} \rangle_{\partial\Omega} + \langle \hat{g}_4, \hat{\sigma}|_{\partial\Omega} \rangle_{\partial\Omega}, \quad \forall \mathfrak{u} = (u, \boldsymbol{\sigma}, \hat{u}, \hat{\sigma}) \in \mathcal{U},$$

and $g_1 \in L^2(\Omega)$, $\boldsymbol{g}_2 \in \boldsymbol{L}^2(\Omega)$, $\hat{g}_3 \in \left(H^{1/2}_{\mathrm{D}}(\partial\Omega)\right)'$, and $\hat{g}_4 \in \left(H^{-1/2}_{\mathrm{N}}(\partial\Omega)\right)'$. Clearly, this encompasses the scenarios of linear quantities of interest involving internal temperature and heat flux, as well as temperature and normal heat flux on the boundary. Notice that if $\overline{\Gamma_{\mathrm{D}}} = \partial\Omega$, then $\left(H^{-1/2}_{\mathrm{N}}(\partial\Omega)\right)' = \left(H^{-1/2}(\partial\Omega)\right)' = H^{1/2}(\partial\Omega)$.

- 11.4. **Refinement indicators.** We now present specific refinement indicators for the DPG* methods from Sections 8–10 in the context of Poisson's problem featured above. The last two refinement indicators can be easily derived from the derivations in Sections 9 and 10. However, the first one, in (11.6), requires the coming Theorem 11.1 for its full justification.
- 11.4.1. Explicit refinement indicators. Recall (8.4). Namely,

$$\left(\eta_{K}^{*,\text{expl}}\right)^{2} = \|\mathcal{L}^{*}\boldsymbol{\mathfrak{v}}_{h,r}^{\text{opt}} - \boldsymbol{\mathfrak{g}}\|_{K}^{2} + \|[\boldsymbol{\mathfrak{v}}_{h,r}^{\text{opt}} - \hat{\boldsymbol{\mathfrak{g}}}_{0}]\|_{\partial K,w}^{2}, \quad \forall K \in \mathcal{T}.$$

For Poisson's problem, $\mathfrak{g}=(g_1,\boldsymbol{g}_2),\,\hat{\mathfrak{g}}_0=(\hat{g}_4,\hat{g}_3),\,\mathcal{L}^*\mathfrak{v}=(\operatorname{div}_{\mathcal{T}}\boldsymbol{\tau},\boldsymbol{\tau}+\operatorname{grad}_{\mathcal{T}}\boldsymbol{v}),\,\text{and}\,\,\mathfrak{v}_{h,r}^{\operatorname{opt}}=(v_{h,r}^{\operatorname{opt}},\boldsymbol{\tau}_{h,r}^{\operatorname{opt}}).$ Define \mathcal{F}_{D} and \mathcal{F}_{N} to be the interior faces in \mathcal{T} union the faces in common with Γ_{D} and Γ_{N} , respectively. Also,

define $\operatorname{grad}_{\partial \mathcal{T}} = \prod_{K \in \mathcal{T}} \operatorname{grad}_{\partial K}$ to be the surface gradient operator on the mesh boundary [53, Section 3.4]. As we shall see, Theorem 11.1 suggests that we use

(11.6)
$$(\eta_{K}^{*,\text{expl}})^{2} = \|\operatorname{div}\boldsymbol{\tau}_{h,r}^{\text{opt}} - g_{1}\|_{K}^{2} + \|\operatorname{grad}\boldsymbol{v}_{h,r}^{\text{opt}} + \boldsymbol{\tau}_{h,r}^{\text{opt}} - \boldsymbol{g}_{2}\|_{K}^{2}$$

$$+ h_{K} \sum_{F \in \partial K \cap \mathcal{F}_{N}} \|[\boldsymbol{\tau}_{h,r}^{\text{opt}} \cdot \hat{\boldsymbol{n}} - \hat{g}_{3}]\|_{F}^{2}$$

$$+ h_{K} \sum_{F \in \partial K \cap \mathcal{F}_{D}} \left(\|[\boldsymbol{v}_{h,r}^{\text{opt}} - \hat{g}_{4}]\|_{F}^{2} + \|[\hat{\boldsymbol{n}} \times \operatorname{grad}_{\partial \mathcal{T}}(\boldsymbol{v}_{h,r}^{\text{opt}} - \hat{g}_{4})]\|_{F}^{2} \right),$$

for all $K \in \mathcal{T}$, if the functions \hat{g}_3 and \hat{g}_4 are sufficiently regular.

11.4.2. Implicit refinement indicators. Recall (9.6) and (9.7). That is,

$$a_{R,\kappa}(\boldsymbol{\varepsilon}_{\kappa}, \boldsymbol{\mathfrak{u}}_{H}) = g(\boldsymbol{\mathfrak{u}}_{H}) - b(\boldsymbol{\mathfrak{u}}_{H}, \boldsymbol{\mathfrak{v}}_{h,r}^{\mathrm{opt}}), \quad \forall \, \boldsymbol{\mathfrak{u}}_{H} \in \mathcal{U}_{H,\kappa},$$

and

$$(\eta_K^{*,\mathrm{impl}})^2 = a_{R,K}(\boldsymbol{\varepsilon}_K, \boldsymbol{\varepsilon}_K), \quad \forall K \in \mathcal{T}.$$

Let us only consider the artificial boundary condition technique of Section 9.2.3 to introduce uniqueness of solutions to the equation defining ε_K . We performed experiments with the other techniques presented in Section 9.2 and the results were similar. In Poisson's problem, Dirichlet boundary conditions on any nontrivial subset of the domain boundary induces uniqueness of solutions. Likewise, nontrivial Dirichlet boundary on an element boundary will induce uniqueness of the solution to (9.9), $\varepsilon = (\varepsilon_1, \varepsilon_2, \hat{\varepsilon}_3, \hat{\varepsilon}_4) \in \hat{U}$.

For every $K \in \mathcal{T}$, define the affine subspace

$$\mathfrak{U}_{\boldsymbol{\varepsilon},K} = L^2(K) \times \boldsymbol{L}^2(K) \times \{\hat{\varepsilon}_3|_{\partial K}\} \times H^{-1/2}(\partial K),$$

and the (linear) subspace

$$\mathcal{U}_{0,K} = L^2(K) \times \boldsymbol{L}^2(K) \times \{0\} \times H^{-1/2}(\partial K).$$

For each local problem (9.9), we would *ideally* like to approximate the unique $\varepsilon_K \in \mathcal{U}_{H,K} \cap \mathcal{U}_{\varepsilon,K}$ such that

(11.7)
$$a_{R,\kappa}(\boldsymbol{\varepsilon}_{\kappa}, \boldsymbol{\mathfrak{u}}_{H}) = g(\boldsymbol{\mathfrak{u}}_{H}) - b(\boldsymbol{\mathfrak{u}}_{H}, \boldsymbol{\mathfrak{v}}_{h,r}^{\text{opt}}), \quad \forall \, \boldsymbol{\mathfrak{u}}_{H} \in \mathcal{U}_{H,\kappa} \cap \mathcal{U}_{0,\kappa}.$$

Because $\hat{\varepsilon}_3$ is unknown, we instead solve for the unique $\varepsilon_{0,K} \in \mathfrak{u}_H \in \mathcal{U}_{H,K} \cap \mathcal{U}_{0,K}$ satisfying (11.7). This may be a good estimate of ε_K if $\hat{\varepsilon}_3 \approx 0$.

In this scenario, we define the following goal-oriented error estimator:

(11.8)
$$\left(\eta_K^{*,\text{impl}}\right)^2 = a_{R,K}(\boldsymbol{\varepsilon}_{0,K}, \boldsymbol{\varepsilon}_{0,K}).$$

11.4.3. Ad hoc refinement indicators. Recall (10.1). Namely,

$$\eta_{\scriptscriptstyle{K}}^{*,\mathrm{a.h.}}(\boldsymbol{\omega}_{h,r}^{\mathrm{opt}}) = \|\mathfrak{g} - \omega_{h,r}^{\mathrm{opt}}\|_{\scriptscriptstyle{K}} \,, \quad \forall \, K \in \mathcal{T} \,.$$

Recall that $\boldsymbol{\omega}_{h,r}^{\mathrm{opt}} = \left((\omega_1)_{h,r}^{\mathrm{opt}}, (\boldsymbol{\omega}_2)_{h,r}^{\mathrm{opt}}, (\hat{\omega}_3)_{h,r}^{\mathrm{opt}}, (\hat{\omega}_4)_{h,r}^{\mathrm{opt}} \right) \in \mathcal{U}_h$. Here, $\boldsymbol{\mathfrak{g}} = (\boldsymbol{\mathfrak{g}}, \hat{\boldsymbol{\mathfrak{g}}})$ and $\boldsymbol{\omega}_{h,r}^{\mathrm{opt}} = (\omega_{h,r}^{\mathrm{opt}}, \hat{\omega}_{h,r}^{\mathrm{opt}})$, where $\boldsymbol{\mathfrak{g}} = (g_1, \boldsymbol{g}_2)$ and $\omega_{h,r}^{\mathrm{opt}} = ((\omega_1)_{h,r}^{\mathrm{opt}}, (\boldsymbol{\omega}_2)_{h,r}^{\mathrm{opt}})$. Therefore,

(11.9)
$$(\eta_K^{*,a.h.})^2 = \|g_1 - (\omega_1)_{h,r}^{\text{opt}}\|_K^2 + \|g_2 - (\omega_2)_{h,r}^{\text{opt}}\|_K^2 .$$

11.5. **Efficiency of the explicit error estimator.** Before proving Theorem 11.1, we require the following lemma which readily follows from the many identities proved in [14, Section 2].

Lemma 11.1. Let $\tau \in H(\text{div}, \mathcal{T})$ and $v \in H^1(\mathcal{T})$. Then

(11.10)
$$\sup_{\hat{u}\in H_{\mathbf{r}}^{1/2}(\mathcal{S})} \frac{\langle \hat{u}, \boldsymbol{\tau} \cdot \hat{\boldsymbol{n}} \rangle_{\partial \mathcal{T}}^2}{\|\hat{u}\|_{H^{1/2}(\partial \mathcal{T})}^2} = \sup_{u\in H_{\mathbf{D}}^1(\Omega)} \frac{\langle \operatorname{tr}_{\mathrm{grad}}^{\partial \mathcal{T}} u, \boldsymbol{\tau} \cdot \hat{\boldsymbol{n}} \rangle_{\partial \mathcal{T}}^2}{\|u\|_{H^1(\Omega)}^2}$$

and

(11.11)
$$\sup_{\hat{\sigma} \in H_{N}^{-1/2}(\mathcal{S})} \frac{\langle \hat{\sigma}, v \rangle_{\partial \mathcal{T}}^{2}}{\|\hat{\sigma}\|_{H^{-1/2}(\partial \mathcal{T})}^{2}} = \sup_{\boldsymbol{\sigma} \in \boldsymbol{H}_{N}(\operatorname{div}, \Omega)} \frac{\langle \operatorname{tr}_{\operatorname{div}}^{\partial \mathcal{T}} \boldsymbol{\sigma}, v \rangle_{\partial \mathcal{T}}^{2}}{\|\boldsymbol{\sigma}\|_{\boldsymbol{H}(\operatorname{div}, \Omega)}^{2}}.$$

Theorem 11.1. Assume that $\Omega \subseteq \mathbb{R}^3$ is convex and let \mathcal{T} be an associated partition of Ω . Assume that $\overline{\Gamma_D \cup \Gamma_N} = \partial \Omega$ and $\Gamma_D \cap \Gamma_N = \emptyset$ are relatively open in $\partial \Omega$ and $\Gamma_D \neq \emptyset$. Define \mathcal{F}_N and \mathcal{F}_D to be the sets of faces in \mathcal{T} excluding those in common with Γ_D and Γ_N , respectively, and take \mathcal{U}_h to be a closed subset of \mathcal{U} . As above, let

$$b(\mathbf{u}, \mathbf{v}) = (u, \operatorname{div}_{\tau} \boldsymbol{\tau})_{\Omega} + (\boldsymbol{\sigma}, \boldsymbol{\tau} + \operatorname{grad}_{\tau} v)_{\Omega} - \langle \hat{u}, \boldsymbol{\tau} \cdot \hat{\boldsymbol{n}} \rangle_{\partial \tau} - \langle \hat{\sigma}, v \rangle_{\partial \tau}$$

and

$$g(\mathfrak{u}) = (g_1, u)_{\Omega} + (\boldsymbol{g}_2, \boldsymbol{\sigma})_{\Omega} + \langle \hat{g}_3, \hat{u} |_{\partial \Omega} \rangle_{\partial \Omega} + \langle \hat{g}_4, \hat{\sigma} |_{\partial \Omega} \rangle_{\partial \Omega},$$

where $g_1 \in L^2(\Omega)$, $g_2 \in L^2(\Omega)$, $\hat{g}_3 \in L^2(\Gamma_N) \subsetneq (H_D^{1/2}(\partial\Omega))'$, and $\hat{g}_4 \in H_0^1(\Gamma_D) \subsetneq (H_N^{-1/2}(\partial\Omega))'$. Here, without loss of generality, we may implicitly assume that \hat{g}_3 and \hat{g}_4 are extended by zero throughout Γ_D and Γ_N , respectively. If $\mathfrak{v}_r = (v_r, \tau_r) \in \mathcal{V}_r \subseteq \mathcal{V}$ satisfies

$$(11.12) b(\mathbf{v}_r, \mathbf{u}_h) = g(\mathbf{u}_h), \quad \forall \, \mathbf{u}_h \in \mathcal{U}_h,$$

then

$$\begin{split} \left\| \mathcal{B}' \boldsymbol{v}_r - g \right\|_{\mathcal{U}'}^2 &\leq \sum_{K \in \mathcal{T}} \left(\left\| \operatorname{div} \boldsymbol{\tau}_r - g_1 \right\|_K^2 + \left\| \boldsymbol{\tau}_r + \operatorname{grad} \boldsymbol{v}_r - \boldsymbol{g}_2 \right\|_K^2 \right) \\ &+ C \sum_{K \in \mathcal{T}} h_K \left(\sum_{F \in \partial K \cap \mathcal{F}_{\mathbf{N}}} \left\| \left\| \boldsymbol{\tau}_r \cdot \hat{\boldsymbol{n}} - \hat{g}_3 \right\| \right\|_F^2 \\ &+ \sum_{F \in \partial K \cap \mathcal{F}_{\mathbf{D}}} \left(\left\| \left\| \boldsymbol{v}_r - \hat{g}_4 \right\| \right\|_F^2 + \left\| \left\| \hat{\boldsymbol{n}} \times \operatorname{grad}_{\partial \mathcal{T}} (\boldsymbol{v}_r - \hat{g}_4) \right\| \right\|_F^2 \right) \right), \end{split}$$

where C > 0 is a constant independent of the mesh diameters h_K and $\operatorname{grad}_{\partial \mathcal{T}} = \prod_{K \in \mathcal{T}} \operatorname{grad}_{\partial K}$ is the surface gradient operator on the mesh boundary.

Remark 11.1. The convexity assumption in Theorem 11.1 can be relaxed at the expense of a possibly larger constant C>0 having an additional dependence on the shape of the domain Ω . This will follow if a decomposition other than (11.17) is used at that step in the proof. In particular, one would require the fact that, for all $\sigma \in H(\text{div})$, there exists $E, \sigma_1 \in H^1(\Omega)$, and $C_1 > 0$ depending on the shape of the domain such that $\sigma = \text{curl } E + \sigma_1$ and $\|E\|_{H^1(\Omega)} + \|\sigma_1\|_{H^1(\Omega)} \le C_1 \|\sigma\|_{H(\text{div})}$ (see [3] for details).

Remark 11.2. Reliability of the explicit estimator defined in Theorem 11.1—that is, a complementary lower bound on the residual of the dual problem $\|\mathcal{B}'\mathbf{v}_r - g\|_{\mathcal{U}'}$ —can be proven with Verfürth's bubble function technique [69]. We have chosen not to include the proof here because it is not absolutely necessary for our analysis.

Proof of Theorem 11.1. Begin by observing that

$$\begin{split} \left\| \mathcal{B}' \mathbf{v}_r - g \right\|_{\mathcal{U}'}^2 &= \left(\sup_{\mathbf{u} \in \mathcal{U}} \frac{b(\mathbf{u}, \mathbf{v}_r) - g(\mathbf{u})}{\|\mathbf{u}\|_{\mathcal{U}}} \right)^2 \\ &= \left(\sup_{u \in L^2(\Omega)} \frac{(u, \operatorname{div}_{\mathcal{T}} \boldsymbol{\tau}_r - g_1)_{\Omega}}{\|u\|_{\Omega}} \right)^2 + \left(\sup_{\boldsymbol{\sigma} \in \boldsymbol{L}^2(\Omega)} \frac{(\boldsymbol{\sigma}, \boldsymbol{\tau}_r + \operatorname{grad}_{\mathcal{T}} v_r - \boldsymbol{g}_2)_{\Omega}}{\|\boldsymbol{\sigma}\|_{\Omega}} \right)^2 \\ &+ \left(\sup_{\hat{u} \in H_{\mathrm{D}}^{1/2}(\mathcal{S})} \frac{\langle \hat{u}, \boldsymbol{\tau}_r \cdot \hat{\boldsymbol{n}} - \hat{g}_3 \rangle_{\partial \mathcal{T}}}{\|\hat{u}\|_{H^{1/2}(\partial \mathcal{T})}} \right)^2 + \left(\sup_{\hat{\sigma} \in H_{\mathrm{N}}^{-1/2}(\mathcal{S})} \frac{\langle \hat{\sigma}, v_r - \hat{g}_4 \rangle_{\partial \mathcal{T}}}{\|\hat{\sigma}\|_{H^{-1/2}(\partial \mathcal{T})}} \right)^2. \end{split}$$

Indeed, this is a simple consequence of Lemma 3.1. We will now deal with each term in the expression above, individually.

Notice that

$$\sup_{u \in L^2(\Omega)} \frac{(u, \operatorname{div}_{\tau} \boldsymbol{\tau}_r - g_1)_{\Omega}^2}{\|u\|_{\Omega}^2} = \|\operatorname{div}_{\tau} \boldsymbol{\tau}_r - g_1\|_{\Omega}^2 = \sum_{K \in \mathcal{T}} \|\operatorname{div} \boldsymbol{\tau}_r - g_1\|_{K}^2$$

and

$$\sup_{\boldsymbol{\sigma} \in \boldsymbol{L}^2(\Omega)} \frac{(\boldsymbol{\sigma}, \boldsymbol{\tau}_r + \operatorname{grad}_{\mathcal{T}} v_r - \boldsymbol{g}_2)_{\Omega}^2}{\|\boldsymbol{\sigma}\|_{\Omega}^2} = \left\|\boldsymbol{\tau}_r + \operatorname{grad}_{\mathcal{T}} v_r - \boldsymbol{g}_2\right\|_{\Omega}^2 = \sum_{K \in \mathcal{T}} \left\|\boldsymbol{\tau}_r + \operatorname{grad} v_r - \boldsymbol{g}_2\right\|_K^2.$$

We are now left with only the last two terms which are far more delicate to handle.

Let $(u, \sigma, \hat{u}, \hat{\sigma}) \in \mathcal{U}$ and $(u_h, \sigma_h, \hat{u}_h, \hat{\sigma}_h) \in \mathcal{U}_h$ be arbitrary. Invoking (11.12), notice that

$$(11.13) \quad \langle \hat{u}, \boldsymbol{\tau}_r \cdot \hat{\boldsymbol{n}} - \hat{g}_3 \rangle_{\partial \tau} = \langle \hat{u} - \hat{u}_h, \boldsymbol{\tau}_r \cdot \hat{\boldsymbol{n}} - \hat{g}_3 \rangle_{\partial \tau} \quad \text{and} \quad \langle \hat{\sigma}, v_r - \hat{g}_4 \rangle_{\partial \tau} = \langle \hat{\sigma} - \hat{\sigma}_h, v_r - \hat{g}_4 \rangle_{\partial \tau}.$$

Because $(\hat{u} - \hat{u}_h)|_{\partial K} \in L^2(\partial K)$, for all $K \in \mathcal{T}$, we see that

$$(11.14) \quad \langle \hat{u} - \hat{u}_h, \boldsymbol{\tau}_r \cdot \hat{\boldsymbol{n}} - \hat{g}_3 \rangle_{\partial \mathcal{T}} = \sum_{K \in \mathcal{T}} (\hat{u} - \hat{u}_h, [\![\boldsymbol{\tau}_r \cdot \hat{\boldsymbol{n}} - \hat{g}_3]\!])_{\partial K} \lesssim \sum_{F \in \mathcal{F}_N} \|\hat{u} - \hat{u}_h\|_F \|[\![\boldsymbol{\tau}_r \cdot \hat{\boldsymbol{n}} - \hat{g}_3]\!]\|_F,$$

where $[\![\cdot]\!]$ denotes the inter-element jump across the mesh \mathcal{T} and \mathcal{F}_N denotes the set of faces in the mesh excluding those in common with Γ_D , where \hat{u} and \hat{u}_h vanish. Using a Clément interpolation operator, $\mathcal{I}: u \mapsto u_h$, where $(0,0,\operatorname{tr}_{\operatorname{grad}}^{\partial\mathcal{T}}u_h,0) \in \mathcal{U}_h$, it can be shown that $\|\operatorname{tr}_{\operatorname{grad}}^{\partial K}(\widetilde{u}-\mathcal{I}\widetilde{u})\|_F \lesssim h_K^{1/2}\|\widetilde{u}\|_{H^1(\widetilde{K})}$, for any face F of an element $K \in \mathcal{T}$, where $\widetilde{u} \in H^1(\Omega)$ is an extension of \widehat{u} , and \widetilde{K} is the patch of elements associated with the element K [9]. Therefore, by (11.10), (11.13), and (11.14),

$$\sup_{\hat{u}\in H^{1/2}_{\Gamma_{D}}(\mathcal{S})} \frac{\langle \hat{u}, \boldsymbol{\tau}_{r} \cdot \hat{\boldsymbol{n}} - \hat{g}_{3} \rangle_{\partial \mathcal{T}}^{2}}{\|\hat{u}\|_{H^{1/2}(\partial \mathcal{T})}^{2}} = \sup_{u\in H^{1}_{\Gamma_{D}}(\Omega)} \frac{\langle \operatorname{tr}_{\mathrm{grad}}^{\partial \mathcal{T}}(u - \mathcal{I}u), \boldsymbol{\tau}_{r} \cdot \hat{\boldsymbol{n}} - \hat{g}_{3} \rangle_{\partial \mathcal{T}}^{2}}{\|u\|_{H^{1}(\Omega)}^{2}}$$

$$\lesssim \sup_{u\in H^{1}_{\Gamma_{D}}(\Omega)} \sum_{F\in\mathcal{F}_{N}} \frac{\|\operatorname{tr}_{\mathrm{grad}}^{\partial \mathcal{T}}(u - \mathcal{I}u)\|_{F}^{2} \|[\boldsymbol{\tau}_{r} \cdot \hat{\boldsymbol{n}} - \hat{g}_{3}]\|_{F}^{2}}{\|u\|_{H^{1}(\Omega)}^{2}}$$

$$\lesssim \sup_{u\in H^{1}_{\Gamma_{D}}(\Omega)} \sum_{K\in\mathcal{T}} \sum_{F\in\partial K\cap\mathcal{F}_{N}} \frac{h_{K}\|u\|_{H^{1}(\widetilde{K})}^{2} \|[\boldsymbol{\tau}_{r} \cdot \hat{\boldsymbol{n}} - \hat{g}_{3}]\|_{F}^{2}}{\|u\|_{H^{1}(\Omega)}^{2}}$$

$$\leq \sum_{K\in\mathcal{T}} h_{K} \sum_{F\in\partial K\cap\mathcal{F}_{N}} \|[\boldsymbol{\tau}_{r} \cdot \hat{\boldsymbol{n}} - \hat{g}_{3}]\|_{F}^{2}.$$

$$(11.15)$$

Finally, we consider the term

(11.16)
$$\sup_{\hat{\sigma} \in H_{\mathbf{N}}^{-1/2}(\mathcal{S})} \frac{\langle \hat{\sigma}, v_r - \hat{g}_4 \rangle_{\partial \mathcal{T}}^2}{\|\hat{\sigma}\|_{H^{1/2}(\partial \mathcal{T})}^2} = \sup_{\boldsymbol{\sigma} \in \boldsymbol{H}_{\mathbf{N}}(\operatorname{div}, \Omega)} \frac{\langle \operatorname{tr}_{\operatorname{div}}^{\partial \mathcal{T}} \boldsymbol{\sigma} - \hat{\sigma}_h, v_r - \hat{g}_4 \rangle_{\partial \mathcal{T}}^2}{\|\boldsymbol{\sigma}\|_{\boldsymbol{H}(\operatorname{div}, \Omega)}^2},$$

where, by Galerkin orthogonality (11.13), $\hat{\sigma}_h$ is arbitrary, as above. Because we *cannot* claim that $\operatorname{tr}_{\operatorname{div}}^{\partial \mathcal{T}} \sigma|_{\partial K}$ is in $L^2(\partial K)$, the treatment of this term is more delicate than before. We choose to begin by considering the decomposition

(11.17)
$$\boldsymbol{H}_{N}(\operatorname{div},\Omega) = \boldsymbol{H}_{N,0}(\operatorname{div},\Omega) \oplus \boldsymbol{H}_{N,1}(\operatorname{div},\Omega),$$

where

$$\boldsymbol{H}_{N,0}(\operatorname{div},\Omega) = \{ \boldsymbol{\sigma}_0 \in \boldsymbol{H}_N(\operatorname{div},\Omega) \mid \operatorname{div} \boldsymbol{\sigma}_0 = 0 \}$$

and

$$\boldsymbol{H}_{\mathrm{N},1}(\mathrm{div},\Omega) = \{ \boldsymbol{\sigma}_1 \in \boldsymbol{H}_{\mathrm{N}}(\mathrm{div},\Omega) \mid (\boldsymbol{\sigma}_1,\boldsymbol{\sigma}_0)_{\Omega} = 0 \ \forall \boldsymbol{\sigma}_0 \in \boldsymbol{H}_{\mathrm{N},0}(\mathrm{div},\Omega) \}.$$

Now, in three spatial dimensions, it can be shown [53] that $\mathbf{H}_{N,0}(\operatorname{div},\Omega) \subseteq \operatorname{curl}(\mathcal{H}(\Omega))$, where

$$\boldsymbol{\mathcal{H}}(\Omega) = \left\{\boldsymbol{E} \in \boldsymbol{H}(\operatorname{curl},\Omega) \cap \boldsymbol{H}(\operatorname{div},\Omega) \mid \operatorname{div} \boldsymbol{E} = 0 \, \wedge \, \operatorname{tr}_{\operatorname{div}}^{\partial\Omega} \boldsymbol{E} = 0 \, \wedge \, \operatorname{tr}_{\operatorname{curl},\dashv}^{\partial\Omega} \boldsymbol{E}|_{\Gamma_{\mathrm{N}}} = 0\right\},$$

where $\operatorname{tr}_{\operatorname{curl},\dashv}^{\partial\Omega} E = \hat{\boldsymbol{n}} \times \boldsymbol{E}|_{\partial\Omega}$. Meanwhile, it can be shown that $\boldsymbol{H}_{N,1}(\operatorname{div},\Omega) \subseteq \boldsymbol{H}^1(\Omega)$, where $\boldsymbol{H}^1(\Omega) = (H^1(\Omega))^3$. Likewise, because Ω is convex with Lipschitz boundary, it can be shown that $\boldsymbol{\mathcal{H}}(\Omega) \subseteq \boldsymbol{H}^1(\Omega)$. Using this decomposition, we can separate the right-hand side of (11.16) into two terms:

$$\begin{split} \sup_{\boldsymbol{\sigma} \in \boldsymbol{H}_{\mathrm{N}}(\mathrm{div},\Omega)} \frac{\langle \mathrm{tr}_{\mathrm{div}}^{\partial \mathcal{T}} \boldsymbol{\sigma} - \hat{\sigma}_{h}, v_{r} - \hat{g}_{4} \rangle_{\partial \mathcal{T}}^{2}}{\|\boldsymbol{\sigma}\|_{\boldsymbol{H}(\mathrm{div},\Omega)}^{2}} &= \sup_{\boldsymbol{\sigma}_{0} \in \boldsymbol{H}_{\mathrm{N},0}(\mathrm{div},\Omega)} \frac{\langle \mathrm{tr}_{\mathrm{div}}^{\partial \mathcal{T}} \boldsymbol{\sigma}_{0} - \hat{\sigma}_{h}, v_{r} - \hat{g}_{4} \rangle_{\partial \mathcal{T}}^{2}}{\|\boldsymbol{\sigma}_{0}\|_{\boldsymbol{H}(\mathrm{div},\Omega)}^{2}} \\ &+ \sup_{\boldsymbol{\sigma}_{1} \in \boldsymbol{H}_{\mathrm{N},1}(\mathrm{div},\Omega)} \frac{\langle \mathrm{tr}_{\mathrm{div}}^{\partial \mathcal{T}} \boldsymbol{\sigma}_{0} - \hat{\sigma}_{h}, v_{r} - \hat{g}_{4} \rangle_{\partial \mathcal{T}}^{2}}{\|\boldsymbol{\sigma}_{1}\|_{\boldsymbol{H}(\mathrm{div},\Omega)}^{2}} \,. \end{split}$$

Let $\mathcal{I}: \sigma_1 \mapsto \sigma_h$ be a new Clément interpolation operator where $(0,0,0,\operatorname{tr}_{\operatorname{div}}^{\partial \tau}\sigma_h) \in \mathcal{U}_h$. Considering the second term first, we find

$$\sup_{\boldsymbol{\sigma}_{1} \in \boldsymbol{H}_{\mathrm{N},1}(\mathrm{div},\Omega)} \frac{\left\langle \operatorname{tr}_{\mathrm{div}}^{\partial \mathcal{T}}(\boldsymbol{\sigma}_{1} - \boldsymbol{\mathcal{I}}\boldsymbol{\sigma}_{1}), v_{r} - \hat{g}_{4}\right\rangle_{\partial \mathcal{T}}}{\|\boldsymbol{\sigma}_{1}\|_{\boldsymbol{H}(\mathrm{div},\Omega)}} \leq \sup_{\substack{\boldsymbol{\sigma}_{1} \in \boldsymbol{H}^{1}(\Omega) \\ \operatorname{tr}_{\mathrm{div}}^{\partial \Omega} \boldsymbol{\sigma}_{1}|_{\Gamma_{\mathrm{N}}} = 0}} \frac{\left\langle \operatorname{tr}_{\mathrm{div}}^{\partial \mathcal{T}}(\boldsymbol{\sigma}_{1} - \boldsymbol{\mathcal{I}}\boldsymbol{\sigma}_{1}), v_{r} - \hat{g}_{4}\right\rangle_{\partial \mathcal{T}}}{\|\boldsymbol{\sigma}_{1}\|_{\boldsymbol{H}^{1}(\Omega)}}$$
$$\lesssim \sum_{K \in \mathcal{T}} h_{K} \sum_{F \in \partial K \cap \mathcal{F}_{\mathrm{D}}} \left\| \left[v_{r} - \hat{g}_{4}\right]\right\|_{F}^{2},$$

where the second inequality is developed similar to (11.15).

Let $\widetilde{g}_4 \in H^1(\Omega)$ be an arbitrary extension of the function $\widehat{g}_4 \in H^1(\partial\Omega)$ into the domain Ω and define $\operatorname{tr}_{\operatorname{curl},\top}^{\partial \tau} = \prod_{K \in \mathcal{T}} \operatorname{tr}_{\operatorname{curl},\top}^{\partial K}$, where $\operatorname{tr}_{\operatorname{curl},\top}^{\partial K} \boldsymbol{E} = (\hat{\boldsymbol{n}} \times \boldsymbol{E}|_{\partial K}) \times \hat{\boldsymbol{n}}$. Then the remaining term delivers

$$\sup_{\boldsymbol{\sigma}_{0} \in \boldsymbol{H}_{N,0}(\operatorname{div},\Omega)} \frac{\langle \operatorname{tr}_{\operatorname{div}}^{\partial \tau} \boldsymbol{\sigma}_{0}, v_{r} - \hat{g}_{4} \rangle_{\partial \tau}^{2}}{\|\boldsymbol{\sigma}_{0}\|_{\boldsymbol{H}(\operatorname{div},\Omega)}^{2}} = \sup_{\boldsymbol{\sigma}_{0} \in \boldsymbol{H}_{N,0}(\operatorname{div},\Omega)} \frac{\left((\boldsymbol{\sigma}_{0}, \operatorname{grad}_{\tau}(v_{r} - \tilde{g}_{4}))_{\Omega} - (\operatorname{div}\boldsymbol{\sigma}_{0}, v_{r} - \tilde{g}_{4})_{\Omega}^{2}}{\|\boldsymbol{\sigma}_{0}\|_{\boldsymbol{H}(\operatorname{div},\Omega)}^{2}}$$

$$= \sup_{\boldsymbol{E} \in \mathcal{H}(\Omega)} \frac{\left(\operatorname{curl}\boldsymbol{E}, \operatorname{grad}_{\tau}(v_{r} - \tilde{g}_{4})\right)_{\Omega}^{2}}{\|\operatorname{curl}\boldsymbol{E}\|_{\Omega}^{2}}$$

$$= \sup_{\boldsymbol{E} \in \mathcal{H}(\Omega)} \frac{\langle \operatorname{tr}_{\operatorname{curl}, \top}^{\partial \tau}\boldsymbol{E}, \hat{\boldsymbol{n}} \times \operatorname{grad}_{\partial \tau}(v_{r} - \hat{g}_{4})\rangle_{\partial \tau}}{\|\operatorname{curl}\boldsymbol{E}\|_{\boldsymbol{H}(\operatorname{curl},\Omega)}^{2}}$$

$$\lesssim \sup_{\boldsymbol{E} \in \mathcal{H}^{1}(\Omega)} \frac{\langle \operatorname{tr}_{\operatorname{curl}, \top}^{\partial \tau}\boldsymbol{E}, \hat{\boldsymbol{n}} \times \operatorname{grad}_{\partial \tau}(v_{r} - \hat{g}_{4})\rangle_{\partial \tau}}{\|\boldsymbol{E}\|_{\boldsymbol{H}(\operatorname{curl},\Omega)}^{2}}$$

$$\lesssim \sup_{\boldsymbol{E} \in \mathcal{H}^{1}(\Omega)} \frac{\langle \operatorname{tr}_{\operatorname{curl}, \top}^{\partial \tau}\boldsymbol{E}, \hat{\boldsymbol{n}} \times \operatorname{grad}_{\partial \tau}(v_{r} - \hat{g}_{4})\rangle_{\partial \tau}}{\|\boldsymbol{E}\|_{\boldsymbol{H}^{1}(\Omega)}^{2}}$$

$$= \sup_{\boldsymbol{E} \in \mathcal{H}^{1}(\Omega)} \sum_{\operatorname{tr}_{\operatorname{curl}, \top}^{\partial \Omega}} \sum_{\boldsymbol{E} \in \mathcal{T}} \frac{\langle \boldsymbol{E}, \hat{\boldsymbol{n}} \times \operatorname{grad}_{\partial \boldsymbol{K}}(v_{r} - \hat{g}_{4})\rangle_{\partial \boldsymbol{K}}}{\|\boldsymbol{E}\|_{\boldsymbol{H}^{1}(\Omega)}^{2}}.$$

Likewise,

$$\sup_{\boldsymbol{\sigma}_{0} \in \boldsymbol{H}_{\mathrm{N},0}(\mathrm{div},\Omega)} \frac{\langle \mathrm{tr}_{\mathrm{div}}^{\partial \mathcal{T}} \boldsymbol{\sigma}_{0}, v_{r} - \hat{g}_{4} \rangle_{\partial \mathcal{T}}^{2}}{\|\boldsymbol{\sigma}_{0}\|_{\boldsymbol{H}(\mathrm{div},\Omega)}^{2}} \lesssim \sup_{\substack{\boldsymbol{E} \in \boldsymbol{H}^{1}(\Omega) \\ \mathrm{tr}_{\mathrm{curl},\dashv}^{\partial \Omega} \boldsymbol{E}|_{\Gamma_{\mathrm{N}}}}} \sum_{K \in \mathcal{T}} \frac{(\boldsymbol{E} - \boldsymbol{\mathcal{I}} \boldsymbol{E}, \hat{\boldsymbol{n}} \times \mathrm{grad}_{\partial K}(v_{r} - \hat{g}_{4}))_{\partial K}}{\|\boldsymbol{E}\|_{\boldsymbol{H}^{1}(\Omega)}^{2}}$$
$$\lesssim \sum_{K \in \mathcal{T}} h_{K} \sum_{F \in \partial K \cap \mathcal{F}_{\mathrm{D}}} \left\| \left[\hat{\boldsymbol{n}} \times \mathrm{grad}_{\partial K}(v_{r} - \hat{g}_{4}) \right] \right\|_{F}^{2}.$$

12. NUMERICAL EXPERIMENTS

Throughout this section, we demonstrate the efficacy of goal-oriented adaptive mesh refinement (GMR) using the refinement indicators for the DPG and DPG* problems presented in Section 7 and Sections 8–10, respectively. All experiments pertain to the broken ultraweak formulation of Poisson's boundary value problem presented in Section 11.2 with quantities of interest of the form discussed in Section 11.3. Thereupon, recall that $\mathbf{u} = (u, \boldsymbol{\sigma}, \hat{u}, \hat{\sigma}) \in \mathcal{U}$ and $\mathbf{v} = (v, \boldsymbol{\tau}) \in \mathcal{V}$, $\eta_K = \|\mathcal{B}\mathbf{u}_{h,r}^{\text{opt}} - \ell\|_{\mathcal{V}_{K,r}'}$, and η_K^* is defined in (11.6), (11.8), and (11.9), depending on the specific indicator type.

12.1. **Set-up.** To compare the GMR algorithms with the conventional solution-adaptive mesh refinement (SMR) algorithm, we used a manufactured solution with separate and isolated steep and shallow gradients in a convex domain $\Omega = [0,4] \times [0,1] \times [0,1]$ (see Figure 12.2 (a)). The exact expression for this manufactured solution, $u^{\star} = u^{\text{man}} \in C_0^{\infty}(\Omega)$, is given by

(12.1)
$$u^{\text{man}}(x, y, z) = f(x/4)f(y)f(z)$$
, where $f(x) = x(1-x)((x/4) + (1-4x)^2)$.

The remaining components of $\mathbf{u}^* = (u^*, \boldsymbol{\sigma}^*, \hat{u}^*, \hat{\sigma}^*)$ can easily be derived from the expression above.

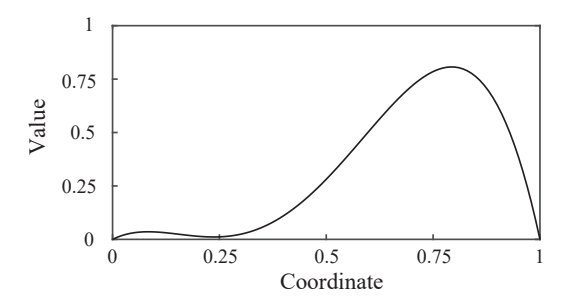


FIGURE 12.1. Graph of the function f(x) in (12.1).

With such a solution, the expected behavior of an SMR strategy is to induce the majority of mesh refinements in the region with the highest gradients in the solution. That is, where the length scale of the solution is the smallest and the solution is the most difficult to resolve. This behavior is illustrated in Figures 12.2 (a)–(c) with the manufactured solution given in (12.1).

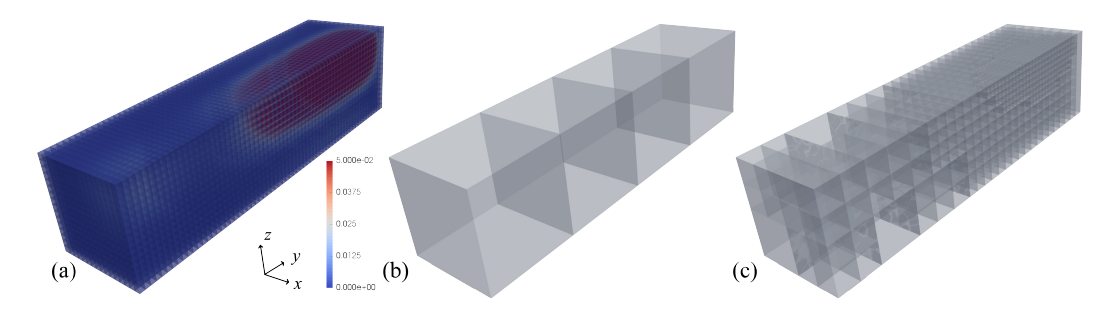


FIGURE 12.2. (a) Converged solution; (b) initial mesh; (c) mesh after twelve SMRs.

Now, consider a goal functional $g \in \mathcal{U}'$ defined in terms of the solution in a region far away from the largest solution gradients. In this circumstance, for a fixed computational expenditure, it is conceivable that the best possible approximate QoI, $g(\mathbf{u}_h)$, would require a mesh with a refinement pattern very different than one coming from a standard series of SMRs. The following results will verify this conjecture and the utility of our GMR strategies.

12.2. **Experimental design.** Beginning with the four-element mesh depicted in Figure 12.2 (a), we analyzed four different QoIs with goal functionals of the type considered in (11.5) and one pointwise-value QoI (see Section 12.7). In our experiments, $g_1 \in L^2(\Omega)$, $g_2 \in L^2(\Omega)$, $\hat{g}_3 \in L^2(\Gamma_N)$, and $\hat{g}_4 \in H^1_0(\Gamma_D)$ are each piecewise polynomial. Here, is it convenient to express $g \in \mathcal{U}$ as

(12.2)
$$g(\mathbf{u}) = \int_{\Omega} g_1 \cdot u + \int_{\Omega} \mathbf{g}_2 \cdot \boldsymbol{\sigma} + \int_{\Gamma_{\mathcal{N}}} \hat{g}_3 \cdot \hat{u} + \int_{\Gamma_{\mathcal{D}}} \hat{g}_4 \cdot \hat{\sigma}, \quad \forall \, \mathbf{u} = (u, \boldsymbol{\sigma}, \hat{u}, \hat{\sigma}) \in \mathcal{U}.$$

Because the ad hoc indicator $\eta_K^{*,\mathrm{a.h.}}$, given in Section 10, is not suitable for goal functionals with nonzero boundary contributions, we used a sequence of modified goal functionals when $g(\mathfrak{u})$ involved nonzero \hat{g}_3 or nonzero \hat{g}_4 (see Sections 12.5 and 12.6). In Section 12.7, an extension of this technique is presented for a pointwise-value QoI, $g_{\widetilde{\mathbf{x}}}(\mathfrak{u}) = u(\widetilde{\mathbf{x}})$.

All of our computations were performed with the finite element software hp3D which has complete 3D support for local hierarchical anisotropic h and p refinements with one level of hanging nodes [22,31] and shape functions for all standard elements conforming in each of the canonical 3D exact sequence energy spaces [38]:

$$H^1(K) \xrightarrow{\operatorname{grad}} \boldsymbol{H}(\operatorname{curl}, K) \xrightarrow{\operatorname{curl}} \boldsymbol{H}(\operatorname{div}, K) \xrightarrow{\operatorname{div}} L^2(K)$$
.

In our third experiment (Section 12.5), non-homogeneous Neumann boundary conditions were applied to a non-trivial subset of the boundary $\Gamma_N \subseteq \partial \Omega$. In order to apply this essential boundary condition to the $\hat{\sigma}$ -variable, we used projection-based interpolation [23]. In each of the energy space above, this is a fully-supported feature of the hp3D software.

To implement the practical DPG and DPG* methods, (4.5) and (4.6), corresponding to the ultraweak form of Poisson's boundary value problem (11.2), polynomial discretizations of \mathcal{U}_h and \mathcal{V}_r were inferred from previous studies [36, 37, 47, 49]. For the discrete trial space \mathcal{U}_h , $L^2(\Omega)$ and $L^2(\Omega)$ were taken from a fixed p-order exact sequence. Meanwhile, the interface spaces $H^{1/2}(\partial \mathcal{T})$ and $H^{-1/2}(\partial \mathcal{T})$, were discretized by the H^1 - and H(div)-elementwise traces of the $H^1(\Omega)$ - and $H(\text{div},\Omega)$ -conforming shape functions from the same fixed p-order exact sequence. Roughly speaking, our assembly of the trace variables \hat{u} and $\hat{\sigma}$ follows established procedure in their respective energy spaces, with the additional extra step of removing the interior bubbles from the final stiffness matrix (see [27, Section 5]). Finally, for the discrete test space \mathcal{V}_r , discretizations of $H^1(\mathcal{T})$ and $H(\text{div},\mathcal{T})$ were taken from a fixed, non-conforming and enriched (p+dp)-order exact sequence.

For a careful account of DPG assembly algorithms, see [63] and [49, Section 4]. Notably, we constructed the normal equation [49, Section 4.1]. In the DPG* setting, the stiffness matrix is identical and so, on any one mesh, only a single assembly and factorization of the DPG stiffness matrix was ever performed to solve for both $\mathbf{u}_{h,r}^{\text{opt}}$ and $\mathbf{v}_{h,r}^{\text{opt}}$.

Parameters. Before finally presenting the results of our experiments, we now list the outstanding parameters in our algorithms and our choices for them:

- Discretizations of the trial space \mathcal{U}_h and the test space \mathcal{V}_r came from an exact sequence of polynomial order p=2 and $p+\mathrm{d}p=3$, respectively. Note that the polynomial order of the manufactured solution (12.1) is too high for it to be exactly recovered with this trial space discretization.
- In the implicit refinement indicator $\eta_K^{*,\mathrm{impl}}$, the local problems (11.7) were solved on individual elements from the same mesh as the global DPG and DPG* problems. Here, the enriched trial space \mathcal{U}_H and further enriched test space \mathcal{V}_R were constructed just as described above for \mathcal{U}_h and \mathcal{V}_r , but with exact sequences of polynomial order P=p+1=3 and $P+\mathrm{d}p=4$, respectively.
- For the test space, the adjoint graph norm (11.3) was used, $\|\cdot\|_{\mathcal{V}} = \|\cdot\|_{\mathcal{L}^*,\alpha}$, with $\alpha = 1$.
- The refinement factor of $\theta = 0.5$ was set for both the SMR and GMR marking strategies (see Section 6.2).

12.3. **Temperature in a subdomain.** In this subsection, we consider the goal functional given in (12.2) where

(12.3)
$$g_1(x, y, z) = \begin{cases} 1, & x \le 1, \\ 0, & \text{otherwise,} \end{cases}$$
 $g_2 = \mathbf{0}, \quad \hat{g}_3 = 0, \quad \text{and} \quad \hat{g}_4 = 0.$

Physically, this corresponds to a QoI which is the average value of the temperature u in the subdomain $0 \le x \le 1$. In our experiments, we used homogeneous Dirichlet boundary conditions, $u|_{\partial\Omega} = 0$, when studying this QoI.

12.3.1. Results. Define the relative error in the QoI to be $|g(\mathfrak{u}^{\star} - \mathfrak{u}_{h,r}^{\text{opt}})|/|g(\mathfrak{u}^{\star})|$. In Figure 12.3 (a), we present the relative error vs. the degrees of freedom in each successive solution as the mesh was refined using each AMR strategy. Here, it is immediately evident that each GMR step was far more efficient at reducing the relative error in the QoI than each SMR step. Moreover, taking into account their entire sequence of refinements, each GMR strategy performed nearly equally, until nearly the final refinement.

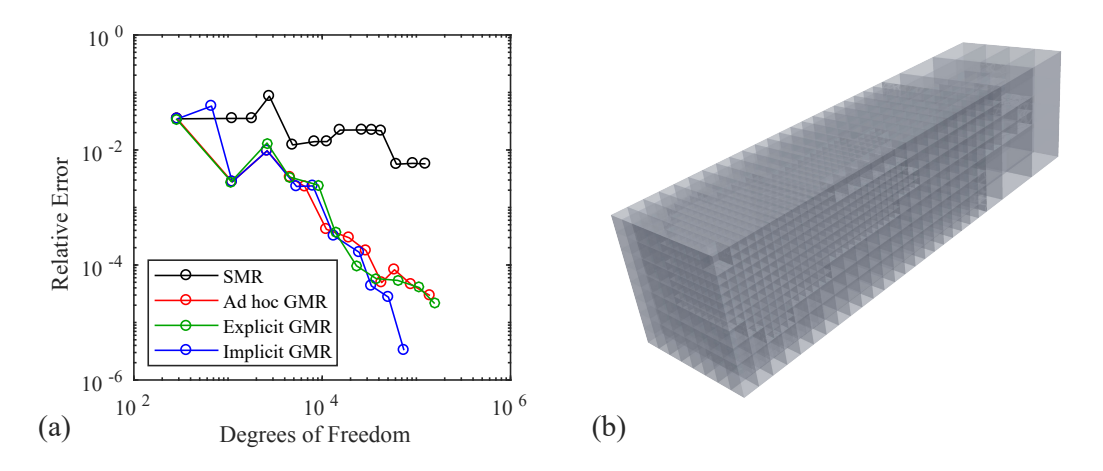


FIGURE 12.3. (a) The error in the QoI for the first example: average temperature u; (b) the final adaptively refined mesh using the ad hoc GMR approach.

In Figure 12.3 (b), we see the final refined mesh after twelve adaptive mesh refinements with the GMR marking strategy and the ad hoc refinement indicator $\eta_K^{*,\mathrm{a.h.}}$. However, because there are two other classes of DPG* refinement indicators which preformed well for this problem and QoI, Figure 12.4 is provided to compare all three corresponding final solution and meshes. Here, it is visibly evident that the final meshes are extremely similar, but significantly different from the SMR mesh in Figure 12.2 (c). A strong visual similarity in the final GMR meshes was also exhibited in each of the later studies. Therefore, from now on, we will only provide one representative GMR mesh for illustration.

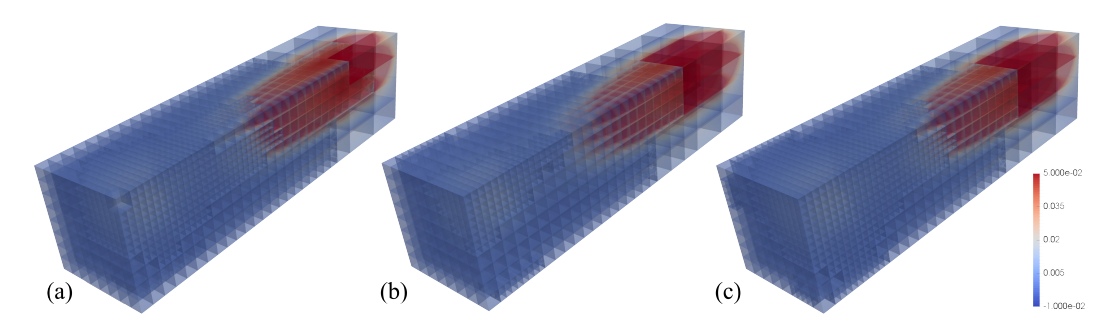


FIGURE 12.4. The solution after twelve GMR steps using the: (a) ad hoc approach; (b) explicit approach; (c) implicit approach.

Finally, we provide Figure 12.5 for a visual depiction of the local temperature error in the region $0 \le x \le 1$. In some contexts, a goal functional of the form (12.3) is chosen to drive adaptivity with the intention of significantly

reducing the error in a particular solution variable—in this case, it is the temperature u—in a region of interest. Although this can also be done more accurately by considering a nonlinear goal functional [57], simply using GMR with a closely related linear QoI often provides a sufficient improvement. With this understanding, Figure 12.5 clearly demonstrates that, the total error in the temperature variable u in the region of interest, is far lower as a result of the GMRs as opposed to the conventional SMR for a similar number of degrees of freedom. In Figure 12.5 (b), we have only visualized the error from the ad hoc approach, however, the results from the other two approaches were nearly indistinguishable in comparison.

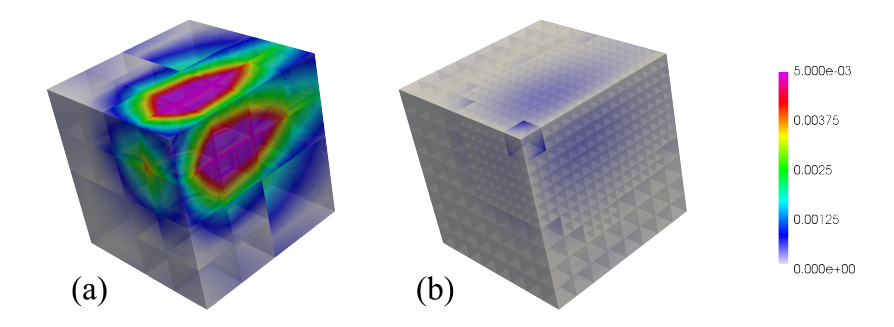


FIGURE 12.5. The error in the solution component u in $0 \le x \le 1$ at the final mesh using: (a) conventional SMR; (b) GMR with the ad hoc refinement indicators $\eta_K^{*,\mathrm{a.h.}}$ for the DPG* problem.

12.3.2. The influence function. It is worth remarking, once again, that the ad hoc refinement indicator $\eta^{*,a.h.}$ can not even be expected to converge to zero asymptotically. Therefore, the success of the DPG* refinement indicator $\eta_K^{*,proj}$ in a goal-oriented AMR strategy depends upon the quality of resolution of the optimal test functions and the difference between the optimal test norm and the norm chosen for computation.

Recall that $g_1=1$, if $x\leq 1$, and $g_1=0$, otherwise, while ${\boldsymbol g}_2={\boldsymbol 0}$ everywhere. Our driving assumption in Section 10 is that $(\omega_1,{\boldsymbol \omega}_2)\approx (g_1,{\boldsymbol g}_2)$ when using the adjoint graph norm instead of the optimal test norm. The affirmative results in Figure 12.3 (a) indicate that this assumption was reasonably valid for this problem. Figure 12.6 is also provided to further justify this conclusion. Here, the ω_1 -component of the approximated influence function ${\boldsymbol \omega}_{h,r}^{\rm opt}$ is visualized on both the initial and final mesh. Clearly, even when computing on the initial mesh, which had only four elements, the difference between the computed ω_1 and its idealized value, $\omega_1 \stackrel{\star}{=} g_1$, was only marginal.

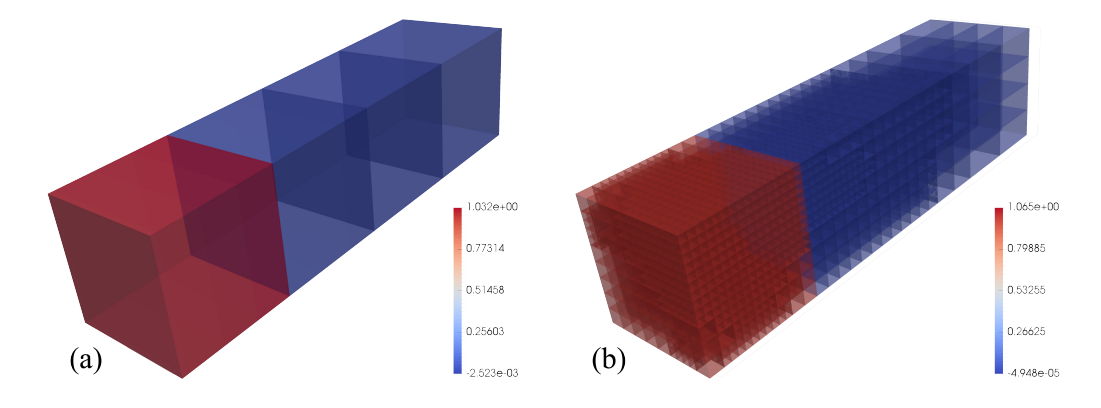


FIGURE 12.6. The influence function ω_1 for: (a) the initial mesh; (b) final adaptively refined mesh using the ad hoc GMR approach.

12.4. Flux in a subdomain. In this subsection, we consider the goal functional given in (12.2) where

(12.4)
$$g_1 = 0$$
, $g_2(x, y, z) = \begin{cases} (1, 0, 0)^\mathsf{T}, & x \le 1, \\ \mathbf{0}, & \text{otherwise,} \end{cases}$ $\hat{g}_3 = 0$, and $\hat{g}_4 = 0$.

Physically, this corresponds to a QoI which is the average value of the x-component of the flux, σ_x , in the subdomain $0 \le x \le 1$. In our experiments, homogeneous Dirichlet boundary conditions, $u|_{\partial\Omega} = 0$, were used when studying this QoI.

Define the relative error in the QoI to be $|g(\mathbf{u}^* - \mathbf{u}_{h,r}^{\text{opt}})|/|g(\mathbf{u}^*)|$. As in the previous study, we present the relative error in this QoI with each of the AMR strategies. Again, by inspecting Figure 12.7 (a), it is clear that each of the GMR strategies are far more efficient than conventional SMR.

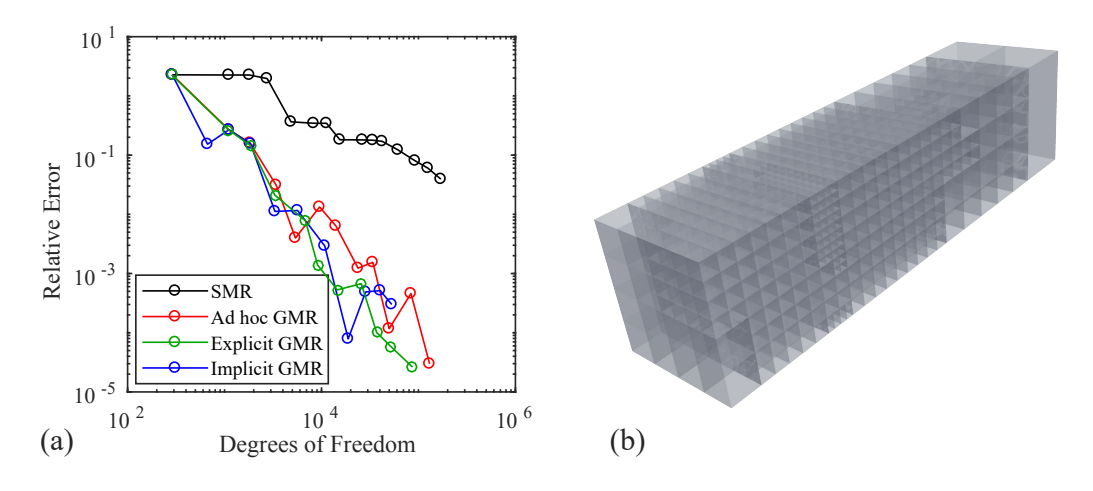


FIGURE 12.7. (a) The error in the QoI for the second example: average flux σ_x ; (b) the final adaptively refined mesh using the explicit GMR approach.

For a visual comparison of the error in σ_x in the region of interest $0 \le x \le 1$, we provide Figure 12.8. Notice that the local error with the GMR strategy is at least two orders of magnitude smaller than with the SMR strategy even though both meshes have a similar number of degrees of freedom.

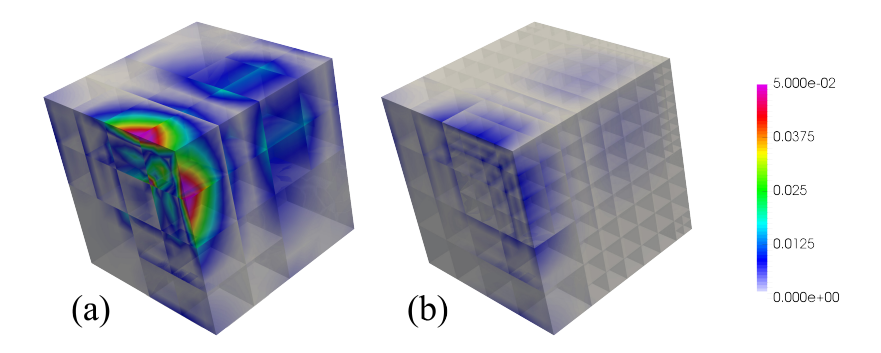


FIGURE 12.8. The final error in the solution component σ_x in the subdomain $0 \le x \le 1$ using: (a) conventional SMR; (b) GMR with the explicit refinement indicators $\eta_K^{*,\text{expl}}$ for the DPG* problem.

12.5. **Temperature on the boundary.** In this subsection, consider the goal functional g given in (12.2) where

(12.5)
$$g_1 = 0$$
, $g_2 = 0$, $\hat{g}_3(x, y, z) = \begin{cases} 1, & x = 0, \\ 0, & \text{otherwise,} \end{cases}$ and $\hat{g}_4 = 0$.

Physically, this corresponds to a QoI which is the average value of the temperature u on the subboundary x=0. Here, homogeneous Dirichlet and homogeneous Neumann boundary conditions were used on disjoint regions of the boundary, $u|_{\Gamma_{\rm D}}=0$ and $\frac{\partial u}{\partial n}|_{\Gamma_{\rm N}}=0$, where $\Gamma_{\rm D}=\{(x,y,z)\in\partial\Omega\mid x>0\}$ and $\overline{\Gamma_{\rm D}\cup\Gamma_{\rm N}}=\partial\Omega$.

Given that the ad hoc refinement indicators $\eta_K^{*,a.h.}$ were not derived for goal functionals involving nonzero \hat{g}_3 or \hat{g}_4 , in this case only, we actually used a different goal functional (12.6).

12.5.1. An alternative functional for ad hoc refinement indicators. Let $\Gamma = \{(x,y,z) \in \partial\Omega \mid x=0\}$ and define the set of all elements neighboring Γ as $\mathcal{T}_{\Gamma} = \{K \in \mathcal{T} \mid \overline{K} \cap \Gamma \neq \varnothing\}$. Lastly, define the subdomain occupied by this set of elements as $\Omega_{\Gamma} = \bigcup_{K \in \mathcal{T}_{\Gamma}} \overline{K}$.

Instead of (12.5), consider the modified goal functional

$$(12.6) \hspace{1cm} g_1(\mathbf{x}) = \begin{cases} h_{K,x}^{-1} \,, & \mathbf{x} \in \Omega_\Gamma \,, \\ 0 \,, & \text{otherwise,} \end{cases} \hspace{1cm} \boldsymbol{g}_2 = \mathbf{0} \,, \qquad \hat{g}_3 = 0 \,, \qquad \text{and} \qquad \hat{g}_4 = 0 \,,$$

where, $h_{K,x}$ is the length, in the x-dimension, of the element $K \in \mathcal{T}_{\Gamma}$ enclosing the point $\mathbf{x} \in K$. Notice that because g_1 operates on the u-component of the solution in (12.2), as the mesh becomes finer near Γ , this functional will also limit to a characterization of the average temperature on the boundary. The primary novelty of (12.6) is that the definition is mesh dependent. This is demonstrated in Figure 12.9, where Ω_{Γ} is highlighted in red on different adaptively refined meshes.

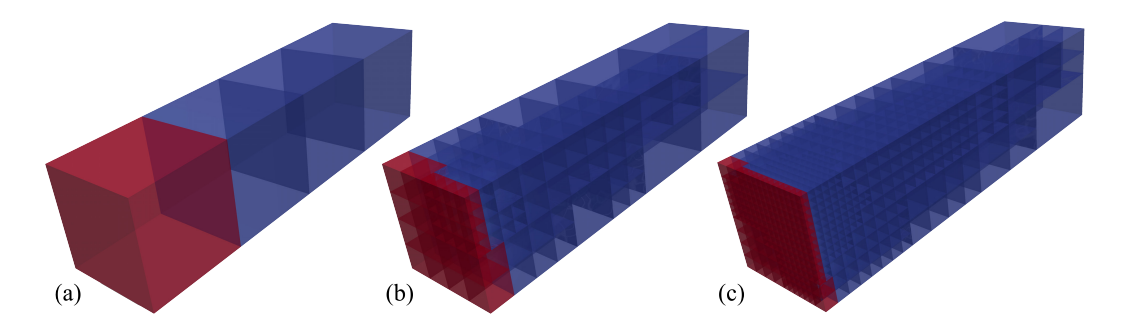


FIGURE 12.9. The region of interest Ω_{Γ} , marked in red, for: (a) the initial mesh; (b) the mesh after six GMR steps with the ad hoc approach; (c) the mesh after twelve GMR steps.

12.5.2. Results. Notice that $u^\star|_{\partial\Omega}=0$ from (12.1). Therefore, from the definition of g given in (12.5), $g(\mathbf{u}^\star)=\int_{\Gamma_{\rm N}}u^\star=\int_{\Gamma}u^\star=0$. Define the relative error in the QoI to be $\left|\int_{\Gamma}\hat{u}_{h,r}^{\rm opt}\right|/\left|\int_{\Gamma}\hat{u}_{h_{\rm init},r}^{\rm opt}\right|$, where $\hat{u}_{h_{\rm init},r}^{\rm opt}$ is the third component of approximate solution $\mathbf{u}_{h,r}^{\rm opt}$ computed on the initial mesh, which all approaches having in common (see Figure 12.2 (a)).

From only a cursory inspection of Figure 12.10, it is again evident that each of the GMR strategies were far more efficient than conventional SMR.

In Figure 12.11, the visual comparison given of the error in the temperature variable on the region of interest, x = 0, demonstrates a substantial improvement over the conventional SMR strategy, even with the ad hoc GMR approach which employed the modified goal functional (12.6).

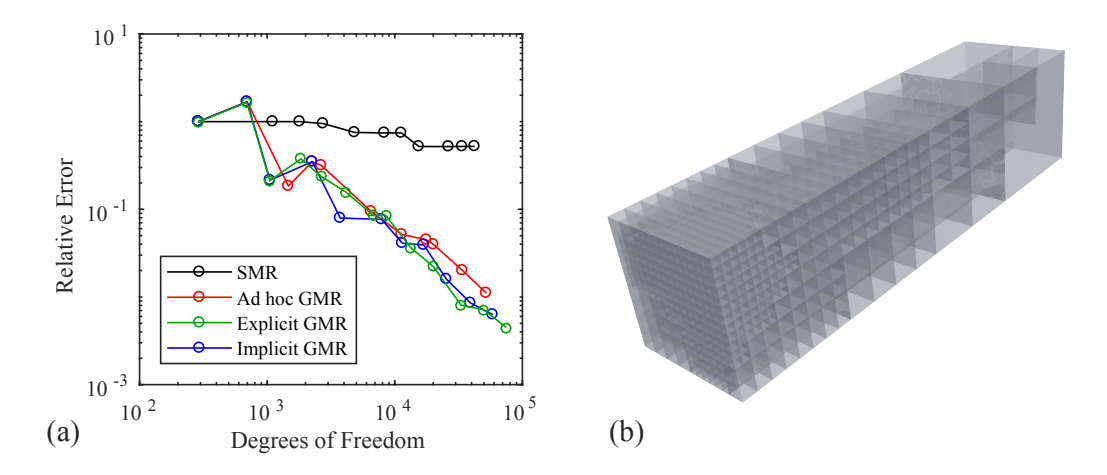


FIGURE 12.10. (a) The error in the QoI for the third example: average temperature \hat{u} ; (b) the final adaptively refined mesh using the ad hoc GMR approach.

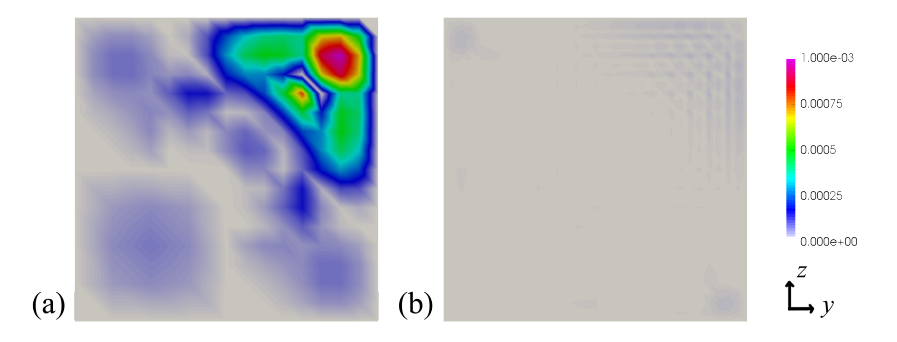


FIGURE 12.11. The final error in the solution \hat{u} on x=0 from: (a) conventional SMR; (b) the ad hoc GMR approach.

12.6. Flux on the boundary. Consider the goal functional given in (12.2) where

(12.7)
$$g_1 = 0$$
, $g_2 = 0$, $\hat{g}_3 = 0$, and $\hat{g}_4(x, y, z) = \begin{cases} 1, & x = 0, \\ 0, & \text{otherwise.} \end{cases}$

Physically, this corresponds to the QoI being the average value of the flux $\sigma \cdot \hat{n}$ through the subboundary x = 0. In our experiments, we used homogeneous Dirichlet boundary conditions everywhere, $u|_{\partial\Omega} = 0$.

12.6.1. Energy space considerations. In this experiment, $\Gamma_D = \partial \Omega$ and so $\left(H_N^{-1/2}(\partial \Omega)\right)' = H^{1/2}(\partial \Omega)$ and $H_0^1(\Gamma_D) = H^1(\partial \Omega)$. Notice that $\hat{g}_4 \in L^2(\partial \Omega)$ but $\hat{g}_4 \notin H^1(\partial \Omega)$. Therefore, there is no perquisite reason why g, as defined by (12.7), should be a bounded linear functional on $\mathcal U$. In fact, because it has a nontrivial jump discontinuity, $\hat{g}_4 \notin H^{1/2}(\partial \Omega)$ and so $g \notin \mathcal U'$.

Unfortunately, violating the energy setting is not simply a mathematical concern. Indeed, we found spuriously concentrated refinements near the discontinuity in \hat{g}_4 , when using (12.7). Therefore, instead of (12.7) in our experiments we chose to mollify the physically ideal (but discontinuous) \hat{g}_4 to an extent that it obeys the proper energy setting. Specifically, for our explicit and implicit GMR experiments, we ended up using the ramp function depicted in Figure 12.12, in place of the function \hat{g}_4 defined in (12.7).

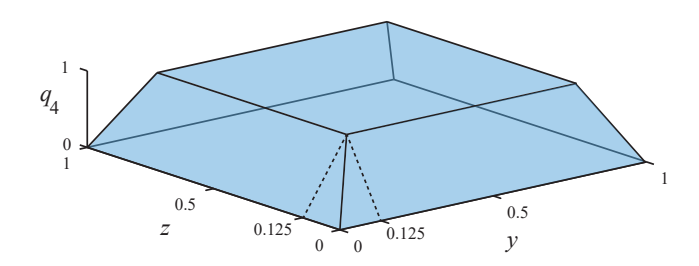


FIGURE 12.12. Illustration of the function $\hat{g}_4 \in H^1(\partial\Omega)$ (on the face x=0) used for explicit and implicit GMR.

12.6.2. Another alternative functional for ad hoc refinement indicators. Analogous to the previous experiment, here we considered an alternative to the goal functional (12.7) for the ad hoc DPG* refinement indicator. Namely, we used

$$(12.8) g_1 = 0 g_2(\mathbf{x}) = \begin{cases} (h_{K,x}^{-1}, 0, 0)^\mathsf{T}, & \mathbf{x} \in \Omega_\Gamma, \\ \mathbf{0}, & \text{otherwise}, \end{cases}, \quad \hat{g}_3 = 0, \quad \text{and} \quad \hat{g}_4 = 0,$$

with the same definitions for Ω_{Γ} and $h_{K,x}$ as in (12.6). Fortunately, with this definition, $g_2 \in L^2(\Omega)$ and so $g \in \mathcal{U}'$, for all meshes, and the energy space issues we documented for the explicit and implicit approaches are avoided.

12.6.3. Results. Define the relative error in the QoI to be $\left|\int_{\Gamma}(\sigma^{\star}\cdot\hat{n}-\hat{\sigma}_{h,r}^{\mathrm{opt}})\right|/\left|\int_{\Gamma}\sigma^{\star}\cdot\hat{n}\right|$. An inspection of Figure 12.13 clearly illustrates that the GMR strategies were far more efficient than the conventional SMR strategy for this QoI. In fact, with the conventional strategy, the error in this QoI did not even decrease until the eighth mesh refinement was performed!

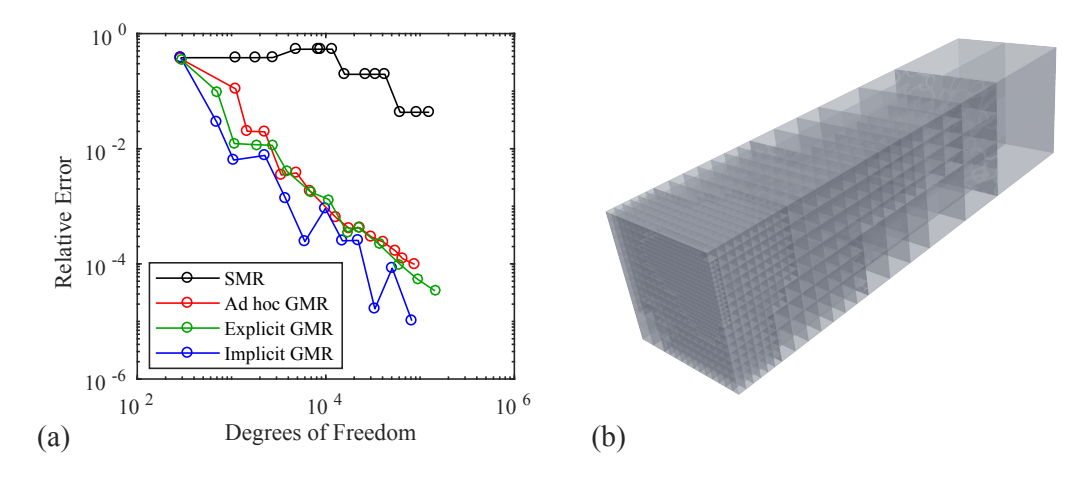


FIGURE 12.13. (a) The error in the QoI for the fourth example: average normal flux $\hat{\sigma}$; (b) the final adaptively refined mesh using the implicit GMR approach.

As for the visual comparison of the error in the flux on the region of interest, Figure 12.14 again demonstrates a significant improvement over conventional DPG SMR.

12.7. **Temperature at a point.** In this final experiment, we consider the quantity of interest $g_{\widetilde{\mathbf{x}}}(\mathbf{u}) = u(\widetilde{\mathbf{x}})$, where $\widetilde{\mathbf{x}} \in \Omega$ is a specified point in the domain. Markedly, this QoI does not fall into the theory of this article because $g_{\widetilde{\mathbf{x}}} \notin \mathcal{U}'$. To overcome this issue, we a mesh-dependent goal functional like (12.6) and (12.8). Define

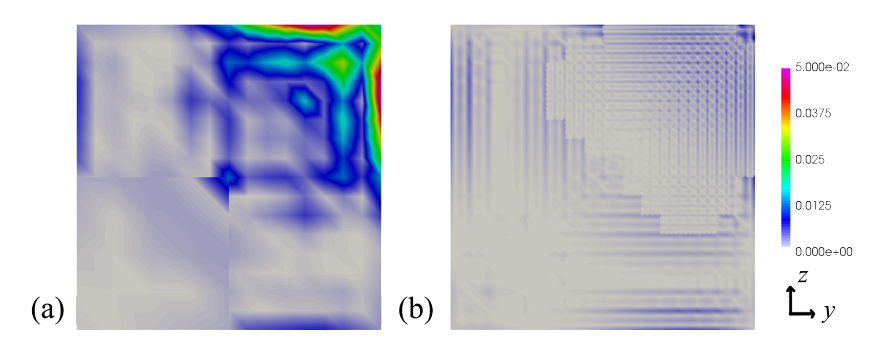


FIGURE 12.14. The final error in the solution $\hat{\sigma}$ at x=0 using: (a) conventional SMR; (b) the implicit GMR approach.

the set of all elements containing the point $\widetilde{\mathbf{x}}$ in their closure as $\mathcal{T}_{\widetilde{\mathbf{x}}} = \{K \in \mathcal{T} \mid \widetilde{\mathbf{x}} \in \overline{K}\}$ and define the subdomain occupied by this set of elements $\Omega_{\widetilde{\mathbf{x}}} = \bigcup_{K \in \mathcal{T}_{\widetilde{\mathbf{x}}}} \overline{K}$. Now, redefine the goal functional as

$$g_1(\mathbf{x}) = \begin{cases} \operatorname{vol}(\Omega_{\widetilde{\mathbf{x}}})^{-1}, & \mathbf{x} \in \Omega_{\widetilde{\mathbf{x}}}, \\ 0, & \text{otherwise}, \end{cases}$$
 $\mathbf{g}_2 = \mathbf{0}, \qquad \hat{g}_3 = 0, \qquad \text{and} \qquad \hat{g}_4 = 0.$

All results presented in this section are from our experiments with the mesh-dependent definition above and $\widetilde{\mathbf{x}} = (0.3, 0.3, 0.3)^T$. The evolution of this functional is visually depicted in Figure 12.15, where the region of interest $\Omega_{\widetilde{\mathbf{x}}}$ is highlighted in red on a selection of meshes.

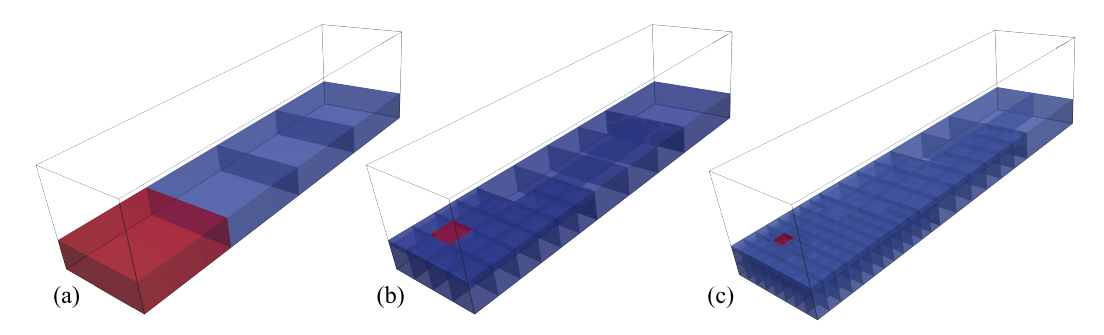


FIGURE 12.15. The region of interest $\Omega_{\widetilde{\mathbf{x}}}$ enclosing the point $\widetilde{\mathbf{x}} = (0.3, 0.3, 0.3)^{\mathsf{T}}$ for: (a) the initial mesh; (b) the mesh after six refinements with the implicit approach; (c) the mesh after twelve refinements. For the sake of illustration, only $y \leq 0.3$ is shown.

Inspect Figure 12.16. Here, the relative error is defined to be $|u^{\star}(\widetilde{\mathbf{x}}) - u_{h,r}^{\text{opt}}(\widetilde{\mathbf{x}})|/|u^{\star}(\widetilde{\mathbf{x}})|$. As in every previous experiment, each GMR approach vastly outperformed conventional SMR. However, in this experiment, the convergence behavior of each GMR approach was far more erratic.

APPENDIX A. A PYTHAGOREAN THEOREM FOR BOUNDED PROJECTIONS

The purpose of this appendix is to prove Theorem 7.3. For convenience, we restate it here, as Theorem A.1.

Theorem A.1 (Pythagoras). Let W be a Hilbert space and $W_0 \subseteq W$ be a nontrivial closed subspace. Let $\mathcal{P}: \mathcal{W} \to \mathcal{W}_0$ be the orthogonal projection onto W_0 and let $\Pi: \mathcal{W} \to \mathcal{W}_0$ be any other bounded projection onto $W_0 = \Pi(\mathcal{W})$. Then

$$\|\Pi - \mathcal{P}\|^2 + 1 = \|\Pi\|^2.$$

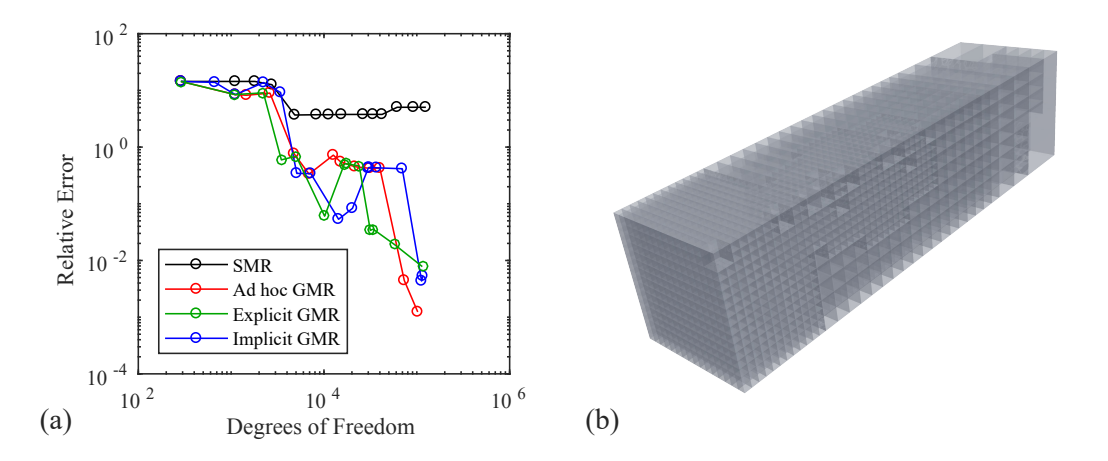


FIGURE 12.16. (a) The error in the QoI for the fifth example: temperature u at a fixed point; (b) the final adaptively refined mesh using the explicit GMR approach.

Proof. Throughout this proof, the subscript-w in norms and inner products is suppressed.

Note that, if $\Pi = \mathcal{P}$, we are done. Therefore, assume that $\Pi \neq \mathcal{P}$ and so $\{\mathfrak{w} \in \mathcal{W} \mid \|(\mathcal{P} - \Pi)\mathfrak{w}\| > 0\} \neq \emptyset$. Define $\mathcal{W}_1 = \mathcal{W}_0^{\perp}$. By Lemma 3.1, observe that

$$(A.1) \qquad \qquad \sup_{\mathfrak{w} \in \mathcal{W}} \frac{(\widetilde{\mathfrak{w}}, \Pi\mathfrak{w})^2}{\|\mathfrak{w}\|^2} = \sup_{\mathfrak{w}_0 \in \mathcal{W}_0} \frac{(\widetilde{\mathfrak{w}}, \Pi\mathfrak{w}_0)^2}{\|\mathfrak{w}_0\|^2} + \sup_{\mathfrak{w}_1 \in \mathcal{W}_1} \frac{(\widetilde{\mathfrak{w}}, \Pi\mathfrak{w}_1)^2}{\|\mathfrak{w}_1\|^2} \,, \quad \forall \, \widetilde{\mathfrak{w}} \in \mathcal{W} \,.$$

Note that $\Pi \mathfrak{w}_0 = \mathfrak{w}_0$ and $\Pi \mathfrak{w}_1 = \Pi(1 - P)\mathfrak{w}_1 = (\Pi - P)\mathfrak{w}_1$ for any $\mathfrak{w}_0 \in \mathcal{W}_0$ and $\mathfrak{w}_1 \in \mathcal{W}_1$, respectively. Therefore,

$$\begin{split} \|\Pi\|^2 &= \sup_{\mathfrak{w} \in \mathcal{W}} \frac{\|\Pi\mathfrak{w}\|^2}{\|\mathfrak{w}\|^2} = \sup_{\widetilde{\mathfrak{w}}, \mathfrak{w} \in \mathcal{W}} \frac{(\widetilde{\mathfrak{w}}, \Pi\mathfrak{w})^2}{\|\widetilde{\mathfrak{w}}\|^2 \|\mathfrak{w}\|^2} = \sup_{\widetilde{\mathfrak{w}} \in \mathcal{W}} \left(\sup_{\mathfrak{w}_0 \in \mathcal{W}_0} \frac{(\widetilde{\mathfrak{w}}, \Pi\mathfrak{w}_0)^2}{\|\widetilde{\widetilde{\mathfrak{w}}}\|^2 \|\mathfrak{w}_0\|^2} + \sup_{\mathfrak{w}_1 \in \mathcal{W}_1} \frac{(\widetilde{\mathfrak{w}}, \Pi\mathfrak{w}_1)^2}{\|\widetilde{\mathfrak{w}}\|^2 \|\mathfrak{w}_1\|^2} \right) \\ &= \sup_{\widetilde{\mathfrak{w}} \in \mathcal{W}} \left(\sup_{\mathfrak{w}_0 \in \mathcal{W}_0} \frac{(\widetilde{\mathfrak{w}}, \mathfrak{w}_0)^2}{\|\widetilde{\mathfrak{w}}\|^2 \|\mathfrak{w}_0\|^2} + \sup_{\mathfrak{w}_1 \in \mathcal{W}_1} \frac{(\widetilde{\mathfrak{w}}, (\Pi - \mathcal{P})\mathfrak{w}_1)^2}{\|\widetilde{\mathfrak{w}}\|^2 \|\mathfrak{w}_1\|^2} \right), \end{split}$$

$$(A.2)$$

where the third equality follows from (A.1). Clearly

$$\|\Pi\|^2 \leq \sup_{\widetilde{\mathfrak{w}}, \mathfrak{w} \in \mathcal{W}} \frac{(\widetilde{\mathfrak{w}}, \mathfrak{w})^2}{\|\widetilde{\mathfrak{w}}\|^2 \|\mathfrak{w}\|^2} + \sup_{\widetilde{\mathfrak{w}}, \mathfrak{w} \in \mathcal{W}} \frac{(\widetilde{\mathfrak{w}}, (\Pi - \mathcal{P})\mathfrak{w})^2}{\|\widetilde{\mathfrak{w}}\|^2 \|\mathfrak{w}\|^2} = 1 + \|\Pi - \mathcal{P}\|^2.$$

Now, define $\mathfrak{w}_{\pi} = \arg\max_{\|\mathfrak{w}\|=1} \|(\Pi - \mathfrak{P})\mathfrak{w}\| \neq 0$ and then $\mathfrak{w}_{\pi,0} = (\Pi - \mathfrak{P})\mathfrak{w}_{\pi} \neq 0$. Consider $\widetilde{\mathfrak{w}} = \mathfrak{w}_{\pi,0}$ in (A.2) and observe that

$$\|\Pi\|^2 \geq \sup_{\mathfrak{w}_0 \in \mathcal{W}_0} \frac{(\mathfrak{w}_{\pi,0},\mathfrak{w}_0)^2}{\|\mathfrak{w}_{\pi,0}\|^2 \|\mathfrak{w}_0\|^2} + \sup_{\mathfrak{w}_1 \in \mathcal{W}_1} \frac{(\mathfrak{w}_{\pi,0}, (\Pi - \mathcal{P})\mathfrak{w}_1)^2}{\|\mathfrak{w}_{\pi,0}\|^2 \|\mathfrak{w}_1\|^2}.$$

Note that $\mathfrak{w}_{\pi,0} \in \mathcal{W}_0$, $\mathfrak{w}_{\pi} \in \mathcal{W}_1$, $\|\mathfrak{w}_{\pi,0}\| = \|\Pi - \mathcal{P}\|$, and $\|\mathfrak{w}_{\pi}\| = 1$. Finally, consider $\mathfrak{w}_0 = \mathfrak{w}_{\pi,0}$ and $\mathfrak{w}_1 = \mathfrak{w}_{\pi}$ and observe that

$$\|\Pi\|^2 \geq \frac{(\mathfrak{w}_{\Pi,0},\mathfrak{w}_{\Pi,0})^2}{\|\mathfrak{w}_{\Pi,0}\|^4} + \frac{((\Pi - \mathcal{P})\mathfrak{w}_\Pi, (\Pi - \mathcal{P})\mathfrak{w}_\Pi)^2}{\|\Pi - \mathcal{P}\|^2} = 1 + \|\Pi - \mathcal{P}\|^2.$$

REFERENCES

- [1] M. AINSWORTH AND J. T. ODEN, A posteriori error estimation in finite element analysis, vol. 37, John Wiley & Sons, 2011.
- [2] B. AKSOYLU, S. D. BOND, E. C. CYR, AND M. HOLST, Goal-oriented adaptivity and multilevel preconditioning for the Poisson–Boltzmann equation, J. Sci. Comput., 52 (2012), pp. 202–225.
- [3] C. AMROUCHE, C. BERNARDI, M. DAUGE, AND V. GIRAULT, Vector potentials in three-dimensional non-smooth domains, Math. Methods Appl. Sci., 21 (1998), pp. 823–864.
- [4] I. BABUŠKA AND A. MILLER, The post-processing approach in the finite element method-part 1: Calculation of displacements, stresses and other higher derivatives of the displacements, Int. J. Numer. Meth. Eng., 20 (1984), pp. 1085–1109.
- [5] I. BABUŠKA, R. B. KELLOGG, AND J. PITKÄRANTA, Direct and inverse error estimates for finite elements with mesh refinements, Numer. Math., 33 (1979), pp. 447-471.
- [6] R. BECKER, E. ESTECAHANDY, AND D. TRUJILLO, Weighted marking for goal-oriented adaptive finite element methods, SIAM J. Numer. Anal., 49 (2011), pp. 2451–2469.
- [7] R. BECKER AND R. RANNACHER, An optimal control approach to a posteriori error estimation in finite element methods, Acta Numer., 10 (2001), pp. 1–102.
- [8] J. BRAMWELL, L. DEMKOWICZ, J. GOPALAKRISHNAN, AND Q. WEIFENG, A locking-free hp DPG method for linear elasticity with symmetric stresses, Numer. Math., 122 (2012), pp. 671–707.
- [9] S. BRENNER AND R. SCOTT, The Mathematical Theory of Finite Element Methods, vol. 15, Springer Science & Business Media, 2007.
- [10] F. Brezzi, On the existence, uniqueness and approximation of saddle-point problems arising from Lagrangian multipliers, Rev. fr. autom. inform. rech. opér., Anal. numér., 8 (1974), pp. 129–151.
- [11] T. Bui-Thanh, L. Demkowicz, and O. Ghattas, Constructively well-posed approximation methods with unity inf-sup and continuity constants for partial differential equations, Math. Comp., 82 (2013), pp. 1923–1952.
- [12] C. CARSTENSEN, P. BRINGMANN, F. HELLWIG, AND P. WRIGGERS, Nonlinear discontinuous Petrov-Galerkin methods, arXiv:1710.00529 [math.NA], (2017).
- [13] C. CARSTENSEN, L. DEMKOWICZ, AND J. GOPALAKRISHNAN, A posteriori error control for DPG methods, SIAM J. Numer. Anal., 52 (2014), pp. 1335–1353.
- [14] C. CARSTENSEN, L. DEMKOWICZ, AND J. GOPALAKRISHNAN, Breaking spaces and forms for the DPG method and applications including Maxwell equations, Comput. Math. Appl., 72 (2016), pp. 494–522.
- [15] C. CARSTENSEN, M. FEISCHL, M. PAGE, AND D. PRAETORIUS, Axioms of adaptivity, Comput. Math. Appl., 67 (2014), pp. 1195–1253.
- [16] C. CARSTENSEN AND F. HELLWIG, Low-order discontinuous Petrov-Galerkin finite element methods for linear elasticity, SIAM J. Numer. Anal., 54 (2016), pp. 3388–3410.
- [17] J. CHAN, N. HEUER, T. BUI-THANH, AND L. DEMKOWICZ, A robust DPG method for convection-dominated diffusion problems II: Adjoint boundary conditions and mesh-dependent test norms, Comput. Math. Appl., 67 (2014), pp. 771–795.
- [18] J. L. CHAN, A DPG method for convection-diffusion problems, PhD thesis, The University of Texas at Austin, Austin, Texas, U.S.A., 2013.
- [19] J. H. CHAUDHRY, E. C. CYR, K. LIU, T. A. MANTEUFFEL, L. N. OLSON, AND L. TANG, Enhancing least-squares finite element methods through a quantity-of-interest, SIAM J. Numer. Anal., 52 (2014), pp. 3085–3105.
- [20] P. G. CIARLET, Linear and Nonlinear Functional Analysis with Applications, SIAM, 2013.
- [21] W. DAHMEN, C. HUANG, C. SCHWAB, AND G. WELPER, Adaptive Petrov-Galerkin methods for first order transport equations, SIAM J. Numer. Anal., 50 (2012), pp. 2420–2445.
- [22] L. Demkowicz, Computing with hp Finite Elements. I. One and Two Dimensional Elliptic and Maxwell Problems, Chapman & Hall/CRC Press, New York, October 2006.
- [23] L. Demkowicz, Polynomial exact sequences and projection-based interpolation with application to Maxwell equations, in Mixed Finite Elements, Compatibility Conditions, and Applications, D. Boffi and L. Gastaldi, eds., vol. 1939 of Lecture Notes in Mathematics, Springer, Berlin, 2008, pp. 101–158.
- [24] L. Demkowicz and J. Gopalakrishnan, A class of discontinuous Petrov-Galerkin methods. Part I: The transport equation, Comput. Methods Appl. Mech. Engrg., 199 (2010), pp. 1558–1572.
- [25] L. DEMKOWICZ AND J. GOPALAKRISHNAN, A class of discontinuous Petrov-Galerkin methods. II. Optimal test functions, Numer. Methods Partial Differential Equations, 27 (2011), pp. 70–105.
- [26] L. Demkowicz and J. Gopalakrishnan, *An overview of the DPG method*, in Recent Developments in Discontinuous Galerkin Finite Element Methods for Partial Differential Equations, X. Feng, O. Karakashian, and Y. Xing, eds., vol. 157 of The IMA Volumes in Mathematics and its Applications, Springer, 2014, pp. 149–180.
- [27] L. DEMKOWICZ AND J. GOPALAKRISHNAN, Discontinuous Petrov-Galerkin (DPG) method, ICES Report 15-20, The University of Texas at Austin, 2015.
- [28] L. DEMKOWICZ, J. GOPALAKRISHNAN, S. NAGARAJ, AND P. SEPULVEDA, A spacetime DPG method for the Schrödinger equation, SIAM J. Numer. Anal., 55 (2017), pp. 1740–1759.
- [29] L. DEMKOWICZ, J. GOPALAKRISHNAN, AND A. H. NIEMI, A class of discontinuous Petrov-Galerkin methods. Part III: Adaptivity, Appl. Numer. Math., 62 (2012), pp. 396-427.

- [30] L. DEMKOWICZ AND N. HEUER, Robust DPG method for convection-dominated diffusion problems, SIAM J. Numer. Anal., 51 (2013), pp. 2514–2537.
- [31] L. DEMKOWICZ, J. KURTZ, D. PARDO, M. PASZYŃSKI, W. RACHOWICZ, AND A. ZDUNEK, Computing with hp Finite Elements. II. Frontiers: Three Dimensional Elliptic and Maxwell Problems with Applications, Chapman & Hall/CRC, New York, October 2007.
- [32] W. DÖRFLER, A convergent adaptive algorithm for Poisson's equation, SIAM J. Numer. Anal., 33 (1996), pp. 1106-1124.
- [33] T. ELLIS, L. DEMKOWICZ, AND J. CHAN, Locally conservative discontinuous Petrov-Galerkin finite elements for fluid problems, Comput. Math. Appl., 68 (2014), pp. 1530–1549.
- [34] K. ERIKSSON, D. ESTEP, P. HANSBO, AND C. JOHNSON, Introduction to adaptive methods for differential equations, Acta Numer., 4 (1995), pp. 105–158.
- [35] M. FEISCHL, D. PRAETORIUS, AND K. G. VAN DER ZEE, An abstract analysis of optimal goal-oriented adaptivity, SIAM J. Numer. Anal., 54 (2016), pp. 1423–1448.
- [36] F. FUENTES, L. DEMKOWICZ, AND A. WILDER, Using a DPG method to validate DMA experimental calibration of viscoelastic materials, Comput. Methods Appl. Mech. Engrg., 325 (2017), pp. 748–765.
- [37] F. FUENTES, B. KEITH, L. DEMKOWICZ, AND P. LE TALLEC, Coupled variational formulations of linear elasticity and the DPG methodology, J. Comput. Phys., 348 (2017), pp. 715–731.
- [38] F. FUENTES, B. KEITH, L. DEMKOWICZ, AND S. NAGARAJ, Orientation embedded high order shape functions for the exact sequence elements of all shapes, Comput. Math. Appl., 70 (2015), pp. 353–458.
- [39] T. FÜHRER AND N. HEUER, Robust coupling of DPG and BEM for a singularly perturbed transmission problem, Comput. Math. Appl., 74 (2017), pp. 1940–1954.
- [40] T. FÜHRER, N. HEUER, AND E. P. STEPHAN, On the DPG method for Signorini problems, IMA J. Numer. Anal., in press (2017).
- [41] M. B. GILES AND E. SÜLI, Adjoint methods for PDEs: a posteriori error analysis and postprocessing by duality, Acta Numer., 11 (2002), pp. 145–236.
- [42] J. GOPALAKRISHNAN AND W. QIU, An analysis of the practical DPG method, Math. Comp., 83 (2014), pp. 537-552.
- [43] B. N. Granzow, M. S. Shephard, and A. A. Oberai, Output-based error estimation and mesh adaptation for variational multiscale methods, Comput. Methods Appl. Mech. Engrg., 322 (2017), pp. 441–459.
- [44] N. HEUER AND M. KARKULIK, A robust DPG method for singularly perturbed reaction-diffusion problems, SIAM J. Numer. Anal., 55 (2017), pp. 1218–1242.
- [45] M. HOLST AND S. POLLOCK, Convergence of goal-oriented adaptive finite element methods for nonsymmetric problems, Numer. Methods Partial Differential Equations, 32 (2016), pp. 479–509.
- [46] B. KEITH, L. DEMKOWICZ, AND J. GOPALAKRISHNAN, DPG* method, arXiv:1710.05223 [math.NA], (2017).
- [47] B. KEITH, F. FUENTES, AND L. DEMKOWICZ, The DPG methodology applied to different variational formulations of linear elasticity, Comput. Methods Appl. Mech. Engrg., 309 (2016), pp. 579–609.
- [48] B. KEITH, P. KNECHTGES, N. V. ROBERTS, S. ELGETI, M. BEHR, AND L. DEMKOWICZ, An ultraweak DPG method for viscoelastic fluids, J. Non-Newton. Fluid Mech., 247 (2017), pp. 107–122.
- [49] B. KEITH, S. PETRIDES, F. FUENTES, AND L. DEMKOWICZ, Discrete least-squares finite element methods, Comput. Methods Appl. Mech. Engrg., in press (2017).
- [50] P. LADEVÈZE, Strict upper error bounds on computed outputs of interest in computational structural mechanics, Comput. Mech., 42 (2008), pp. 271–286.
- [51] P. LADEVÈZE, F. PLED, AND L. CHAMOIN, New bounding techniques for goal-oriented error estimation applied to linear problems, Int. J. Numer. Meth. Eng., 93 (2013), pp. 1345–1380.
- [52] M. S. MOMMER AND R. STEVENSON, A goal-oriented adaptive finite element method with convergence rates, SIAM J. Numer. Anal., 47 (2009), pp. 861–886.
- [53] P. MONK, Finite Element Methods for Maxwell's Equations, Numerical Analysis and Scientific Computation Series, Oxford University Press, New York, 2003.
- [54] S. NAGARAJ, S. PETRIDES, AND L. F. DEMKOWICZ, Construction of DPG Fortin operators for second order problems, Comput. Math. Appl., 74 (2017), pp. 1964–1980.
- [55] J. T. ODEN, L. DEMKOWICZ, W. RACHOWICZ, AND T. WESTERMANN, Toward a universal h-p adaptive finite element strategy, part 2. A posteriori error estimation, Comput. Methods Appl. Mech. Engrg., 77 (1989), pp. 113–180.
- [56] J. T. ODEN AND S. PRUDHOMME, New approaches to error estimation and adaptivity for the Stokes and Oseen equations, Int. J. Numer. Methods Fluids, 31 (1999), pp. 3–15.
- [57] J. T. ODEN AND S. PRUDHOMME, Goal-oriented error estimation and adaptivity for the finite element method, Comput. Math. Appl., 41 (2001), pp. 735–756.
- [58] M. PARASCHIVOIU, J. PERAIRE, AND A. T. PATERA, A posteriori finite element bounds for linear-functional outputs of elliptic partial differential equations, Comput. Methods Appl. Mech. Engrg., 150 (1997), pp. 289–312.
- [59] A. T. PATERA AND J. PERAIRE, A general Lagrangian formulation for the computation of a posteriori finite element bounds, in Error Estimation and Adaptive Discretization Methods in Computational Fluid Dynamics, Springer, 2003, pp. 159–206.
- [60] S. PETRIDES AND L. F. DEMKOWICZ, An adaptive DPG method for high frequency time-harmonic wave propagation problems, Comput. Math. Appl., 74 (2017), pp. 1999–2017.

- [61] S. PRUDHOMME AND J. T. ODEN, On goal-oriented error estimation for elliptic problems: application to the control of pointwise errors, Comput. Methods Appl. Mech. Eng., 176 (1999), pp. 313–331.
- [62] N. V. Roberts, A discontinuous Petrov-Galerkin methodology for incompressible flow problems, PhD thesis, The University of Texas at Austin, Austin, Texas, U.S.A., 2013.
- [63] N. V. Roberts, Camellia: A software framework for discontinuous Petrov-Galerkin methods, Comput. Math. Appl., 68 (2014), pp. 1581–1604.
- [64] N. V. ROBERTS, Camellia v1.0 manual: Part I, Tech. Rep. ANL/ALCF-16/3, Argonne National Laboratory, Argonne, Illinois, 2016.
- [65] N. V. ROBERTS, T. BUI-THANH, AND L. DEMKOWICZ, The DPG method for the Stokes problem, Comput. Math. Appl., 67 (2014), pp. 966–995.
- [66] N. V. ROBERTS, L. DEMKOWICZ, AND R. MOSER, A discontinuous Petrov-Galerkin methodology for adaptive solutions to the incompressible Navier-Stokes equations, J. Comput. Phys., 301 (2015), pp. 456–483.
- [67] D. B. SZYLD, The many proofs of an identity on the norm of oblique projections, Numer. Algorithms, 42 (2006), pp. 309-323.
- [68] A. VAZIRI ASTANEH, F. FUENTES, J. MORA, AND L. DEMKOWICZ, High-order polygonal discontinuous Petrov-Galerkin (PolyDPG) methods using ultraweak formulations, arXiv:1706.06754 [math.NA], (2017).
- [69] R. VERFÜRTH, A posteriori error estimation and adaptive mesh-refinement techniques, J. Comput. Appl. Math., 50 (1994), pp. 67–83
- [70] J. ZITELLI, I. MUGA, L. DEMKOWICZ, J. GOPALAKRISHNAN, D. PARDO, AND V. M. CALO, A class of discontinuous Petrov-Galerkin methods. Part IV: The optimal test norm and time-harmonic wave propagation in 1D, J. Comput. Phys., 230 (2011), pp. 2406–2432.

THE INSTITUTE FOR COMPUTATIONAL ENGINEERING AND SCIENCES (ICES), THE UNIVERSITY OF TEXAS AT AUSTIN, 201 E 24TH ST, AUSTIN, TX 78712, USA

E-mail address, corresponding author: brendan@ices.utexas.edu